Performance Characterization of Digital Optical Data Transfer Systems for Use in the Space Radiation Environment

By Robert A. Reed, NASA/GSFC

1.0 Introduction

Radiation effects in photonic and microelectronic components can adversely affect the performance of high-speed digital optical data links in a variety of ways. This segment of the Short Course focuses on radiation effects in digital optical data links operating in the MHz to GHz regime. (Some of the information is applicable to frequencies above and below this regime.) The three basic component level effects that should be considered are effects due to total ionizing dose and displacement damage dose, and single-event effects. In some cases the system performance degradation can be quantified by means of component level tests, while in others a more holistic characterization approach must be taken.

In Section 2 of this segment of the Short Course we will give a brief overview of the space radiation environment followed by a summary of the above listed space radiation effects important for microelectronics and photonics. The last part of this section will discuss an example of radiation environment requirements for a typical mission.

Section 3 gives an overview of intra-satellite digital optical data link systems, including various link topologies and their associated components. Also, we discuss some of the important system performance metrics that are impacted by radiation-induced degradation of optical and optoelectronic component performance.

Section 4 discusses radiation effects in optical and optoelectronic components, focusing on degradation of passive optical components and single-event effects in photodetectors. (The other mechanisms are covered in detail in segment II of this Short Course entitled “Photonic Devices with Complex and Multiple Failure Modes”.)

Section 5 will focus on optical-data-link system response to the space radiation environment. Optical link system level single-event effects ground testing will be discussed. To close, we give a discussion of optical system level assessment of data link performance for optical systems operating in the space radiation environment.

2.0 Summary of the Space Radiation Environment and Basic Radiation Effects in Devices

Earth-orbiting and interplanetary spacecraft face a variety of radiation-related threats. Determining the survival probability of a spacecraft during its mission requires not just accurate ground-based test data for the device and a validated model for predicting the device performance in space from the ground-based data. It also requires accurate prediction of the space radiation environment. Although a complete description of the environment is beyond the scope of this course, its importance demands that we give at least a cursory treatment here. An excellent description of the space radiation environment as well as the use, validity, and limitations of the relevant models thereof, can be found in the Nuclear and Space Radiation Effects Conference 97 Short Course [Bart-97].

The radiation environment encountered by a spacecraft depends on several factors, including the path of the spacecraft relative to the planets, the level of solar activity, and the mission duration determine the radiation levels incident on the spacecraft. For some radiation effects, the spacecraft's ability to shield sensitive components from radiation can be crucial in determining whether radiation effects will degrade the performance of those components. Finally, the threat of man-made radiation environments (not addressed in this course) can be an important consideration. Typically, these variables are used as inputs to computer codes that predict the space radiation environment encountered by a spacecraft and how this environment affects the spacecraft's mission.

There are two major components of the natural space radiation environment: the transient environment and that trapped by the magnetic fields of most planets. As might be expected, Earth's trapped radiation environment is better characterized than that of other planets. Our brief discussion of the radiation environment will focus on the naturally occurring radiation environment as it affects the performance of microelectronic and photonic devices in Earth-orbiting spacecraft. Deep-space missions passing near other planets, radiation dosimetry [Dyer-98] and man-made radiation environments are described elsewhere [Teag-72].

Figure 2.1 is an artist's conception of Earth's radiation environment. The near-Earth trapped particle environment will be discussed first, followed by a discussion of the solar and galactic radiation environments. Next, we will give a brief discussion of the basic concepts of radiation effects in photonic and microelectronic devices. The last part of this section will discuss the typical environmental data needed to evaluate and predict the performance of photonic and microelectronic devices exposed to the radiation environment.

2.1 Space Radiation Environment

The objective of this section is to give a brief summary of the radiation environment encountered by near-earth spacecraft. [Bart-97] gives a more detailed overview of the basic physics and theories that describe solar processes, Earth's magnetic field, charged particle interactions with the magnetic field and many of the other details not covered by this brief summary. Our discussion is divided into two parts: trapped and transient radiation environments.

2.1.1 Trapped Protons and Electrons

Particles with the proper charges, masses, energies and trajectories can be captured by the Earth's magnetic field. See [Bart-97, Dyer-98] for details of the species, origin, confinement processes, subsequent motion, and measurement of these particles. Of the particles confined by

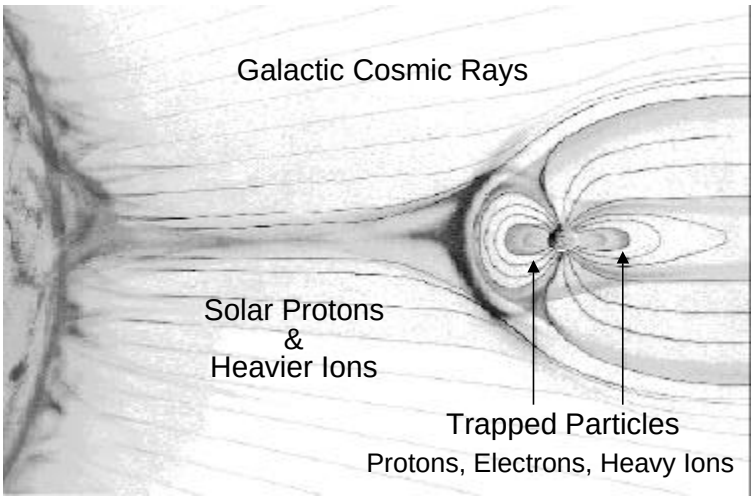

Figure 2.1: Cartoon showing the components of the space radiation environment important for microelectronic and photonic performance degradation evaluations. [Endo]

Earth's magnetic field, electrons and protons have the greatest effect on spaceflight hardware. **Figure 2.2** shows cross sections through dipole plots of these two particle populations as predicted with the AP-8 and AE-8 trapped particle models. The proton environment is given on the left side of the cartoon, and the electron environment is shown on the right. In simplified approximations of these environments, they form a toroid with Earth at the center and Earth's magnetic pole defining the toroid's central axis. (The geographic pole is roughly 11 degrees off center from the magnetic pole.) L is the dipole shell number of the Earth's magnetic field. At the magnetic equator L is the distance in Earth radii from the center of the earth. As the angle of inclination moves away from the magnetic equator, the value of L is corrected for the magnetic field strength. The values of L in **Figure 2.2** refer to that at the magnetic equator.

As shown in the figure, the proton flux is confined to a single toriod, and electrons form two high intensity toriods. The region between the two electron zones is known as the slot region. Earth's atmosphere and magnetic field and their interaction with the solar wind and the solar magnetic field define the details of the flux of each particle toriod. The particles roughly follow Earth's magnetic field lines.

In the inner region, $L < 3.5$, electron and proton toriods overlap, while for $3.5>L>8.5$, the trapped particles are mostly electrons. No significant particle trapping occurs for values of $L>11$. In the trapped regions the flux is considered to be approximately omnidirectional.

Although **Figure 2.2** presents a static view of the shape, regional flux, and orientation of the toriods, in reality, these belts are very dynamic, growing and shrinking over time. Occasionally, new torroidal regions form and disappear, especially in the slot region. The dynamic nature of the trapped radiation belts is not very well understood and is poorly modeled. Research has shown that fluxes can change dramatically with solar activity, but quantitative models of this variability do not yet exist for short term averages.

One temporal variation that has been quantified is the variation of the flux levels in the toriods with the 11 year solar cycle. (During solar maximum the integral fluences for protons are lower for low Earth orbit than during solar minimum, while for electrons the reverse is true.) It is the short duration temporal variations that are the most difficult to quantify. Progress in dynamic modeling techniques has been made by [Bosc-99] with the salambo code.

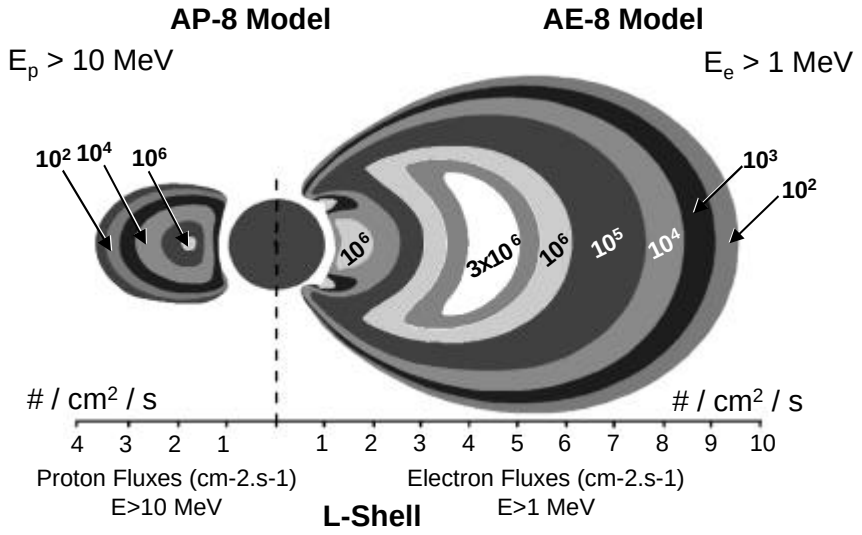

Figure 2.2: Dipole projection of the earth's Van Allen radiation belts as predicted by the AP-8 and AE-8 trapped particle models. A cross section of the protons are depicted on the left and the electrons are shown on the right.

Another modification to the simple toriodal model results from the fact that Earth's magnetic field is multipolar in nature, causing the magnetic field strength contours to sink towards the earth. This multipolar field causes the South Atlantic Anomaly (SAA)—a dip towards the Earth in proton and inner electron flux contours over the South Atlantic. For equal altitudes, the particle flux will be higher for locations in the SAA than for those outside of it.

Further discussion of models for the trapped particle environments are given in [Bart-97, Hous-98]. For example, the NASA's AP8 and AE8, Huston-Pfitzer, CRRESPRO and CRRESELE models are used to model the trapped proton and electron environments [see Bart-97 and references therein].

2.1.2 Trapped Heavier Ions

Ions with Z > 1 can also be trapped by Earth's magnetic field, although the intensities for these ions are lower than those for protons and electrons. The trapped heavy ions have energies on the order of 10s of MeV/amu, so most of them will not penetrate even the thinnest spacecraft shielding [Bart-97 and references therein]. Effects of these particles on microelectronic and photonic systems are second order in most cases.

2.1.3 Transient Environment

Although many types of radiation make up the transient environment, the two most important components for radiation effects in spacecraft are the Galactic Cosmic Rays (GCRs) and particles emitted during solar events.

The sources of GCRs are sufficiently far from our solar system that the fluxes of these particles are essentially isotropic in free space regions. Interactions in the vicinity of Earth between the solar wind and our planet's magnetic field change individual particle trajectories and energies. However, the net GCR flux is still essentially omnidirectional.

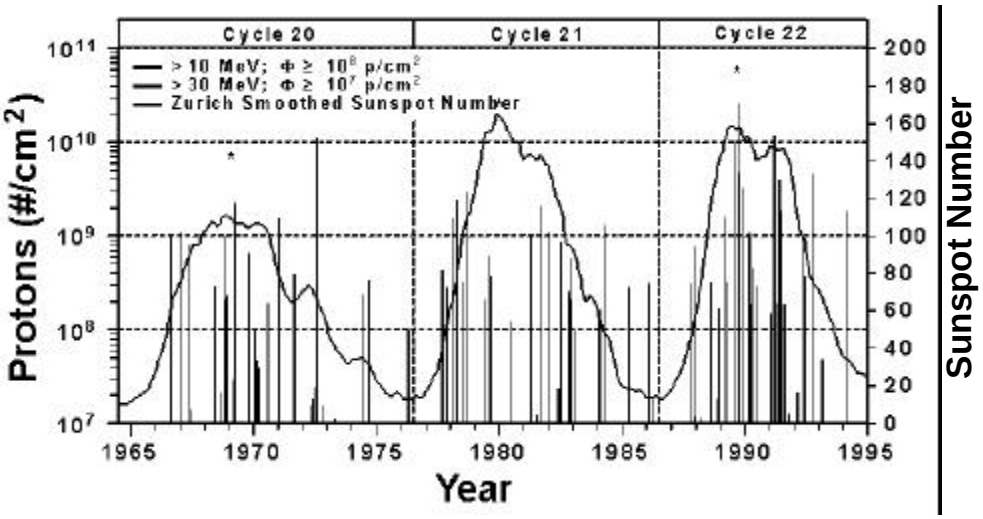

Figure 2.3: Correlation of the occurrence of several large solar proton events over a thirty year period (vertical light lines) with the Zurich sun spot number (single solid dash line). [Bart-97]

The GCR particle composition is roughly 83% protons, 13% alpha particles, 3% electrons, and 1% heavier ions (Z > 2). The ion energies range from 10s of MeV/amu to 100s of GeV/amu and beyond, and most ions are fully ionized. Some of these ions have sufficient energy to penetrate most shielding provided by a spacecraft structure. In [Bart-97], there is a more complete description of the GCR environment, including relative abundances, energy spectra and variation over solar cycle.

Not all of radiation impinging on Earth originates from such distant sources. The Sun can be thought of as a boiling pot of plasma that emits charged particles most of the time. When the Sun is "quiescent," most of the particles it emits do not have sufficient energy to penetrate through even a small amount of spacecraft shielding. However, during times of high activity, conditions occur that can accelerate a spectrum of charged particles with a large range of energies for varying durations. The duration of such events is usually between a few hours and several days. The average frequency of these solar events varies roughly sinusoidally with the eleven-year sunspot cycle. **Figure 2.3** illustrates this variation over the last three solar cycles—showing solar proton integral fluences (the spikes) for large solar proton events over a thirty-year period superimposed over the sunspot numbers (smooth curve).

Two important classes of events that occur during this high activity period are Coronal Mass Ejections (CMEs) and solar flares. CMEs have been correlated with events that have a high probability of producing protons that reach the Earth. Whereas solar flares seem to be correlated to heavy ion rich solar particle events [Ream-95]. Solar flares and CMEs can occur at the same time giving rise to events with very high intensity which contain all naturally occurring elements (Z=1-92) [Tylk-96]. The total integral fluences during these rare events can exceed average GCR fluxes by three orders of magnitude and more. Again, the reference of choice that describes the solar event environment in detail is [Bart-97 and references therein]. Newer models for predicting the solar proton event environment can be found in [Xaps-98, Xaps-00].

2.2 Basic Radiation Effects in Devices

Microelectronic and photonic components are manufactured in very controlled environments. During certain phases of the manufacturing process, even the slightest change in conditions like temperature or impurity concentration can induce changes on the overall molecular structure that cause the component to fail functional or parametric performance metrics. The point here is that devices that rely on such carefully grown, well-defined microscopic structures can have very low tolerance for slight changes in their characteristics. When a component is exposed to radiation, the radiation transfers some of its energy to the component materials, changing the localized material properties. This can have significant effects on component functionality and/or parametrics with the end result depending on the type of radiation, where the energy deposition occurred, and the type of component.

Three important effects that occur when a component is exposed to radiation are: Single-Event Effects (SEEs) and effects due to Total Ionizing Dose (TID) and Displacement Damage Dose (DDD). This section will briefly define these effects and describe the basic mechanisms that cause the effect. It does not attempt to completely describe the impact that these basic interactions have on the performance of the component. The reader will find detailed descriptions and discussions of the effects in other portions of this Short Course, past Short Courses, and in the many years of work published in the IEEE Transactions on Nuclear Science (TNS) and Proceedings from the Radiation Effects in Components and Systems Conference (RADECS). Because much of this segment of the Short Course is dedicated to single-event transient effects, these will be treated and described in the most detail.

2.2.1 Single-Event Effects

An ionizing particle generates electron-hole pairs along its path as it passes through a material, resulting initially in a line charge distribution with equal numbers of holes and electrons. Because the function of many active electronic and optoelectronic devices is governed by the controlled injection of charge into the depletion layers of p-n junctions, the uncontrolled charge injection resulting from ionization can compromise device function. Exactly what effects result from a single-particle event (or single-event), depend on the device type and on how much charge is collected at sensitive junctions in the device [Dodd-99 and references therein].

Once the charge track is generated, it evolves rapidly (on a timescale of picoseconds) in response to the same fields and mechanisms that govern the behavior of any other charges in the medium. On very short timescales, the density of both positive holes and negative electrons along the particle track is quite high, and the dominant process at work is the recombination of these charges. Recombination decreases the charge collected within the device. The initially high charge densities also lead to diffusion of charges away from the ion track. Diffusion increases the average distance between charges, decreasing the recombination rate (and so tending to increase charge collection) over time. Charges will also be swept up by the intrinsic and applied fields in the device—a process called drift, which also tends to separate electrons and holes and increase charge collection. Drift in the vicinity of p-n junctions is especially important because of the strong intrinsic and applied fields in these regions.

Although the processes governing the evolution of the charge track are the same as those governing the behavior of other charges in the medium, the charge densities along the charge track can be high enough to alter the properties of the medium in the track's vicinity. One important manifestation of this is funneling [Hsie-81], which occurs when the charge density along the track is sufficiently high to collapse the usual p-n junction field. (See **Figure 2.4**.)

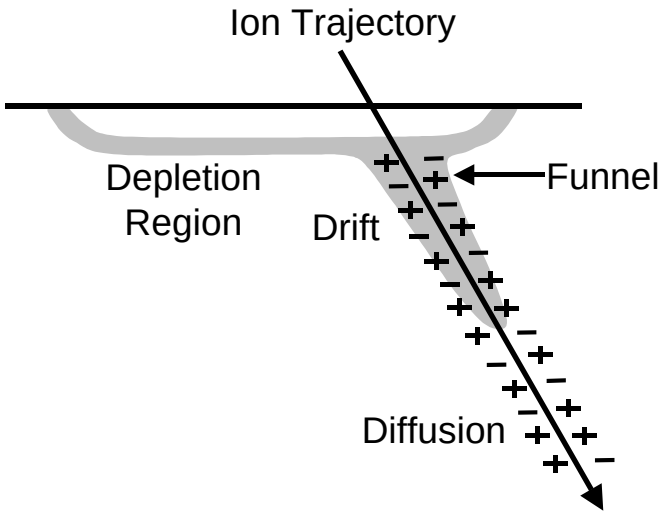

Figure 2.4: Ion strike crossing a p-n junction showing the drift (in the depletion region and funnel) and diffusion components of the charge collected.

When this occurs, charge can be collected from depths along the charge track significantly deeper than would otherwise be possible. Funneling can be an important contributor to charge collection for some devices.

If sufficient charge is collected at a sensitive junction, a variety of single-event effects can occur, with consequences ranging from trivial to catastrophic. Single-event effects that can result in potentially catastrophic failures include Single-Event Latchup (SEL) in complimentary metal-oxide-semiconductor (CMOS), Single-Event Gate Rupture (SEGR) in power MOSFETs, Single-Event Burnout (SEB) in FETs and bipolar transistors, single particle-induced failures of linear bipolar devices, and so on. If the collected charge results in a stable logic change in the device (that is, a bit flip), the event is called a Single-Event Upset (SEU). Alternatively, if the device changes its output state temporarily, the event is called a Single-Event Transient (SET).

Generally, the variable of choice used to characterize SEE is Linear Energy Transfer (LET), which can be looked upon as the energy loss due to direct ionization of orbital electrons as particle passes through a medium (or an energy deposited per unit path length—dE/dx) normalized to the medium's density(ρ)—1/ρ*dE/dx (expressed, for example, in MeV*cm^2/mg) [Zieg-84]. Equivalently, LET can also be expressed as the charge generated per unit length of track (for example, pC/μm). In general, the higher a particle's LET—or, equivalently, the denser its charge track—the higher the probability that it will cause a given SEE in a susceptible device. As in nuclear physics, the probability of a given effect is expressed as a cross-section, with dimensions appropriate to the device (μm^2 or cm^2). In general, for ions with sufficiently high LET, a device's cross-section for a particular effect is related to the physical area on the device that is susceptible to the effect. However, the relationship is usually not a simple one.

In general, if a particle's LET is sufficiently low, it will not generate enough charge to cause SEEs and can be ignored in SEE prediction calculations. However, direct ionization—the creation of electron-hole pairs by ionizing radiation—is not the only means by which radiation can produce charge. It is also possible—although orders of magnitude less likely—that a particle can first interact with a nucleus in the semiconductor lattice. The charged products of this

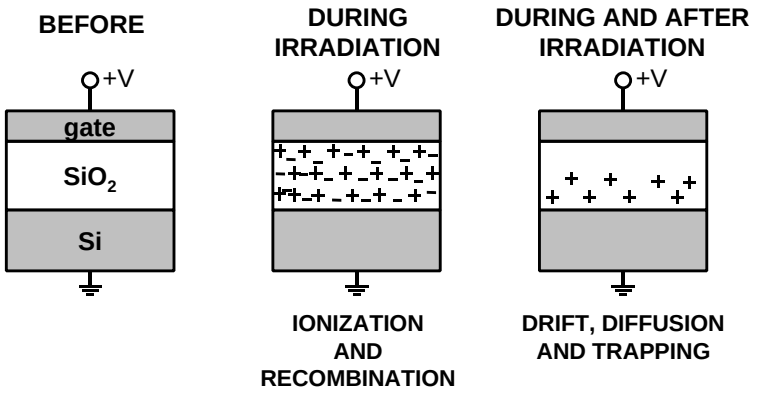

Figure 2.5: Simple model of generation and trapping of charge in an MOS device oxide. [Lera-99]

interaction can then generate electron-hole pairs in their own right. Because nuclear cross sections are so low, such indirect ionization is insignificant for most particles. Nevertheless, because protons are highly penetrating and several orders of magnitude more numerous than other ions, it is often necessary to take indirect ionization due to protons into account in SEE calculations. However, proton LETs are generally so low that proton direct ionization is negligible in SEE in microelectronics. For this reason, and because nuclear cross sections depend on proton energy rather than LET, the formalism for treating proton-induced SEEs has developed along different lines than has that for heavy-ion induced SEEs. This historical artifact has important consequences for the treatment of SEEs in photodetectors, where proton LET is not negligible. (Note: Neutrons are not treated here, however, they can also be important contributors to SEEs, particularly in aircraft avionics or for man-made radiation environments.)

Because optical based subsystems may contain any traditional electronics technology, it should be remembered that they could be susceptible to any of the above mentioned single-event effects. In addition, the optoelectronic components in these devices—particularly the detectors—may be susceptible to similar effects, especially SETs, which we will consider later.

2.2.2 Total Ionizing Dose Effects

As with single-event effects, damage from TID is caused by the electron-hole pairs generated by ionizing radiation passing through a material. These charges can gradually change the performance of an electronic component, with the level of change depending on the total ionizing energy absorbed—that is, on the TID [Dres-98, Lera-99, and references given in these]. Generally, TID changes the characteristics of the materials that make up a component, resulting in gradual parametric degradation and changes in functionality. In most cases, the basic cause of TID degradation is the trapping of charge in the medium. **Figure 2.5** illustrates a simple model of generation and trapping of charge in the dielectric of a MOS device with a positive bias applied to the gate. If enough charge is trapped in the oxide, the device's performance will change. Charge may also be trapped in the field oxide of a linear bipolar device and MOS devices. A third example would be charge trapping in an optical fiber which can results in darkening. This effect is much different than charge trapping in microelectronic device oxides where there are electric fields that separate charge—this topic will be discussed in more detail later.

2.2.3 Displacement Damage Dose Effects

The proper functioning of many devices depends critically on the semiconductor having a pristine crystalline lattice. However, this lattice can be damaged when an energetic particle, such as a neutron, electron, proton or heavy ion displaces one or more nuclei within the crystalline lattice, creating electrically active defects. As this damage to the crystalline lattice—called the displacement damage—increases, the device can degrade parametrically, and eventually stop functioning all together. In microelectronics DDD effects result from the bulk semiconductor material, while TID effects are due to the charge trapping in the dielectric materials used in components.

For the most part, because protons are penetrating, strongly interacting and abundant, the proton environment is predominant in considerations of DDD effects in shielded applications. However, for lightly shielded applications such as solar cells, low-energy electrons may also need to be considered [Dale-93a]. Moreover, for heavily shielded applications, secondary products can also be an important component of the environment. The 1999 NSREC Short Course [Mars-99] and segment II of this Short Course explores DDD effects.

2.3 Case Study: Environment Predictions for a Near-Earth Spacecraft

The primary science objective of the Guided Laser Altimeter System (GLAS) instrument is to obtain day and night, long-term ice-sheet topography measurements with sufficient spatial and temporal resolution to detect regional elevation changes. The GLAS instrument will be placed in a polar orbit over the Earth at an altitude of 600 kilometers. The altimetry subsystem of the instrument uses a high-powered laser and sophisticated optical receiver to detect the outgoing laser pulse and correlate it to return signal reflected from the Earth.

The radiation environment encountered by the microelectronics and photonics on GLAS is a combination of the primary space environment and a secondary environment. The secondary environment is produced when the primary environment interacts with spacecraft materials. For the most part, the primary environment dominates. Although this is true for most spaceflight missions, the use of heavy or composite shielding requires careful consideration of the secondary component of environment inside a spacecraft. An accurate description of the space environment for a specific mission can be crucial when developing an appropriate survivability test plan for microelectronic and photonic components.

This section of the Short Course describes the radiation environment for a spacecraft in a polar orbit at 600 km above Earth's surface. The description focuses on the environments that are important for most microelectronic and photonic devices. The minimum shielding considered is 50 mils of aluminum. By combining these environment predictions with accurate ground testing results, one can estimate the effects of space radiation on microelectronic and photonic components. This requires that validated models exist that allows one to correlate the measurements made using ground-based radiation sources to effects that will be observed in the complex space radiation environment.

2.3.1 SEE Environment

Single-event effects can occur via either direct or indirect ionization. Direct ionization is produced when a primary ionizing particle interacts directly with orbital electrons to free charge which separate in the presence of electric fields and segregates electrons and holes in the

semiconductor structures. The direct-ionization environment is most often characterized by the integral LET flux distributions.

Indirect ionization is a two-step process. First, a primary particle interacts with a nucleus in the semiconductor lattice, producing one or more recoiling ions. These recoiling ions then produce ionization in the medium. Because protons are by far the most numerous particles capable of producing nuclear interactions, the indirect ionization is described by the integral flux curves for protons as a function of energy.

The integral LET flux curves reflect the combined direct ionization effects for all particles (Z = 1 to 92) from all sources. The major sources are the GCR background environment and the environment resulting from solar particle events. **Figure 2.6** depicts eight curves showing the heavy ion (Z=1-92) LET spectra for these two sources (as computed by CREME96 [Tylk-96]), assuming different aluminum shielding thicknesses. The bottom four curves are the GCR background environment. Notice that shielding has little effect after the first few mils of equivalent aluminum.

The four top curves are for the worst case 5 minutes as modeled by the extremely severe October 1989 solar particle event. Notice that these particle fluxes are strongly dependent on shielding thickness. Because such large solar events are quite rare, these curves should only be used to determine the peak SEE rates.

Figure 2.7 shows the LET spectra for the trapped proton environment for four shielding thicknesses. Direct ionization effects from protons are rarely of concern for SEEs. However, as we will discuss later, for certain devices, direct ionization from protons can contribute significantly to the probability of SETs.

Figures 2.8 and **2.9** give the integral flux as a function of energy for the trapped protons and protons from solar particle events for four shielding thicknesses.

2.3.2 TID Environment

The total ionizing dose environment is a combination of several components of the naturally occurring space environment. **Figure 2.10** shows each component and the total for silicon. The total ionizing dose is simply a summation of all the components, with trapped electrons, bremstrahlung, trapped protons, and solar particle event protons being the main contributors.

2.3.3 DDD Environment

Segment II of this Short Course gives a description of the important issues to be considered when determining the DDD environment. We mention this effect here only for completeness. The major contributors to DDD when considering most applications of microelectronic and photonic components within satellite enclosures are the trapped and solar protons. **Figures 2.11** and **2.12** give the differential flux as a function of energy for the trapped protons and protons from solar events for four shielding thicknesses. The details of how to compute the DDD from these data are given in segment II of this Short Course and a Short Course given at the 99 IEEE NSREC [Mars-99].

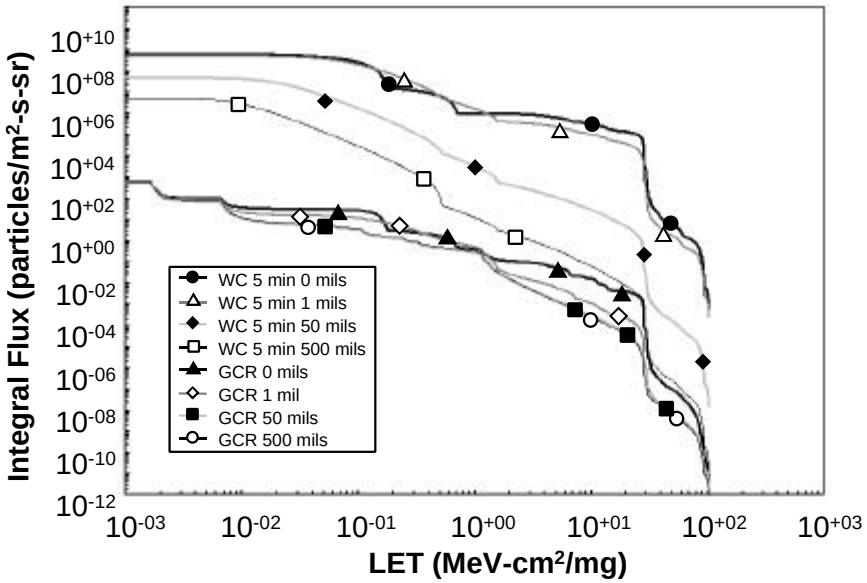

Figure 2.6: Integral LET heavy ion flux spectra for Z=1 to 92 at for a 600 km 99 degrees orbit for various shieldingthicknesess. Computed using the CREME96 codes. Values are given for galactic cosmic ray background levels and for levels modeled from the October 1989 solar particle event (5-min peaks). [Tylk-96]

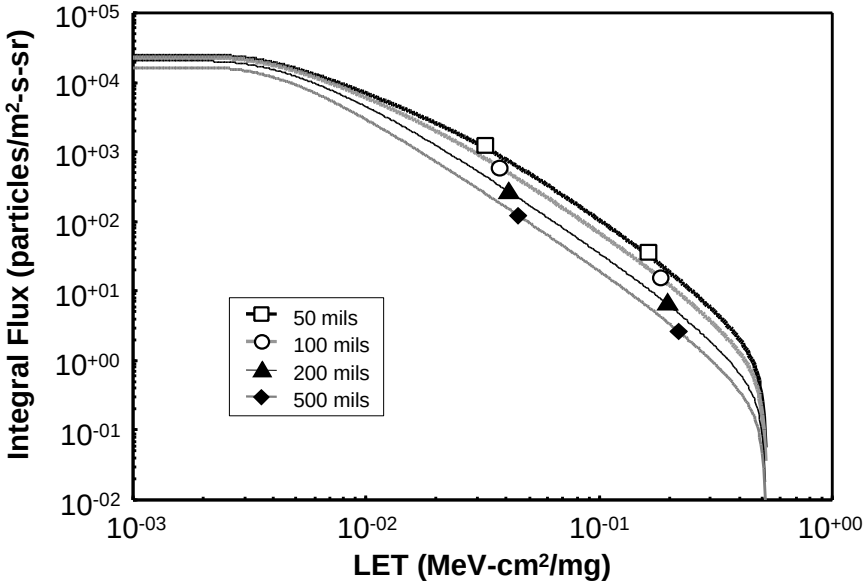

Figure 2.7: Integral LET flux for trapped protons in a 600 km 99 degrees orbit for various Al shielding thicknesses. [Bart-98]

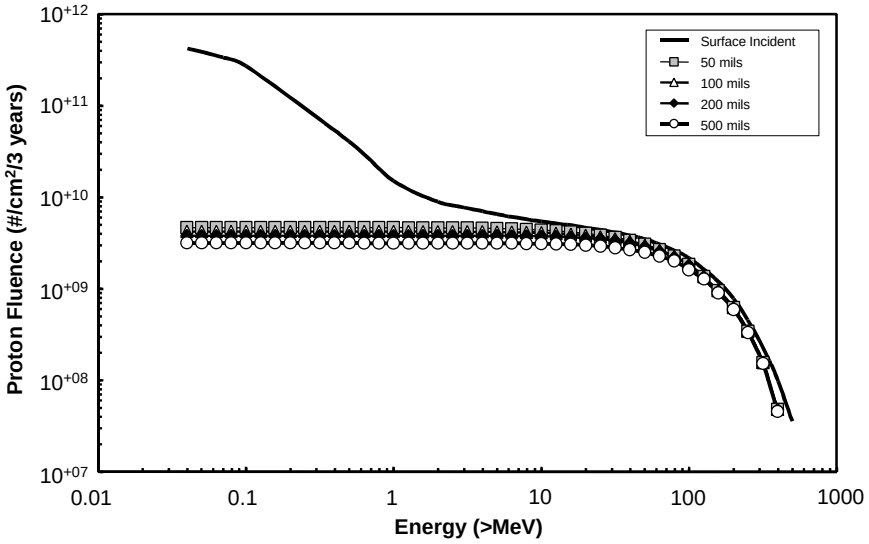

Figure 2.8: Orbit-integrated integral trapped proton fluence for three years in solar maximum for an orbit at altitude 600 km and an inclination of 99 degrees orbit for various Al shielding thicknesses. (AP-8 model with NOAA-PRO correction). [Bart-98]

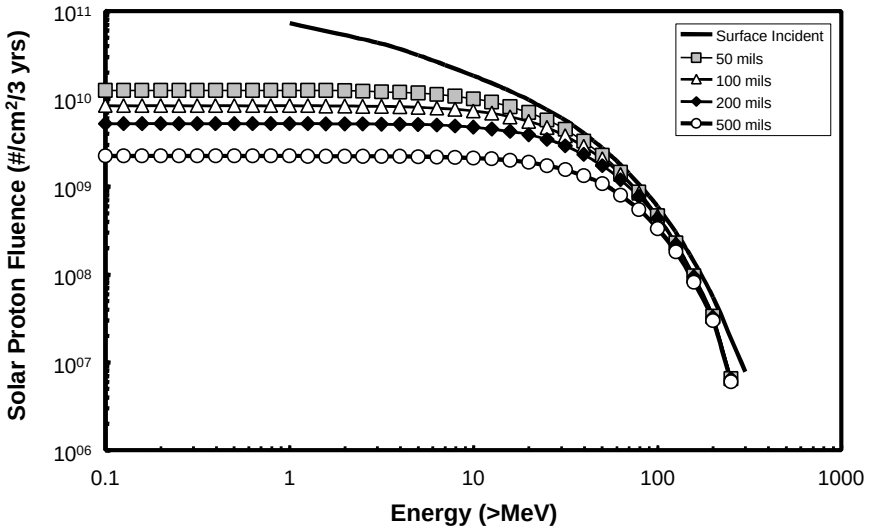

Figure 2.9: Orbit-integrated integral solar proton fluence for three years (95% confidence level) in solar maximum for an orbit at altitude 600 km and an inclination of 99 degrees orbit for various Al shielding thicknesses. [Bart-98]

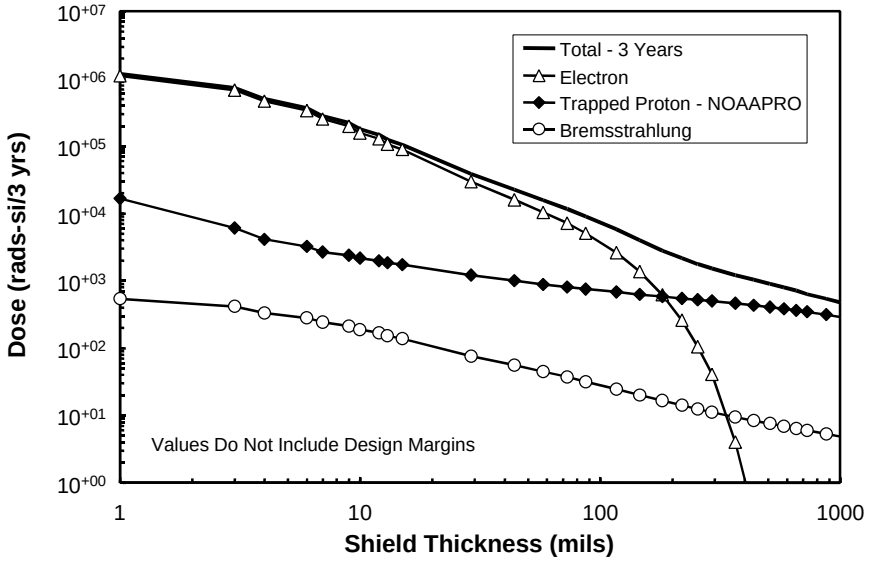

Figure 2.10: Total ionizing dose and contributions for important components thereof are shown as a function of equivalent solid-sphere Al shielding thickness. Orbit altitude of 600 km at an inclination of 99 degrees. [Bart-98]

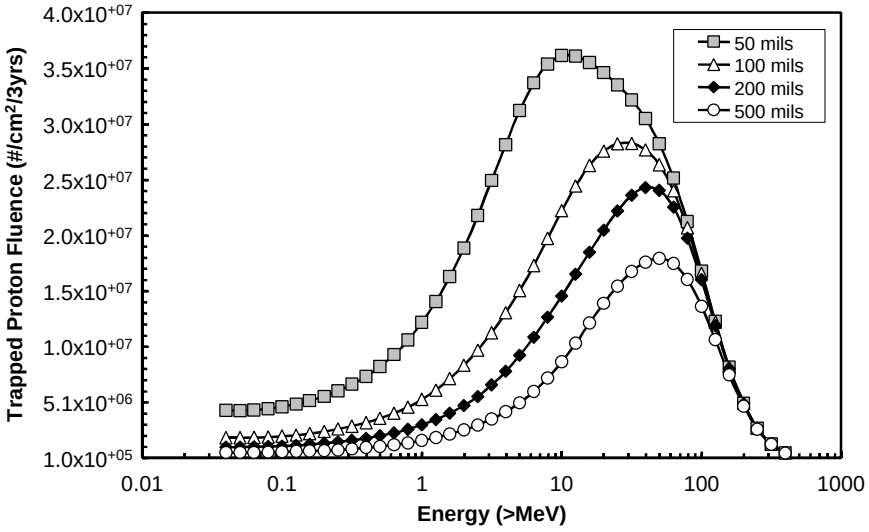

Figure 2.11: Orbit-integrated differential trapped proton fluence as a function of energy for three years in solar maximum for a 600 km 99 degrees orbit for various Al shielding thicknesses. [Bart-98]

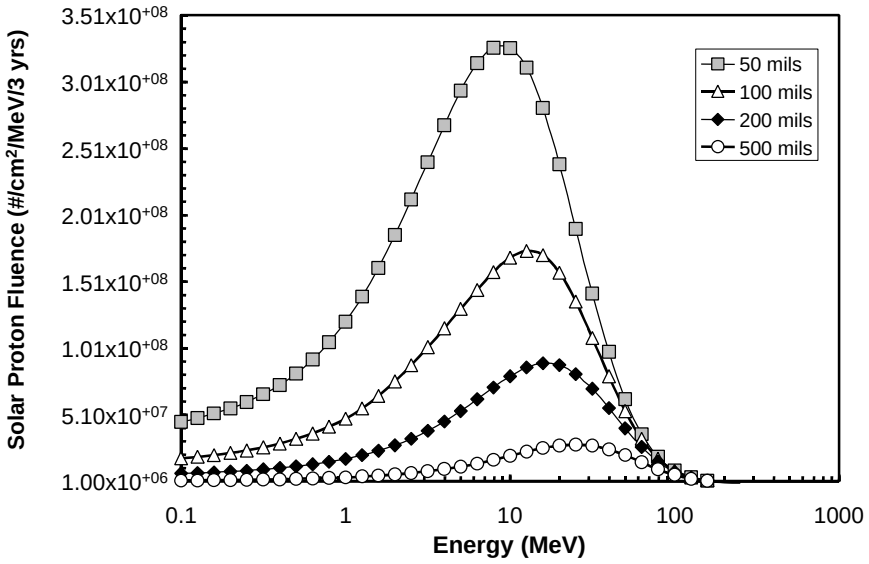

Figure 2.12: Orbit-integrated differential solar proton fluence for three years in solar maximum for a 600 km 99 degrees orbit for various Al shielding thicknesses. [Bart-98]

3.0 Intra-Satellite Digital Optical Data Links

In the search for high-bandwidth digital data transfer systems, spacecraft designers are considering high-speed digital optical links as an alternative to conventional systems. Designers must determine the best link for the mission based on performance metrics of each data link. This Short Course is intended to provide the designer with a clearer understanding of the radiation effects common in optical data links and how those effects affect link performance.

This section introduces digital optical links by giving a general description of optical data transfer systems with a brief overview of each component of the optical portion of a fiber-optic data link. We also discuss the optical system performance metrics that are important when characterizing performance degradation due to radiation exposure. Most of the material in this section represents a summary of the information gathered from these books [Agra-97, Pala-98, Lach-98].

3.1 Overview of the Digital Optical Data Link

Data links transmit large amounts of information at high data rates between spacecraft subsystems. Classically this is done via an electrical connection using standardized data link hardware, i.e., RS232 and MIL-STD 1553. Data transfer at rates in the MHz to GHz range can be achieved using optical data links, where optical fiber and its associated components take the place of wire and electrical components. Some of the advantages and disadvantages of optical links are listed **Table 3.1** [Bris-93, LaBe-98d]. A detailed comparison of optical versus electrical data links is beyond the scope of this Short Course. However, it is obvious from the list of advantages that, for many applications, optical links should be considered seriously.

Table 3.1: List of some of the advantages and disadvantages of digital fiber link systems.

Advantages	Disadvantages
Wide bandwidth	Potential cracking of fiber
Light weight	Limited fiber bending radius
Reduced complexity during spacecraft integration	Additional engineer expertise required to implement optical links
Immunity to electromagnetic interference	Fiber connectors are large
Elimination of cross talk	

Figure 3.1 shows a typical optical data link. Digital data flows from subsystem to subsystem via optical fiber. The support electronics condition the signal. Optoelectronics convert the signal between optical and electrical formats. In the next few sections, different network architectures will be discussed followed by a discussion of the optoelectronics portion of the network (a detailed discussion of each component will be given in section 3.2).

3.1.1 Network Architectures

The network architecture is the baseline for how each subsystem is connected to all the other subsystems on the network. Four popular topologies are illustrated in **Figure 3.2,** namely**,** 1) point-to-point, 2) linear-bus, 3) star-hub, and 4) ring. It is the bus protocol that determines which subsystem has control of the bus. The robustness of the bus to subsystem failure is defined by this protocol.

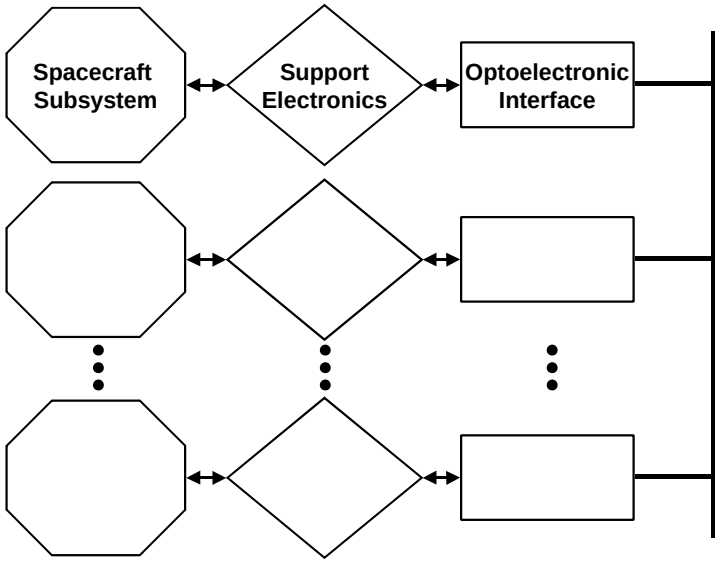

Figure 3.1: Block diagram of fiber-optic data transfer interface between spacecraft subsystems. Optical fiber is the physical medium used to connect each subsystem. Support electronics and an optoelectronic interface handle signal processing and translation of the signal between optical and electronic formats

In the point-to-point network (**Figure 3.2.A),** two subsystems are linked via a single optical fiber. Each subsystem can communicate only with its partner by means of a single optical fiber. To avoid the fiber being a single point failure, the system must use redundant data paths [DeRu-93].

In the linear bus network (**Figure 3.2.B)** the bus forms a backbone structure, with subsystems transmitting and receiving data as required. This network is very robust, in that the functionality of the network does not depend on each subsystem remaining functional. Again, unless the fiber backbone is made to be redundant it could be a potential single point failure of the entire network.

The star hub network's (**Figure 3.2.C)** transmission lines are brought together on the common hub. The receive lines are distributed out from the common hub. One disadvantage of the star hub is that the hub forms a single point failure. However this can be avoided, for example with a redundant second hub in the data path. Like the linear bus, the network functionality is independent of its subsystem's performance. For discussions on star-hub ad its bus protocol for spaceflight application see for example [Frit-94, Bone-96].

Finally, the ring network (**Figure 3.2.D)** subsystems form a continuous loop. When a message is transmitted from a subsystem it must be passed by all subsystems in the ring between the sending subsystem and the receiving subsystem. This simple implementation of the ring network is not as robust as the star hub or the linear bus, in that if one of its subsystems fail the entire network will stop functioning. However, [DeRu-93, Bris-93] discuss a spaceflight hardware application of cross-strapping and bypassing approach that remains functional even if a subsystem failure occurs.

The optical power that is required to support the data link is one of the major factors in determining which network topology to use in a spacecraft design. For example comparing the

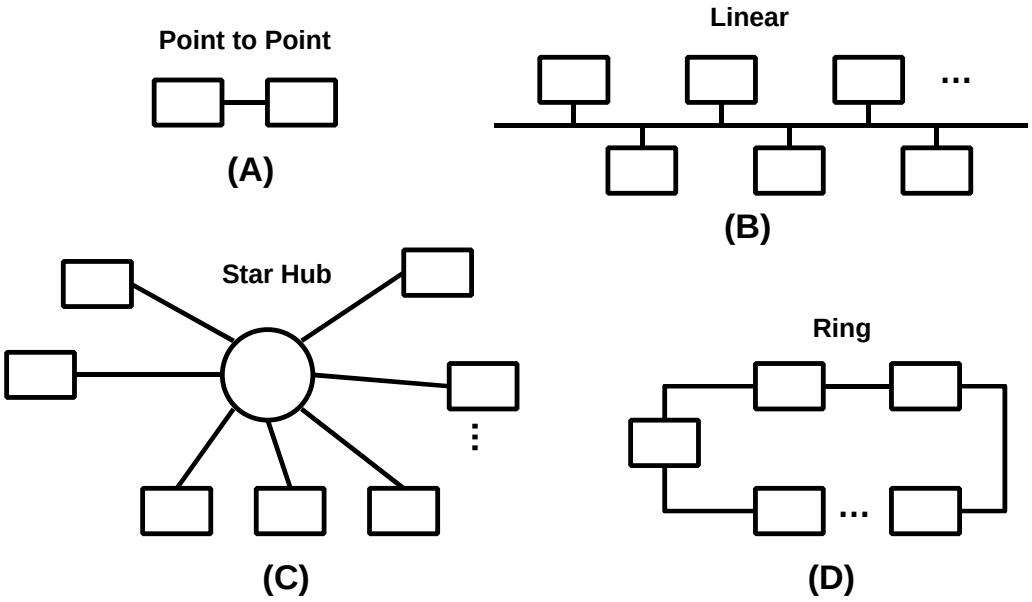

Figure 3.2: Four common network topologies.

last three networks in **Figure 3.2**, the ring and the star hub have inherently lower optical power loss, because the signal passes from subsystem to subsystem [Agra-97]. In the case of the star hub, the power at the receiver decreases linearly with the number of subsystems on the hub. In contrast, the power reaching a specific subsystem in a linear bus configuration decreases exponentially with the number of subsystem between the transmitting subsystem and the receiving subsystem. As we will see later, there is a relationship between radiation exposure degradation of network optical power and data link performance.

3.1.2 Point to Point Digital Optical Data Link

Figure 3.3 is a cartoon of two subsystems connected via an optical data link. The digital data is passed from the subsystem A to the transmitter, through an optical medium, then to the receiver, and finally to the electronics of subsystem B.

The transmitter's function is to convert the electrical signal into an optical format and send the optical signal onto the fiber. **Figure 3.4** gives a block diagram of an optical transmitter.

The light-source's output power is an important parameter. Usually its magnitude is expressed in units of dBm—where the unit optical output power is 1 mW. In general, to convert from power in mW to power in dBm, use:

$$\text{Power (dBm)} = 10 \log_{10}\left(\frac{\text{Power}}{1\ \text{mW}}\right), \qquad \text{(Eq 3.1)}$$

So a 0 dBm source is a 1 mW source. Power loss is defined as the difference between two values, for example power loss in a point to point link is the difference between the sent and received power in dBm. The units for power loss are dB.

The role of optical fiber is to transfer the optical signal from the transmitter to the receiver. The goal is to select fiber that minimizes signal distortion. Signal distortion via loss and dispersion of the optical signal due to optical fiber are important considerations when selecting the optical fiber.

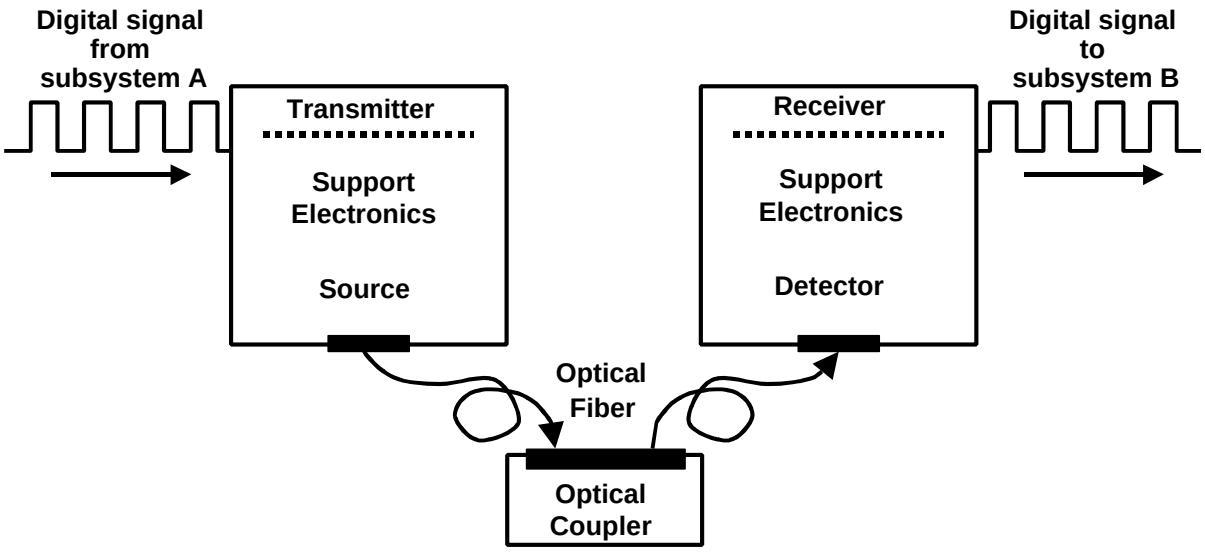

Figure 3.3: Block diagram of simple a point to point architecture. Data flow is from left to right.

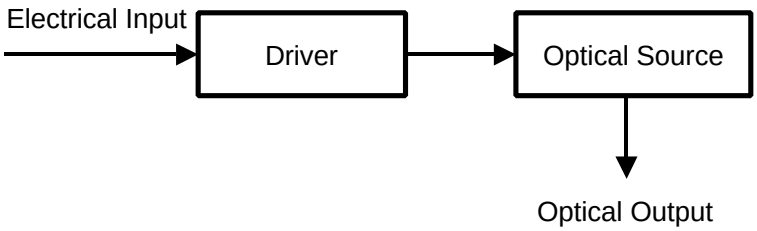

Figure 3.4: Block diagram of an optical transmitter

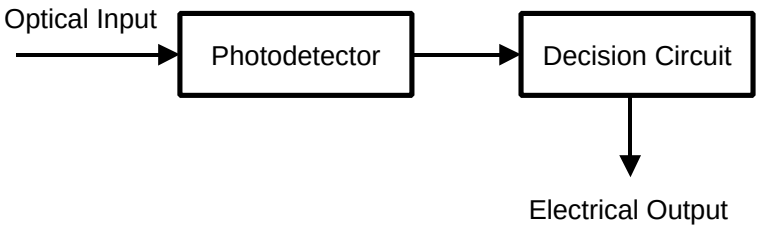

Figure 3.5: Block diagram showing the functions of an optical receiver

The optical receiver's purpose is to convert the optical signal launched by the output end of the optical fiber back into an electrical signal. **Figure 3.5** shows a block diagram of an optical receiver. The optical signal is detected by the photodetector, its output current is related to the intensity of the optical signal. The decision circuitry identifies the value of the data bit by comparing the photodetector's output level to a reference.

In some data link designs, a large number of microelectronic devices support the transmitter and receiver sides of the data link. These support electronics may include voltage level shifters, MUX, DeMUX, encoders, decoders, shift registers, phase lock loops, clock recovery circuitry, protocol chips, and a host of other devices.

Section 3.2 describes in more detail some of the components that form the optical link. We will focus on the key components that are specific to optical data links. (Section 4 will discuss the radiation effects concerns for these components.)

3.2 Brief Description of Digital Optical Data Link Components

The previous section gave an overview of the optical data link. In this section we will focus on the components that make up such a link. The discussion is confined to components that are unique to optical data links—that is, to light sources, optical fiber and other passive components, and receivers (emphasis on photodetector portion). Support electronics will not be discussed in detail.

3.2.1 Optical Digital Transmitter

In this section we review transmitters used in fiber-optic data links. Transmitters contain a drive circuit and a source, as shown in **Figure 3.4**. Typically, Light-Emitting Diodes (LEDs) and laser diodes are used as light sources. The driver converts the input electrical signal to a current. Source modulation is achieved by varying the injection current. (Although it is also possible to modulate the light output directly, this is not as common as injection current modulation.) Sometimes, a lens (not shown) is used to couple the output light to the optical fiber. Optical sources will be described in more detail below. Segment II of the Short Course will give details of source operation, along with a detailed discussion of the radiation effects mechanisms for these devices. Most texts on fiber-optic communications [for example Agra-97, Pala-98, Lach-98] give a detailed discussion of optical sources.

Semiconductor light sources, either LEDs or laser diodes, are used as sources for fiber-optic data links. These devices are quite suitable for use in fiber-based links in terms of their size, range of wavelengths, and power consumption. Sources are classified as long-wavelength or short-wavelength sources. Short-wavelength sources operate in the range of 500-1000 nm, and are typically fabricated with a ternary blend of semiconductors, e.g., GaAlAs. Long-wavelength sources produce light from 1200-1600 nm and are typically fabricated with quaternary semiconductors such as InGaAsP. The light emitting region is a well confined forward biased p-n junction or heterojunction in the semiconductor. Vertical Cavity Surface Emitting Lasers (VCSELs) can be fabricated close together which provides the ability to fabricate a high throughput parallel link (see Section 6).

3.2.1.1 Semiconductor Light Emission and the Resulting Wavelength

Forward biasing a p-n junction causes holes to be injected into the n-doped region and electrons to be injected into the p-doped region. These injected minority carriers recombine with the majority carriers, releasing energy, either as a photon electromagnetic radiation (radiative

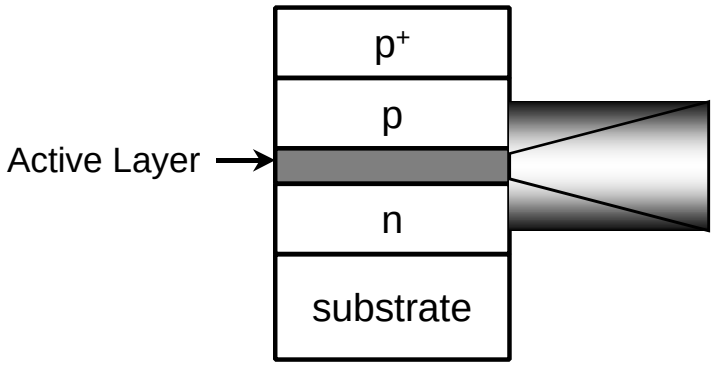

Figure 3.6: Cross section of a light-emitting device. Charge carrier and light confinement occurs in the active layer.

recombination) or as heat (nonradiative recombination). The internal quantum efficiency, η_{int}, is defined as the fraction of recombinations that are radiative.

LEDs emit light by a process called spontaneous emission—that is, each photon is emitted spontaneously with a random direction and polarization. Such light is also called incoherent. In contrast, laser diodes emit coherent light via a process called stimulated emission, in which a photon stimulates the recombining charge pair to emit a second photon with the same direction and polarization as the first.

As current carrier concentration increases, so does the radiative recombination efficiency. Therefore, it is desirable to confine current flow to the active region in a light emitting device (see **Figure 3.6)**. Double heterojunction structure devices are fabricated so that electrons injected into the active region from the n-type region will see the p-type region as an energy barrier. Likewise, holes injected into the active region face an energy barrier from the n-type region. Another feature of the double heterojunction diode is that the different indices of refraction confine the light to the active region, thereby reducing absorption of light in the semiconductor and increasing the output power of the diode.

During radiative recombination, the photon energy is equal to the band-gap energy (E_g) of the semiconductor. It will have a wavelength (λ) defined by :

$$\lambda = \frac{hc}{E_g}, \qquad \text{(Eq 3.2)}$$

h is Planck's constant (6.63×10^{-34} joules sec) and c is the speed of light.

3.2.2 Passive Optical Components

Lenses, gratings, couplers, fibers and other passive optical devices are utilized in building fiber-optic data links. Here we focus our discussion on fiber optic waveguides. To understand how fiber-optic waveguides confine light to a long glass strand, it is useful to review some basic optics. Scattering of light propagating in a medium, other than a vacuum results, in the light travelling less than the speed of light. This allows us to define a medium's refractive index as:

$$n = \frac{c}{v}, \qquad \text{(Eq. 3.3)}$$

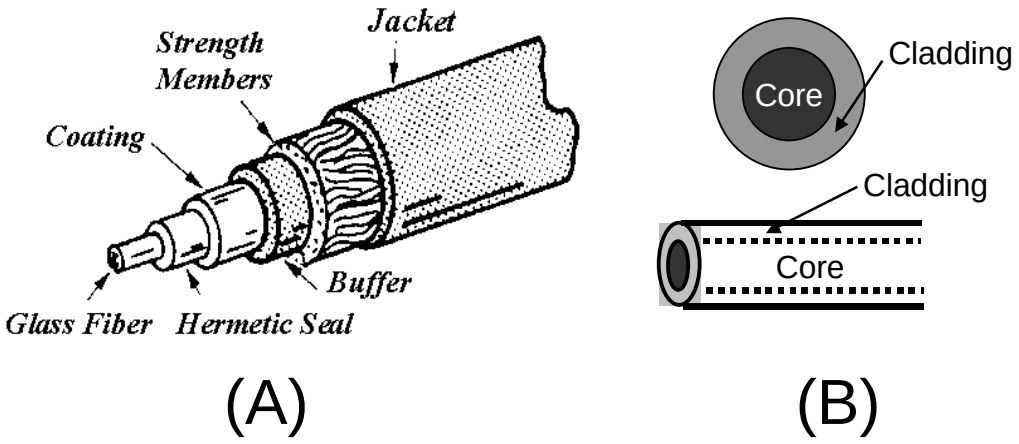

Figure 3.7: (A) Typical optical fiber housing. (B) Core and cladding configuration of a typical optical fiber. [Ott-97]

where c is the velocity of light in a vacuum and v is the velocity of light in the medium. When light passes from one medium to another, its direction of propagation changes according to Snell's law. Snell's law also defines the maximum angle a light ray can make with the normal if it is to pass from a medium with a high refractive index, n_1, to a medium with a lower refractive index, n_2. (See segment II of this Short Course.) This critical angle is given by:

$$\mathrm{Sin}(\theta_c) = \frac{n_2}{n_1}, \qquad \text{(Eq. 3.4)}$$

Light incident at an angle greater than the critical angle will be totally internally reflected back into the first medium.

Optical fibers consist of an inner core with a high refractive index and an outer cladding with a lower refractive index. (See **Figure 3.7**) The optical signal is confined to the core of the fiber by total internal reflection.

Optical fiber can be fabricated with a variety of refractive-index profiles. Step-index fibers have an index of refraction that changes abruptly at the core-cladding interface (**Figure 3.8.A)**. Other fibers may have a triangular profile (**Figure 3.8.B),** or a graded-index profile, like that shown in **Figure 3.8.C**. Yet other fibers may have profiles with several discreet steps in refractive index.

Fibers are classified into two electromagnetic categories: single mode and multimode. The mode refers to the number of electromagnetic modes that exist in the fiber under certain conditions. Each electromagnetic mode in a fiber has its own unique electric and magnetic fields that are setup in the fiber. The mode also has a unique propagation constant.

Optical fiber can attenuate and distort the optical signal. The attenuation per unit length for a typical high-quality fiber is shown in **Figure 3.9.** Notice that there are two minima—located at near 1.3 and at 1.55μm, respectively. Optical fiber can also distort the optical signal through dispersion. One example of such distortion is pulse broadening—a widening of the pulse in the time domain as it travels down the fiber. For a more detailed discussion on optical fibers see almost any text on fiber-optic communications. [For example Agra-97, Pala-98, Lach-98.]

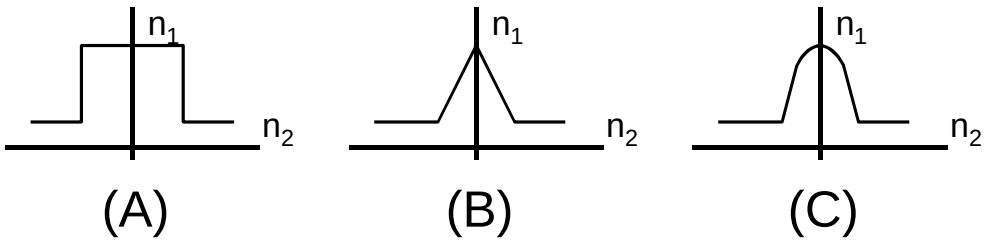

Figure 3.8: Three different profiles of optical-fiber index of refraction. The subscripts (1 and 2) refer to the core and cladding, respectively. [Adapted from Agra-97]

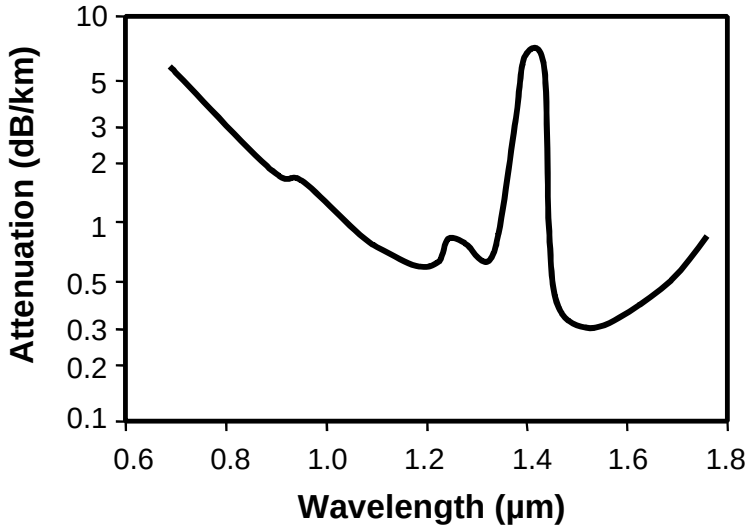

Figure 3.9: Fiber-induced attenuation for various wavelengths. Two minima occur near 1.2 and 1.5 μm, respectively. [Adapted from Miya-79]

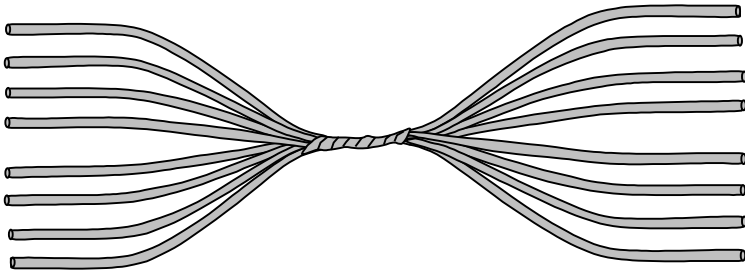

Figure 3.10: Fused biconical tapered star coupler. Optical power sent from one end of the star will be distributed equally over all outputs at the other end of the star. [Adapted from Agra-97].

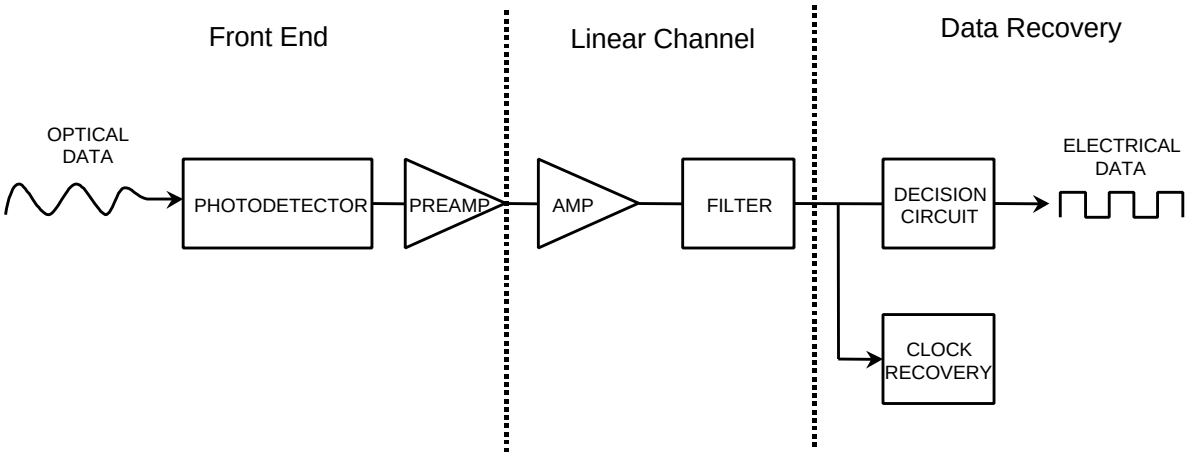

Figure 3.11: Block diagram of an optical receiver. Vertical dashed lines separate the receiver into three groups (see text). [Adapted from Agra-97]

Often fiber is used to form a coupler between data link subsystems. A star coupler can be formed by using a fused biconical-tapering method, see **Figure 3.10**. The role of the star coupler is to combine the optical signals entering from its multiple inputs and distribute the signals equally among its outputs. The input power from all input channels is divided equally among the all output channels. . Typical operation in an optical network utilizes a protocol controller that allows only one transmitting node at any given time. For example, an N x M star coupler has N inputs and M outputs.

3.2.3 Receivers

An optical receiver is a combination of an optical detector, amplifiers, and electronic processing elements used to recover the signal sent from the source. **Figure 3.11** gives a detailed block diagram of a typical optical receiver [Agra-97]. The receiver is made up of three stages: 1) front end, 2) linear channel, and 3) data recovery. We will first give a discussion of the each section of the receiver and then briefly describe photodetectors. Further information may be found in many optical communication texts books. (For example [Agra-97, Pala-98, Lach-98].)

3.2.3.1 Stages of a Receiver

The front end of the receiver contains the photodetector and the preamplifier. The photodetector converts the optical signal to an electrical signal. This signal is very weak and therefore it must be amplified via a preamplifier. A trade off exists between bandwidth and sensitivity of the photodetector-preamplifier pair. Although a high resistive loading across the photodetector increases its sensitivity, this loading also slows the response of the circuit. An equalizer is sometimes added to the circuit to attenuate the low-frequency components of the signal more than the high-frequency components—in effect increasing the bandwidth of the circuit. The most common method used to keep the bandwidth high while maintaining the desired sensitivity level is to use a transimpedance amplifier. Basically, in a transimpedance amplifier application, the load resistor is placed as a feedback resistor around the preamplifier rather than as a load across the photodetector. This results in more amplifier gain with little

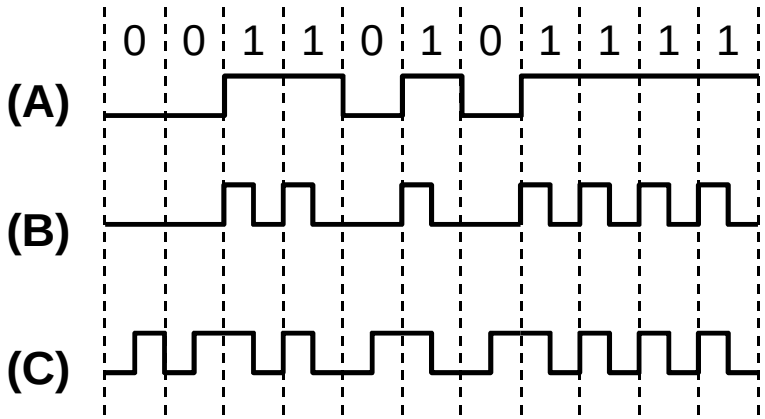

Figure 3.12: Examples of NRZ (A), RZ (B) and Manchester encoded (C) data sequences.

impact on circuit bandwidth. However, stability can be difficult to achieve when using transimpedance amplifiers.

The front end is followed by the linear channel, which consists of a high-gain amplifier and a low-pass filter. The amplifier boosts the electrical signal even more. Sometimes such amplifiers use an automatic gain control mechanism that self-adjusts the gain based on the input signal. The goal here is to limit the average output voltage level regardless of average incident optical power. The low-pass filter shapes the voltage pulse and removes unwanted frequency components generated by signal processing.

The last stage of the receiver is the data recovery portion. In this stage of the receiver, the clock and data are recovered. Transmitters can be designed to encode the clock signal into the data. The clock signal is regenerated using the clock recovery circuitry. Another method of clock recovery is to simply pass the clock signal to the receiver.

The decision circuitry is used to recover the data. It compares the output of the linear channel to a threshold level. If the signal level is above the threshold, it is considered a "1". If the signal is less than the threshold, then it is a "0". The data sampling frequency and sampling duration are determined by the clock frequency. As will be seen later in this tutorial, the radiation sensitivity of the receiver depends strongly on the clock frequency, the sample window width, the delay between data edge and the decision window location within the bit period, and the time relative to the decision window when the radiation event occurred.

3.2.3.2 Digital Data Coding

Some fiber-optic data links utilize encoding schemes to encode the clock in the data sequence, others encode the data for error checking and correcting. Here we describe four types of common encoding schemes. Three are depicted in **Figure 3.12**.

The NonReturn-to-Zero (NRZ) code does not necessarily return to "0" during each data bit, see **Figure 3.12.A**. A sequence on "1s" will hold the data stream high until a "0" is transmitted. This code does not support clock encoding. This code requires less bandwidth than the other two codes in this figure.

The Return-to-Zero (RZ) code does necessarily return to "0" during each data bit, see **Figure 3.12.B**. One example of an RZ code is when the first half of the bit period is coded with the data

bit information, while the last half is coded with a "0". This code does not support clock encoding.

The Manchester code is a RZ code (**Figure 3.12.C).** The signal makes a transition at the center of the bit period, upward for a "0" and downward for a "1." In Manchester coding, the clock is encoded by the center bit transition.

The final data encoding scheme is called 8B10B [Widm-87, Cart-97]. Where 8 bits data sequence is encoded into 10 bit long data sequence. In essence this encoding scheme allows for clock and subsequence recover. The clock is encoded via the minimum number of bit transitions in the 10 bit encoded sequence, the data is encoded via a check technique called disparity. Disparity is the cumulative difference in the number of one's and zero's, disparity for a 10 bit encoded sequence never exceeds ± 1.

3.2.3.3 Receiver Noise and Decision Circuitry

Although the concept of distinguishing a "1" from a "0" seems straightforward at first glance, the presence of noise in the receiver circuit causes some data bits to be interpreted incorrectly. At the frequencies with which we are concerned, there are two inherent sources of noise: shot noise and thermal noise.

Shot noise results from the random nature of charge generation. Although, in general, a particular incident optical power corresponds to a particular average number of photogenerated electron-hole pairs, the actual charge distribution generated in a particular event will vary in time, space, and number. These variations are responsible for introducing shot current into the receiver. When considering shot noise one must include the effects from all components of the receiver.

Thermally generated noise is an intrinsic property of any conductor. Random thermal motion of electrons in some of the front end components of the optical receiver result in the largest current fluctuations. These current fluctuations are called thermal noise.

The total current is the sum of all current sources—photogeneration, shot-noise current, and thermal-noise current, as well as any other current sources in the receiver. The sum of these currents is interpreted as the data signal. If a significant amount of noise exists, the data stream will have bit errors—incorrectly interpreted data. This will be revisited in Section 3.3.

Figure 3.13 is a cartoon of the sampling of a certain data bit (A) in a bit sequence and the distribution of the signal level (B) measured at the sample point over the entire bit sequence. Sampling of the low data bit over the bit sequence will result in a fluctuation, or distribution, of the sampled currents that represent a "0". This distribution is shown as the lower Gaussian distribution in **Figure 3.13.B**, where (i_0) indicates the current value that is most likely to occur. Likewise for the high "1" data bits where the most frequently occurring value is (i_1) peak. The decision circuitry compares each sampled data bit to the threshold value (i_{th}). If the measured value is less than the threshold then it is considered to be a "0", if it is greater than i_{th} then it considered to be a "1". Notice that there is a finite probability (hatched area) that a data bit will be incorrectly interpreted.

3.2.3.4 Photodiodes

This section presents a brief description of photodiodes. For a more detailed discussion on photodetectors see most any semiconductor device physics textbook.

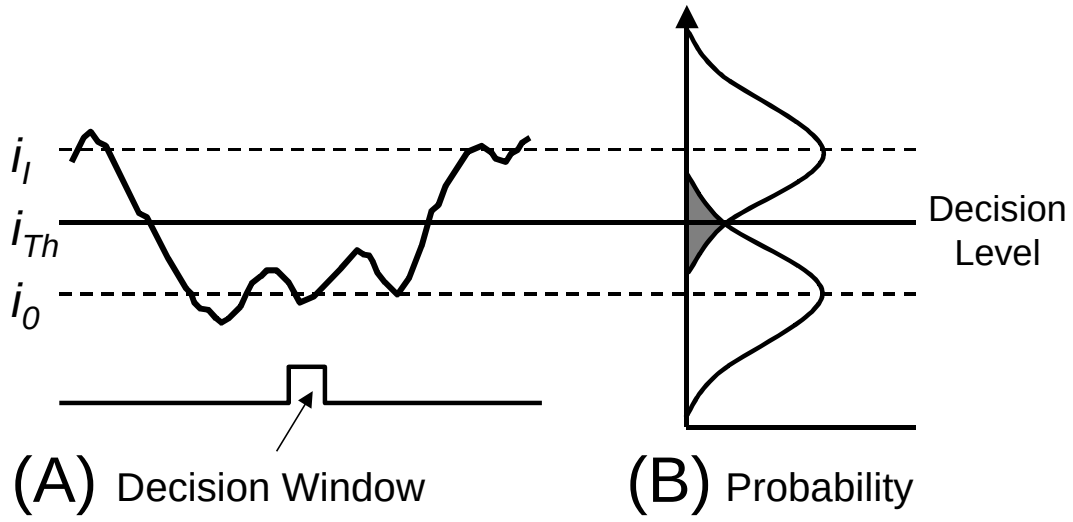

Figure 3.13: (A) Decision circuitry sampling a fluctuating signal from the detector. (B) Gaussian probability distributions of sampled signals. [Adapted from Mars-94a]

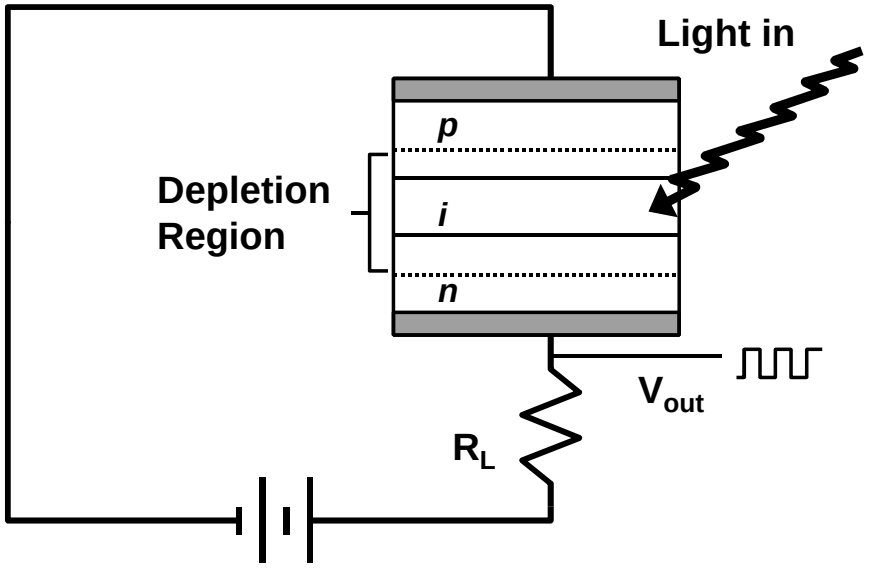

Figure 3.14: Simplified schematic of a p-i-n photodiode used to detect a light signal and convert it into a digital electrical data stream. R_L is the photodiode loading. The output level (V_{out}) depends on the incident optical power. [Adapted from Agra-97]

Typically, if not always, photodiodes are chosen as the photodetector in high-speed fiber-optical data links. Three types of photodiodes used in fiber-optics are p-n photodiode, p-i-n photodiodes (most commonly used), and avalanche photodiodes (APD)—there are others. The first and last are less likely to be used than the p-i-n diode.

The conversion of optical power into an electrical current can be understood by reviewing **Figure 3.14**. The p-i-n photodiode is operated in a reverse bias circuit. The incident light must penetrate to the depletion layer (a region in the diode that has a high electric field due to both the applied voltage and the semiconductor doping concentrations). If the energy of the incident photons exceeds the bandgap energy of the semiconductor (E_g), an electron-hole pair is created. The electric field in the depletion region drives the electrons towards the n-region and the holes towards the p-region. This current is called the photocurrent, and is proportional to the incident optical power. Whether the logic output of the detector is interpreted as a "1" or a "0" is determined by the incident optical power. The proportionality constant between the photocurrent and the incident optical power is called the responsivity. The responsivity depends on the photodiode material and design, as well as the wavelength of the incident light.

A maximum cutoff wavelength (λ) can be determined based on the fact that the band-gap energy (E_g) is the minimum energy needed to create electron-hole pairs. It is given by:

$$\lambda_{max} = \frac{hc}{E_g}, \qquad \text{(Eq. 3.5)}$$

where h is again Planck's constant and c is the speed of light. If the wavelength exceeds this value, the photon is not absorbed and no photocurrent is generated. **Table 3.2** lists some representative photodiode materials and their maximum wavelengths that can be detected. Often short-wavelength photodiodes are fabricated using Si, while long-wavelength applications use InGaAs alloys.

Table 3.2 Approximate cutoff wavelengths for various photodiode materials.

Material	**Wavelength (μm)**
GaAs	0.9
Ge	1.8
InGaAs*	1.0 to 1.7
InP	1.0
Si	1.2

*typical values depending on specific alloy.

A p-i-n diode is fabricated with a large intrinsic semiconductor layer between the p and n-regions—in effect increasing the width of the depletion layer and giving a large region for photon absorption. Because of the high resistance of this intrinsic layer most of the voltage drop occurs across it, and most of the charge that contributes to the signal is generated inside the intrinsic layer. The width of the intrinsic layer determines the how efficient the diode is at converting optical power to current. That is, the diode's responsivity depends on the intrinsic layer thickness. However, the response time of the photodiode increases with increasing intrinsic layer thickness.

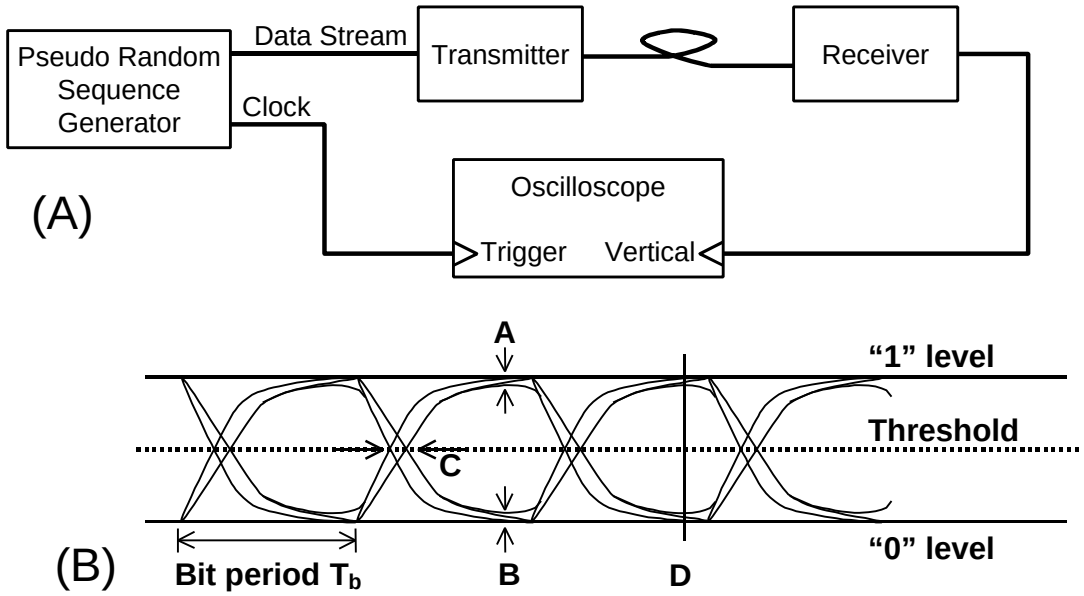

Figure 3.15: (A) Experimental setup used to measure an eye diagram (see text). (B) Representation of an eye diagram. [Adapted from Agra-97]

Indirect bandgap semiconductors, such as Si and Ge require relatively thick intrinsic layers—typically on the order of 20-50 μm. The response times of these devices are > 200ps. In contrast, using direct bandgap semiconductors like InGaAs allows much thinner intrinsic layers (3-5 μm), so these devices will have much faster response times (<50 ps).

A final note: The creation of electron-hole pairs in the photodiode by the high-energy particles found in the space radiation environment can dominate the performance of a photodiode, and in turn the performance of the data link. This topic will be explored in more detail in the sections that follow.

3.2.4 Support Electronics

Most optical data links require support electronics to format the data signal for optical communication. Some examples are buffering, encoding, decoding, voltage level shifting, digital data handing, temperature compensation circuitry, clock recovery circuitry (e.g., phase locked loops), and others. To implement these functions, links may contain MUX, DeMUX, ASICs, RAMs, PROMs, protocol chips, oscillators, and many combinations of the host of linear, digital and passive microelectronics and components. A detailed discussion of the radiation effects of these components is beyond the scope. However, the reader should be warned that radiation effects in the support electronics can dominate the response of the data link, we will give some of the general concerns in Section 4 and some examples of link performance limitations due to radiation degradation of support electronics in Section 5.

3.3 Digital Optical Data Link Performance Metrics

Optical data link operation can be degraded in a high radiation environment. Certain performance metrics can be used to measure the extent of this degradation. These metrics include the optical power budget and the bit-error ratio. In the sections that follow we will

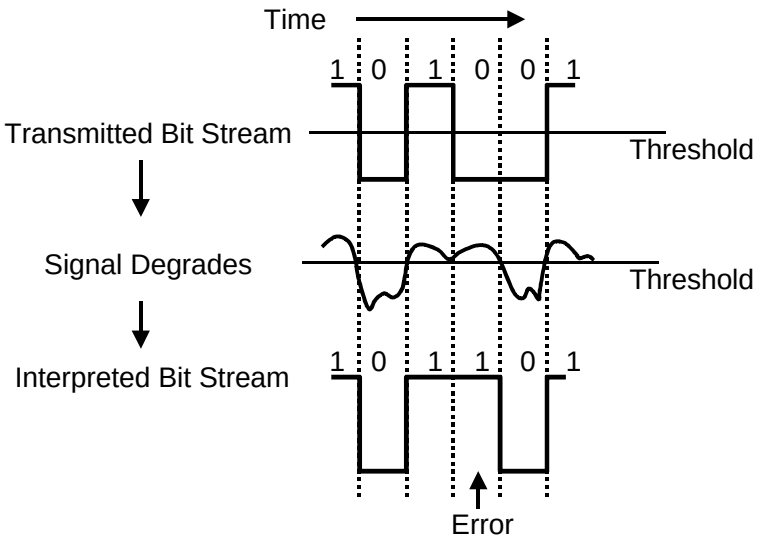

Figure 3.16. Cartoon of a specific bit sequence (101001) as it travels through a data link. The fourth bit in the sequence is interpreted incorrectly (101101). [Adapted from Powe-93]

discuss these metrics. However, first we will look at a measurement technique called eye diagram—a simple technique that results in an easily visualized metric for overall link performance.

3.3.1 Eye Diagram Measurements and Analysis

High-data-rate optical link performance can be measured using the eye-diagram technique [for example see Agra-97]. **Figure 3.15.A** shows a block diagram of the setup to make a time-domain measurement of the bit stream. The pseudorandom sequence generator outputs a repeatable and predictable, but random data-bit stream. The receiver output flows into the vertical trace of the oscilloscope, while the data clock activates the oscilloscope trigger. The result is an eye-shaped trace that represents superposition of several bit sequences, as represented in **Figure 3.15.B**.

The eye diagram contains easily observable information about the overall link performance. Some of its characteristics are:

- The opening of the "eye" gives the optimum sampling time interval for the received signal. The optimum sample time is where the eye is a maximum. In **Figure 3.15.B** this location is labeled "D."
- The voltage spacing labeled "A" is a measure of the noise when a logic "1" is transmitted. Likewise "B" is a measure of the noise when a logic "0" is transmitted.
- The time spacing labeled "C" gives a measure of timing accuracy of the data stream and is called the timing jitter.
- Increasing the frequency to the maximum operating frequency forces the eye to close.

3.3.2 Bit-Error Ratio

Data transfer by optical digital links (or any data link for that matter) can be corrupted by noise. **Figure 3.16** depicts a cartoon bit sequence as it propagates through a data link. The top line shows the "ideal" input signal. The second line shows the degraded signal after it passes through the electronics and optoelectronics. The degradation of the signal is the result of several sources of noise in the data path. The last line represents the signal as received and interpreted. Notice that the fourth bit in the data sequence has been interpreted incorrectly, resulting in a "bit error."

Depending on the operating frequency, several millions to billions of bits travel through a system every second. The probability of incorrectly interpreting a bit is a useful metric commonly known as the Bit Error Ratio (BER):

$$\text{BER} = \frac{\text{number of incorrectly transmitted bits}}{\text{total number of bits transmitted}}, \qquad \text{(Eq. 3.6)}$$

Sometimes this metric is also called the bit-error rate. (However, for the radiation effects community bit-error rate usually implies an on-orbit upset rate, we will use the more commonly accepted meaning for BER.) It can be measured using commercially available Bit Error Ratio Test (BERT) equipment. A general BERT setup will be described in Section 5.1.2.

The relationship between signal level, noise level and BER is fairly simple: the more margin that exists in a digital link, the lower the probability that a bit will be interpreted incorrectly. For a fixed receiver design, increasing the optical power launched on the photodiode lowers the BER until the optical power reaches the design limit of the receiver.

3.3.3 Optical Power Budget

When designing an optical data link, the designer must have a clear understanding of the power budget. There must be sufficient link margin to accommodate power losses as the signal passes through the link. The starting point for this analysis is the source's output optical power. The end point is the optical power that the photodiode requires to achieve the desired BER. The power budget must also consider the other losses in the digital link, including:

- source-to-fiber coupling loss at the transmitter,
- connector insertion loss,
- insertion losses in modulators, couplers, lenses, etc.
- fiber-to-receiver loss,
- aging effects, and
- fiber losses.

Figure 3.17, represents a graphical analysis of the power budget for an optical data link. In this example, the link will transmit data with an acceptable BER as long as the fiber length is less than approximately 2.5 km. To ensure proper operation of fiber-optic data links in space, power budget analyses must include radiation effects resulting from the space radiation environment.

This completes our summary of the optical digital data link, in the next section we will consider radiation effects at the component level, and in Section 5 we will discuss optical data link performance degradation in a radiation environment.

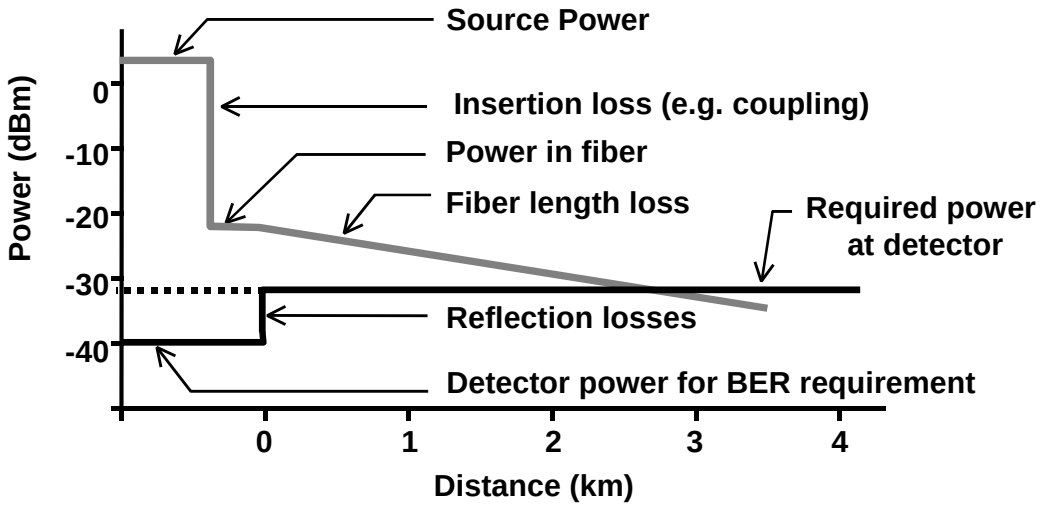

3.17. Graphical analysis of system power budget shows link margin as a function of fiber length. [Adapted from Powe-93] This type of analysis will be revisited when we consider degradation of optical link margin resulting from radiation effects.

4.0 Radiation Effects in Digital Optical Data Link Components

The last half of the previous section gave an overview of the basic components of a Digital Optical Data Link, as well as discussing some of the metrics used to measure the performance of these systems. In this section, we will briefly consider the radiation effects to which these components may be susceptible and how these effects may degrade component performance.

We will first briefly consider DDD effects in light sources—LEDs and laser diodes. This subject will be treated in more detail in segment II of the Short Course. Next we will consider the effects of TID on the passive transmission media used in fiber-optic data links. We will then examine the effects of TID, DDD and single-event transients in photodetectors. Lastly, we will briefly discuss radiation effects in the support electronics.

4.1 Permanent Degradation of Sources

As mentioned in the previous section, the role of light sources in digital optical link systems—usually LEDs and laser diodes—is to convert current signals into light. Because the drive signals for these devices are usually on the order of milliamperes, the small currents generated by ionizing radiation (usually picoamperes) are insufficient to cause SEEs. As such, for these devices, we are generally more concerned with permanent degradation due to DDD, TID is often a second order effect also [Barn-84, Barn-86, Mars-92].

Both LEDs and laser diodes produce light by means of radiative recombination of injected minority charge carriers with majority carriers in the depletion region. As such, any damage that decreases the efficiency of radiative recombination or introduces competing processes will degrade device performance. Irradiation by heavy particles such as protons and neutrons can displace nuclei from the crystalline lattice, causing DDD. These defects can serve as sites for nonradiative recombination, decreasing the efficiency of the light source [Barn-84]. DDD effects will be covered in detail in segment II of this Short Course. Here we merely note that displacement damage decreases the output power of these light sources, as well as increasing the threshold current for laser diodes (see **Figure 4.1**). We also note that with the exception of amphoterically doped LEDs, these devices can remain functional even after exposure to relatively high proton fluences ($>10^{12}$ protons/cm^2), provided the drive currents are sufficiently high to compensate for the effects of DDD. Characterization of light sources continues to be an active area of research, with substantial effort directed toward the study of damage mechanisms and annealing in LEDs and multi-quantum well laser diodes. (See, for example [Hinr-98, Zhao-98, John-99a, Lee-99].)

It is interesting to note that even when one early study observed degradation in the radiation response in optoelectronic systems and found loss of efficiency at relatively modest doses, the light source was vindicated upon further investigation [Mars-92]. It turned out that the degradation actually took place in a graded index lens coupling the laser to the fiber, rather than in the laser diode itself. This anecdote demonstrates not only that most light sources are remarkably hard to radiation, but that in contrast to the situation in microelectronics, in optoelectronics one cannot ignore radiation effects in the so-called passive media.

4.2 TID Degradation of Transmission Media

Although charged particles traversing an optical medium can generate photons, these processes are too weak and the path lengths traversed too short for these events to interfere with signals. For this reason, with respect to transmission media, we are generally more concerned

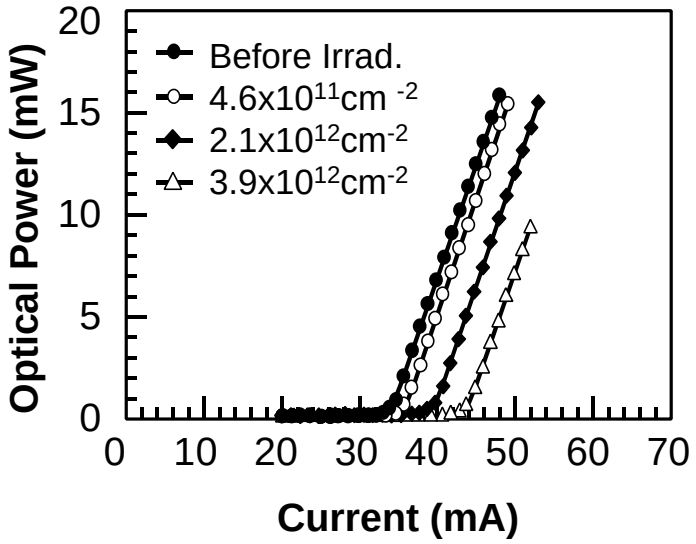

Figure 4.1 Displacement damage from 5.5 MeV proton irradiation increases laser diode's threshold currents and decreases the output power. [Adapted from Evan-93]

with permanent, cumulative degradation resulting from TID. We note in advance that for almost all space applications signal path lengths are relatively short (<75 m), so losses due to TID degradation can be accommodated by selection of rad-hard fibers and other relatively painless measures.

Photonic systems require nearly flawless optical fibers, lenses, and other transmission media to transmit light over long distances with minimal losses. Our discussion will concentrate on optical fibers, because they account for most of the pathlength traversed by the signal. It should be remembered that our treatment applies equally to lenses and other transmission media.

Ionizing radiation causes charge to become trapped by defects in the optical fiber, creating color centers that absorb light and decrease transmission efficiency. TID degradation in passive components should not be overlooked when analyzing the system power budget. For this reason, we will treat it in some detail. Readers who require additional detail are referred to the 1991 Short Course given by E.J. Friebele [Frie-91], the SPIE Photonics for Space Environments journals, as well as several excellent papers in Proceedings of RADECS and TNS [for example see Frie-85, Barn-90, Mars-94b, Gris-94, Hens-97].

As in microelectronics, the phenomenon responsible for TID induced performance degradation of optical fibers is charge trapping by defects in the material. These defects may be radiation-induced themselves, or they may be the result of impurities or fabrication conditions. Regardless of the defect origin, once the color centers form, light transmission efficiency is degraded as the color centers absorb signal photons. The degradation, however, need not be permanent. As is the case for trapped charge in microelectronics, fiber optic color centers can heal by annealing. The processes of formation and annealing of color centers take place in competition, and fiber-optic degradation depends on the relative rates of these mechanisms.

Even after two decades of study, not all of the processes involved in radiation-induced degradation and annealing are completely understood. However, the factors that affect the radiation response of optical fibers are sufficiently understood that the designer now has a good

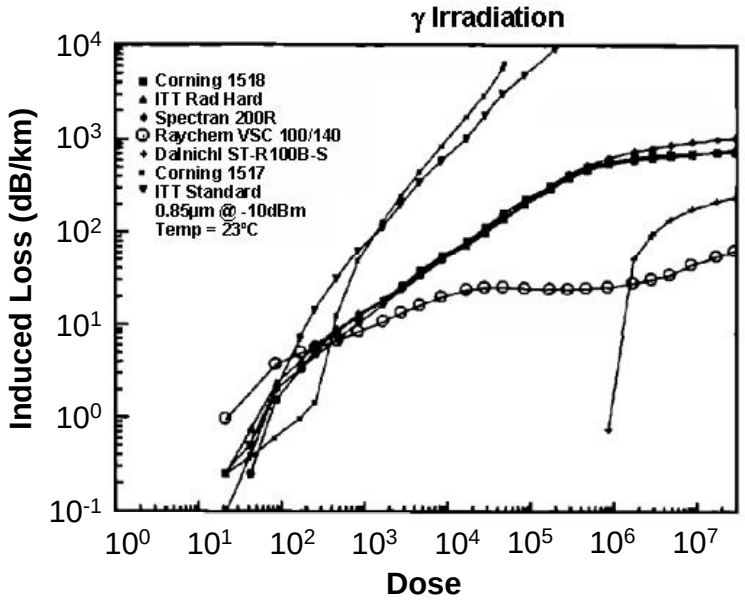

Figure 4.2 Phosphorus-doped, germanium-doped, and pure-silica optical fibers can show quite different susceptibilities to proton-induced attenuation loss. Dose rate is 4000 rads(Si)/minute. Measurement was in situ during the irradiation. The dose is given in rads(Si). [Adapted from Frie-91]

basis for both fiber selection and for formulating a hardness-assurance test program. Among the most important factors that influence both radiation response and annealing are the properties of the fiber itself, the temperature and optical conditions encountered in the application, and the radiation environment to which the fiber is exposed.

A quick glance at **Figure 4.2** is sufficient to indicate that radiation response of various optical fibers can vary widely. Attenuations after the relatively modest dose of 1 krad(Si) range from undetectable to around 100 dB/km. The annealing behavior of different fibers is every bit as variable. Much of the variation can be accounted for by the properties of the fibers themselves. Among the more important fiber properties that affect radiation response is fiber composition. As seen in **Figure 4.2**, pure silica fibers are less susceptible to radiation damage than are those with more complex compositions. However, optical fibers are usually fabricated with dopants to tailor refractive indices of the fiber core and clad to the desired application. Both germanium and phosphorus are commonly added to the core to raise its refractive index, while fluorine is used to lower the clad refractive index. Dopant choice can have important consequences for radiation hardness. In general, phosphorus seems to facilitate the formation of color centers that attenuate light signals, while germanium actually seems to improve some aspects of radiation performance. As might be expected, manufacturing conditions can also influence radiation and annealing response. The manner in which the fiber preform is deposited and under which the fiber is drawn are among the conditions found to correlate with radiation response.

The conditions encountered during the application can also influence requirements for the radiation performance of passive optical components. Annealing in optical media—as in microelectronics—is a thermally activated process. In one study, [Mars-94b] fits to activation

energies for various color-center traps have yielded activation energies on the order of 1 eV, or so, and trap lifetimes ranging from about a thousand to a few tens of thousands of seconds at room temperature. Moreover, studies have shown that the annealing rate of phosphorus-doped fibers does not increase with temperature. As such the temperature range encountered in the application can influence fiber choice as well as testing procedures.

Radiation damage can also be annealed by the light signal itself. This process, called photobleaching [Frie-84a], occurs when the light supplies enough energy to facilitate annealing in the fiber-optic. Even very modest signals can significantly alter the equilibrium between damage and annealing. In space, radiation damage and annealing take place as competing processes, with temperature and signal intensity playing crucial roles in determining the equilibrium point.

One of the most important application conditions in determining the effect of radiation on system performance is the signal wavelength. Most color centers have their peak absorption in the ultraviolet. The further away the source wavelength is from the absorption peak, the less will the signal be absorbed. Thus, systems that use InGaAsP laser diodes operating at 1300 nm or 1550 nm show slightly less signal loss due to radiation darkening than do those operating at shorter wavelengths.

The radiation environment must also be considered when evaluating potential degradation of transmission media. For applications where the transmission length is short (most spacecraft applications are less than 100 m), and where the light source can be driven hard enough to provide sufficient end-of-life margin, radiation-induced darkening of transmission media may be negligible for radiation levels less than 10^5 rad(Si).

The dose rate and the type of radiation also affect the extent of radiation damage. The annealing and photobleaching that compete with radiation damage give rise to an apparent dose-rate effect. To date, however, there is little evidence for true dose rate dependence in optical media, and most studies show good agreement between low-dose rate data and higher-rate tests followed by an anneal. In particular, work by Freibele et al. indicates that a shorter, high rate test coupled with annealing data may suffice to predict radiation behavior in the low-dose-rate, on-orbit environment.

The space radiation environment may include a broad range of radiation types. Because it is not practical to provide such a radiation mixture in the lab, most radiation test sources provide only one type of radiation (for example, 1.25 MeV γ rays from Co^{60}). Several studies have sought to show that, at the very least, such a simplification will not significantly underestimate radiation damage. To date, most studies have shown that equivalent absorbed doses cause roughly equal levels of damage, independent of radiation type [Frie-91]. As such, one can confidently assume that to first order, a rad is a rad, and data obtained with gamma rays can be used to bound the on-orbit behavior of the fiber. It should be noted, however, that different types of radiation might have different damage mechanisms. For example, protons, in addition to generating color centers, may also be captured within the medium forming SiOH, which absorbs strongly in the infrared [Lema-91]. Although these differences have not yet been seen to have any practical effect, care should be taken when using data taken under different conditions.

The preceding discussion is intended primarily to give a reader an indication of the broad variety of factors that affect the radiation performance of optical fibers. For a deeper discussion of these factors, the reader is referred to reference [Frie-91, Mars-94b] and the references contained therein. The reader can also review [Tayl-90, Tayl-91, Tayl-92, Hens-92,] for a discussion on radiation effects in different optical couplers (albeit for dose rates higher than

those encountered in the natural space environment.) Some graded index (GRIN) lenses have been shown to be especially sensitive to darkening via creation of color centers, although this is not an issue in most lenses [Frie-84, Weis-90, Mars-92].

In addition to using spacecraft structures as shielding to minimize radiation exposure, there are a number of techniques for minimizing the effects of radiation damage in optical media. Selecting an optical fiber with known and appropriate radiation response for the mission environment is a first step. It should also be remembered that radiation damage takes place in competition with thermally induced annealing and photobleaching. In most applications, the equilibrium level of radiation damage will be lower if the optical fibers are kept at a higher temperature. (Note that phosphorus-doped fiber optics are an exception [Frie-84, Frie-85].) Moreover, overdriving the light source, if feasible, not only facilitates photobleaching in some fibers, but also can compensate for any attenuation that takes place over time. Properly understanding the processes that contribute to darkening in optical media will ensure that these media are not the weak links in the optoelectronic system. Generally, darkening in well-chosen passive optical components can easily be accommodated in the link margin and does not limit the radiation of on-orbit optical data links.

4.3 Permanent Damage in Optical Detectors

The purpose of the detector in an optical system is to detect a weak optical signal and convert it into an electrical current that can then be amplified sufficiently to allow the resolution of individual data bits. Each of these steps—detection, conversion and amplification—is potentially vulnerable to radiation effects. Here we consider the effects of TID and DDD on the most common optical detectors [Barn-84, Wicz-86, Mars-92], while in the next section we will examine the potentially significant role of single-event transients in these devices. It will be seen that although radiation characteristics play an important role in determining which detectors are suitable for space applications, with proper choice of detector modules, permanent damage due to TID and DDD need not be a significant concern for most space applications.

Optical detectors in optoelectronic devices function by detecting the photocurrent generated by a photon with energy greater than the semiconductor band gap. For this reason, any damage to the semiconductor that changes its global properties, or that degrades the semiconductor's ability to carry a current will potentially compromise the detector's efficiency. Because DDD generates charge traps that significantly decrease minority carrier lifetime, minority-carrier photodetectors—such as phototransistors—are generally unsuitable in high-radiation environments. This is a prime reason why photodiodes predominate in high-radiation applications.

As TID accumulates, photodiodes, like all diodes, degrade, with leakage currents increasing up to several orders of magnitude for doses up to 1 Mrad(Si). Both TID and DDD increase background noise in photodiodes, and DDD tends to decrease receiver current outputs. However, many photodetectors show remarkable robustness to space radiation environments. **Figure 4.3** shows the number of years a typical InGaAs p-i-n photodiode would take to suffer a 3 dB responsivity loss for various circular orbits and behind various shielding thicknesses [Dale-92]. Often the key to success is incorporating adequate margin in source strength to account for EOL degradation in detectors. Segment II of the Short Course discusses DDD in photodetectors in more detail. A detailed discussion of predicting on-orbit performance degradation from ground based data is given in [Mars-94b, Mars-99].

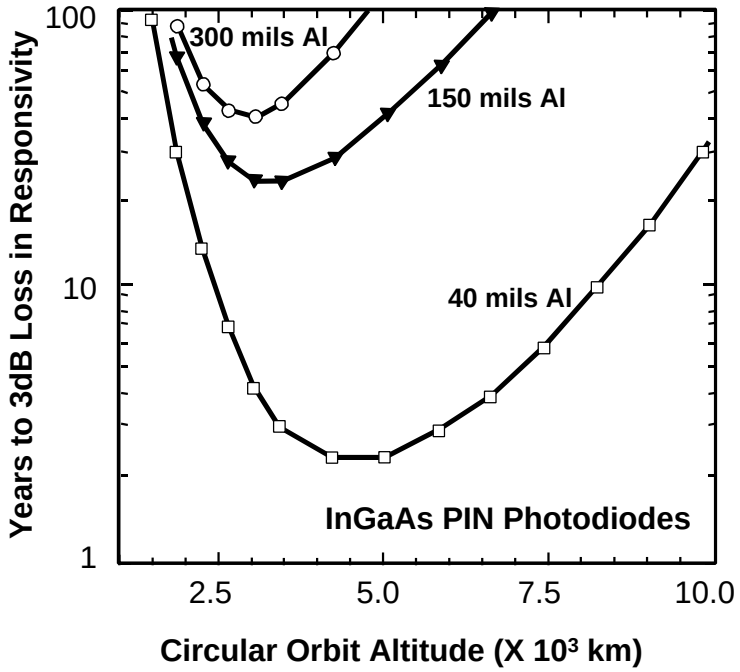

Figure 4.3 Equivalent Al shielding thickness can have a large effect in determining how long a photodetector can operate before the environment inflicts a particular damage level. [Adapted from Dale-92]

4.4 Single-Event Transients in Photodetectors

As outlined previously, photodetectors detect light signals by means of the photocurrents they generate in the semiconductor. However, these photocurrents can be indistinguishable from the single-event transients (SETs) generated by ionizing radiation. For this reason, SETs can combine with other sources of noise (particularly near EOL) to significantly increase the bit error ratio in high-radiation environments. Although the importance of these effects can vary widely from system to system, good receiver design and a robust protocol layer can significantly reduce BER [Mars-94b, Labe-96b, Jack-96, Dale-96].

Fortunately, the SEE susceptibilities of many photodetectors have already been characterized, and this work can be used to guide detector selection for high-radiation environments. Some devices are very susceptible to SETs, while others seem to be virtually immune to them. Indeed, recent work demonstrates that some detectors are even susceptible to proton-induced SETs caused by direct ionization [LaBe-93a, Mars-93a, Mars-93b, Mars-94a, Mars-96, LaBe-97, Reed-98, John-99b].

As discussed in section 2, protons can generate ionization by either direct means—in which the proton, itself generates the charge—or by indirect means—in which the products of a proton-nucleus collision generate the charge. If sufficient charge is generated and collected at a sensitive node in an electronic device, an SET or an SEU may result, see **Figure 4.4**. For most microelectronics, proton direct ionization generates far too little charge to be an SEE concern. The high sensitivity of some photodiode circuits, however, means that even proton direct ionization cannot be ignored by the SEU analyst.

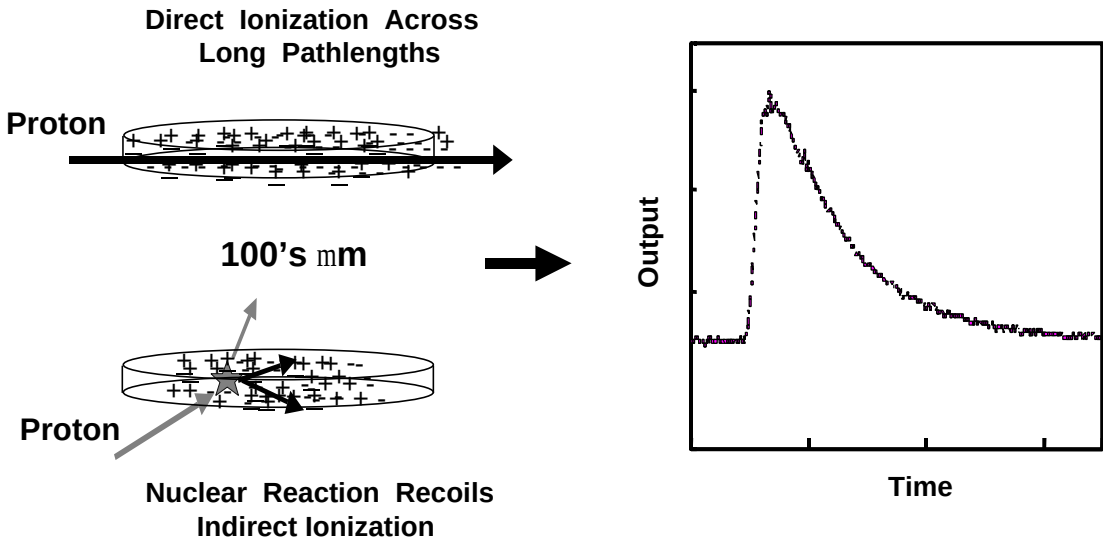

Figure 4.4 Protons can generate charge in a device by either direct or indirect ionization. If sufficient ionization is generated, a single-event transient (SET) may result. [Adapted from LaBe-97]

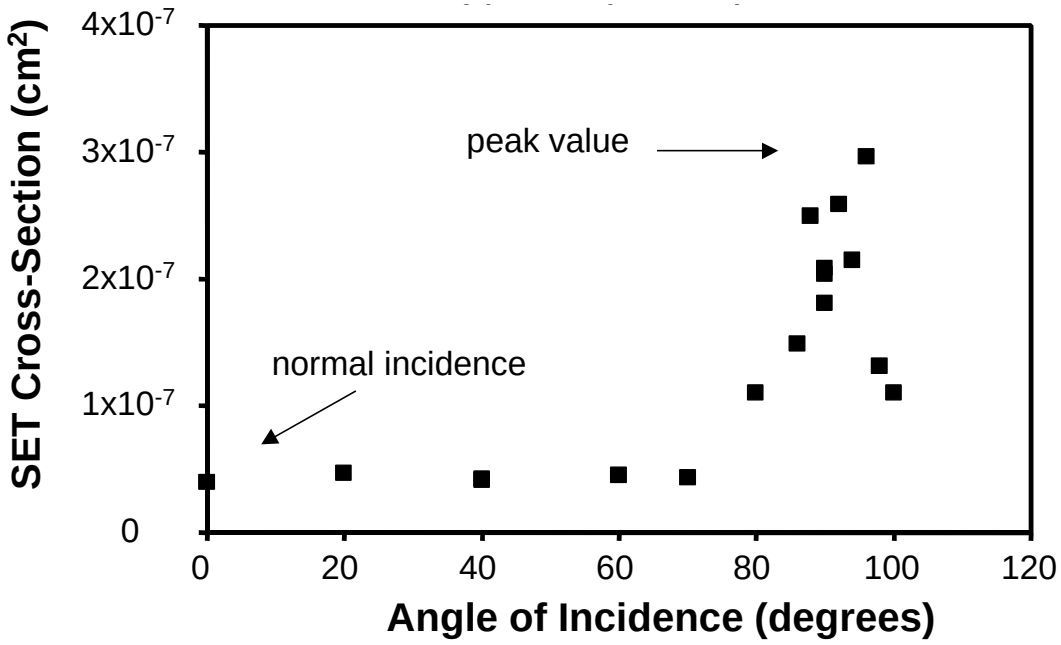

Figure 4.5 The SET cross section for protons incident on a photodiode increases dramatically as the protons approach grazing incidence—an indication that direct ionization is becoming important [LaBe-97].

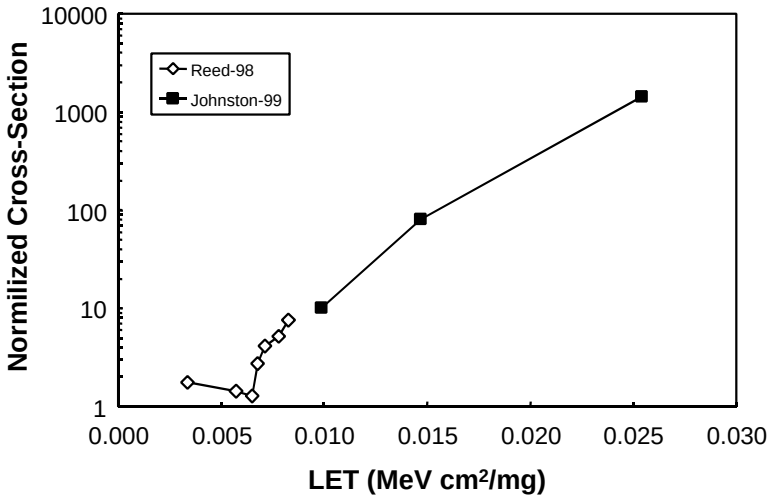

Figure 4.6 More proof of direct-proton-ionization SETs comes from proton experiments at different energies. Protons with higher energies (68-225 MeV [Reed-98]) and therefore low LETs, demonstrating a threshold LET, while for low-energy (15, 30 and 50 MeV [John-99]) protons, which have higher LETs, the cross section increases dramatically.

Figure 4.5 demonstrates this rather surprising result for the photodiode in an optocoupler. (While optocouplers use Si photodiodes the data that follow show clearly that proton-induced direct ionization is important when consider radiation-induced effects on photodetectors). As can be seen, the SET cross section for protons at near-grazing incidence is more than an order of magnitude higher than the cross section for normally incident protons—this despite the fact that the physical device cross section is actually lower for grazing-incidence protons. This result has been interpreted as an indication that for sufficiently long path lengths within the detector, even protons can directly generate enough ionization to cause SETs. Further support for this interpretation is given by comparing results for low-energy protons with those for protons of higher energy, see **Figure 4.6.** The ordinate was computed by normalizing the maximum grazing angle cross-section to that at normal incidence. Because LET decreases with proton energy (over the energy range of interest), direct-ionization would be expected to be less important for higher-energy particles. Indeed, no enhancement is seen at glancing incidence for 225 MeV protons (LET = 3.4×10^{-3} MeV-cm^2/mg), while substantial enhancement is seen at near-grazing incidence for 68, 50 and 30 MeV protons (7.8×10^{-3}, 9.9×10^{-3}, and 1.5×10^{-2} MeV-cm^2/mg, respectively**)** [Reed-98, John-99b]. A consequence of the increase in grazing-angle cross section is that in proton-rich environments, proton-induced SETs can dominate those caused by heavier ions and by indirect ionization [Labe-97].

The susceptibility of photodetectors to direct-ionizing proton SETs demonstrates the importance of minimizing the volume in which the detectors are susceptible to ion-generated photocurrents. This criterion can be extremely important in selecting components that may perform acceptably in space radiation environments. As was discussed in Section 3 of this Short Course, direct-bandgap semiconductors, such as GaAs and InGaAs, require much thinner intrinsic semiconductor layers than do indirect-bandgap semiconductors, such as Si and Ge. As a result, not only are direct-bandgap devices more suitable to high-data-rate applications, they are

also less likely to generate large, ion-induced photocurrents, and so are less susceptible to SETs [Mars-94b].

However, knowing the device SET rate is only one step in determining how these events will affect system performance metrics such as the bit error ratio (BER). Not all SETs cause a bit error. As is the case with most radiation-induced bit errors, system-level characteristics are crucial for understanding whether these bit-errors will affect system performance. System-level aspects of bit-error assessment for fiber-optic data links will be discussed in more detail in Section 5. Here we merely note that it is system-level characteristics that determine whether a SET produced by a radiation-event in a photodiode with a given pulse height and duration will cause a bit error. Because of the periodic nature of the signal, whether an SET causes a bit error depends critically on both its magnitude and on when it occurs with respect to when the signal is read. As such, high-rate applications will be more susceptible to SETs than will slower applications. Moreover, because receivers typically set the threshold for discrimination between '0' and '1' midway between the lowest and highest optical powers, increasing the source intensity significantly lowers the number of SETs that ultimately contribute to the BER. Note that with respect to detector SETs, as with respect to TID and DDD induced degradation in sources, transmission media and detectors, extra margin in light source drive can significantly improve system performance.

4.5 Radiation Effects in Support Circuitry

As indicated in Section 3, the receiver must not only detect a weak light signal and convert it into a current, but also amplify it and then process it. The photodiode can only accomplish the first two of these processes. Amplification and processing require additional support electronics. The devices that perform these functions are inherently vulnerable to the same radiation effects that are found in all electronics. One may devote considerable care to selection of appropriate light sources, transmission media and detectors only to find the most vulnerable component in the system is, for example, an op amp or an A-to-D converter. For this reason, we will briefly discuss how SEE, TID and DDD may affect various support electronics technologies.

Because device technology determines device radiation-effects susceptibility, it is critical to understand the technologies of support devices. Most device technologies can be categorized as either CMOS, bipolar, as a mixture of the two technologies (BiCMOS) or as belonging to various specialty or advanced technologies (GaAs, InP, InGaAs, and so on). In what follows, we merely touch on the effects that are potentially of concern for these technologies. General references include: for general background on radiation effects in semiconductors [Mess-86], for TID concern in CMOS [Dres-89], and [Mess-97]. Other good starting points for the interested reader include the 21 years of NSREC short courses now available and may find additional information in the references in the last paragraph of this section.

The primary concerns for CMOS devices are single-event effects (particularly destructive SEL) and degradation due to TID (particularly leakage current increases). Because CMOS devices are majority carrier devices, displacement damage effects are generally of secondary importance.

Single-event latchup (SEL) is a high-current, positive-feedback state that can be either destructive or nondestructive. Even nondestructive SEL can disrupt operations, because recovery requires cycling power on the device. SEL occurs in pnpn structures in the CMOS (see Figure 4.7). These structures can be thought of as representing a pair of connected parasitic bipolar junction transistors that can form a positive feedback loop, possibly resulting in thermal

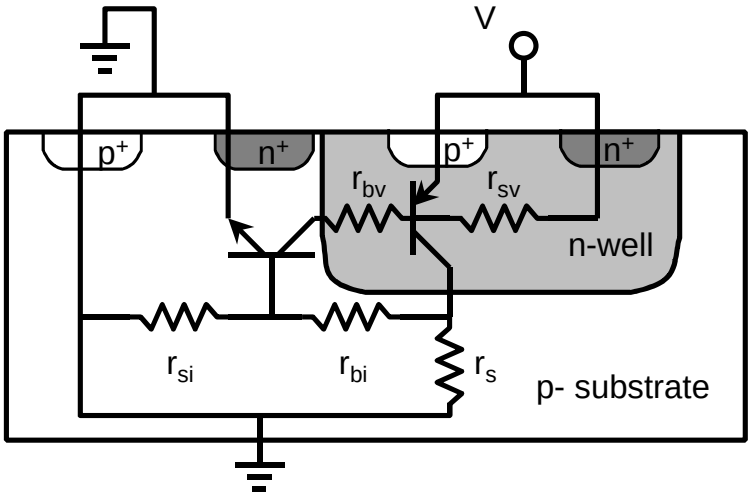

Figure 4.7 Single-event latchup is a potentially destructive effect that occurs in parasitic bipolar junction transistors in p-n-p-n structures—usually in CMOS. [Gall-96]

failure of the device. A large amount of information has been compiled on SEL and on mitigation techniques for the phenomenon [Gall-96]. Here we merely end with the caveat that unless a CMOS device is specifically designed for SEL immunity, it is not possible to predict with certainty whether a device will be susceptible to SEL—or if susceptible, whether one will be able to mitigate the effect—without heavy-ion testing. In addition, CMOS devices may be susceptible to single-event upsets and transients, and at rates ranging from 0 to many times per day.

The basic mechanisms of TID damage were discussed briefly in Section 2. In CMOS devices, the effects of TID manifest as increased leakage currents, shifts in voltage levels (including logic signals) and other parameters and eventually functional failure. Perhaps the most remarkable aspect of TID in CMOS devices is the range of failure levels observed. Devices have been seen to fail at levels as low as a few hundred rads(Si) and to remain functional at levels well above a few Mrads(Si). Again, although similarity of technology may be looked upon as a rough guide to predict device performance, actual device performance cannot be predicted without test data. Moreover, especially for commercial parts, lot-to-lot variations can be significant.

If caution is appropriate when dealing with SEE and TID effects in CMOS, it is doubly so when it comes to radiation effects in bipolar devices. Destructive SEE have been observed in bipolar devices ranging from amplifiers [O'Bry-99, McDo-00] to ADCs [Koga-94]. SEUs and SETs are also possible over a broad range of rates in these devices. It is possible for an op amp or comparator to drive the service outage rate for an entire satellite.

TID degradation in bipolar devices has undergone a bit of a renaissance of late—at the expense of designers' peace of mind. Many of these devices are vulnerable to Enhanced Low Dose Rate Susceptibility (ELDRS)—that is, the devices may suffer more damage when irradiated slowly (as in space) than when irradiated rapidly (as in the lab) [John-94, McCl-94, Emil-96]. We merely note here that our understanding of ELDRS is still evolving, and until the field reaches a more mature state, bipolar devices should probably be assumed to exhibit an

ELDRS sensitivity unless testing has shown otherwise. More generally, as in CMOS devices, TID in bipolar devices results in increased leakage currents, decreased gains, along with other parametric shifts and eventual functional failure. However, TID is not the only mechanism of gradual degradation one must consider for these devices. Bipolar devices, like other minority-carrier devices, are vulnerable to degradation resulting from DDD. Some bipolar devices show significantly more degradation when irradiated with protons than they do when irradiated with gamma rays to an equivalent TID [Rax-99 and references therein]. Parameters that may suffer from DDD include leakage currents, reference voltages and device gains.

The high data rates of the optical components in fiber-optic data links demand support circuitry with commensurate capabilities. Although the development and radiation characterization of such fast technologies—many of them using novel semiconductor materials such as GaAs, InP and so on—are ongoing, a few observations are possible. Because of the technology of these devices, SEL is not an issue. However, the low capacitances of these devices (needed for fast operation) make them inherently vulnerable to SEUs and SETs. Many devices have threshold LETs for upset less than 1 MeVcm^2/mg, leading to high upset rates [Mars-95c]. TID performance for many of these technologies has been found to be generally acceptable and in many cases excellent [Hash-94]. Moreover, displacement-damage tests to date have revealed considerable robustness to displacement damage in these devices [Hash-94, Mars-95c].

Overall, the components in fiber-optic data links can perform well for many missions. However, ensuring such performance is a matter of following good hardness assurance practices for both optical and electronic portions of the system from the component level to the system level.

5.0 Optical System Response to Space Radiation Environments

This section discusses radiation effects as they affect system-level performance of optical digital data links in space radiation environments. The goal is to help the reader better understand how component-level radiation effects (Section 4) affect the link performance metrics (Section 3). We discuss system-level ground testing for single-event effects, as well as performance metric analysis for optical digital data links and how radiation effects on selected components affect such metrics. Finally, we present some on-orbit results for a few fiber links.

An optical data link can contain a host of microelectronic and optoelectronic devices as well as passive optical components. Any of these devices can suffer performance degradation when exposed to space radiation environments. It is beyond the scope of this course to cover every detail of optical-link performance degradation due to all possible devices. Using good engineering practices in selecting devices and in assessing their radiation performance within the system will ensure that any adverse impact on system performance will be minimized. Component-level TID, SEE, and displacement damage screening can be sufficient to assess the performance of some microelectronic and photonic devices in the space radiation environment. However, in-situ testing is especially important for high bandwidth electronic and optoelectronic systems that employ system level mitigation approaches.

The emphasis of this section of the Short Course is the system impacts to optical data links when the performance of their optical and optoelectronic devices degrades as a result of exposure to radiation. Vulnerable devices include optical sources, optical fibers, and photodetectors. Some of the testing techniques and analysis are general, and we have attempted to indicate when a technique or analysis approach can be used to assess other component effects. Three excellent references on radiation-induced effects in fiber-optic data links are [Mars-96, Dale-96, Labe-98d]. These papers provide the basis for the discussion that follows.

The successful use of fiber-optic data links in spaceflight application is discussed in Section 5.3. These successes demonstrate that not only is it possible to develop robust fiber-optic data buses that will survive in the space radiation environment, but it is also feasible to use these systems as a primary means for intra-satellite communications.

5.1 Optical Data Link Single-Event Effects Ground Testing

This section summarizes the impact of single-ionizing-particle events on optical links operating in the MHz to GHz regime. First we will describe radiation-induced bit errors, focusing on radiation events in photodiodes. Then we will describe the implementation of a generic BER test on a photodiode exposed to protons and helium ions—along with the results thereof. An example of subsystem-level testing of a full functional optical data link is then given, followed by a summary of results from in-situ experiments on several other full-functional fiber-optic data buses.

Before we begin we should define the difference between a bit error and a message error. A bit error is a simple data bit that has been changed from its expected value, for example radiation changing a “0” to a “1”. This bit error may or may not induce a system level error. Some systems employ error detection, correction, or mitigation schemes that are robust enough to “repair” a bit error so that it does not impact system performance. So when we refer to bit error we are implying that it is a simple change in a data bit’s state, the system impacts have not been determined. Message errors are manifestation of bit errors at the system level.

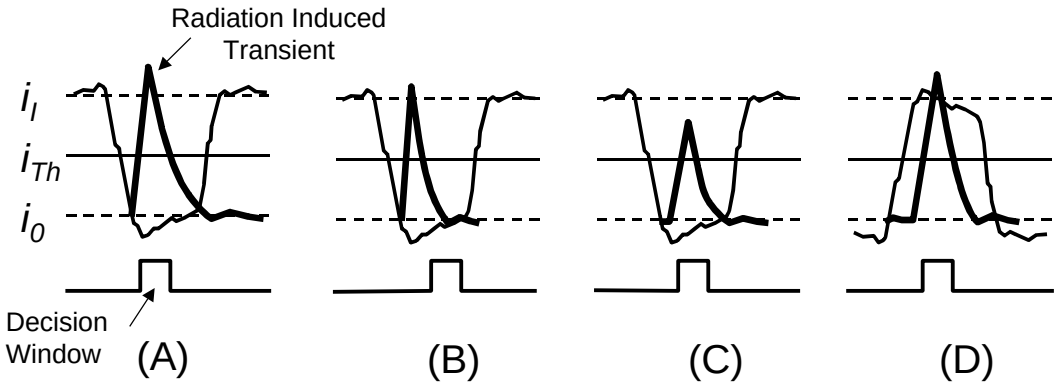

Figure 5.1. Particle-induced SETs occurring at different locations within a bit period and with different intensities [Adapted from Mars-96]. The event in (a) will cause a bit error, those depicted in (b and d) will not induce a bit error, and the event depicted in (c) may or may not cause and bit error. [Adapted from Mars-94a]

5.1.1 Particle Induced Bit Errors

As was shown in Section 3.3, noise can cause bit errors in the data stream. Likewise, single-particle radiation events can induce bit errors in the data sequence [Mars-96, Dale-96, Labe-98d, and references therein]. These single-particle events can occur in any of the digital or linear devices in the data path. Photodiodes are particularly sensitive to ionizing radiation, as described in Section 4.4. The photodiodes used in optical links typically have large junctions, fast time constants, and are incorporated in receiver circuits designed to be highly sensitive [Agra-97, Pala-98, Lach-98]. A key advantage of fiber-optic data links is that the optical signal for a Gbps link may be only microwatts, and conversion to electronic signal during a bit period results in only picocoulombs of charge (a few thousand electrons). Photodiodes used in fiber-optic links make perfect ionizing particle detectors.

The next few paragraphs will examine the particular case of how a radiation-induced current transient in a photodiode can become a bit error when interpreted by the decision circuitry of an optical data link. (The impact of this bit error is defined by the system protocol layer and other mitigation approaches, if interpreted as an system level error we call this a message error). We focus on photodiodes because of their prevalence in optical data links and their susceptibility to radiation-induced transient events. However, the reader should keep in mind that any device in the data path can cause bit errors, which in turn may lead to system level message errors.

Studies on several high-speed digital optical links have shown that photodiodes can be the component most sensitive to single-particle events [Mars-93a, LaBe-93c**,** Mars-94a, Frit-95, Dale-96, LaBe-96b, Mars-96]. These studies have concluded that direct ionization from lightly ionizing particles (protons) is the primary concern for bit errors. As such, bit errors can also be caused by heavy ion cosmic rays traversing the photodiode and energetic products from nuclear interactions between incident protons and semiconductor nuclei in the device. **Figure 5.1** depicts the effects of four different particle events on a data bit. **Figure 5.1.A** depicts a sketch of a "0" level data bit that is part of a NRZ data stream (dark line). Superimposed on this sketch is the current pulse from an ionizing particle interacting with the photodiode (light line). In this case, the radiation event occurs during the decision time-window and with sufficient current to induce a bit error. The current transient depicted in **Figure 5.1.B** does not cause a bit error. The error has sufficient height, but does not occur within the decision time-window. The transient

depicted in **Figure 5.1.C** may or may not cause a bit error. It occurs at a time that is within the decision window, but the induced current level falls in a region that will be ambiguously interpreted by the decision circuitry. The current transient depicted in **Figure 5.1.D** does not cause a bit error. Adding more current when interpreting a level "1" does not affect the decision made by the decision circuitry unless the charge arrives slow relative to the bit period or persists longer than the bit period and the following zero bit is corrupted.

We see that the interpretation process introduces a finite probability of a "0" level bit transitioning to a "1" level when the photodiode is exposed to the space radiation environment. BER assessment must include bit errors caused by radiation events in the photodetector. More generally, any device that is in the data path and is susceptible to radiation-induced bit-errors should be included in the assessment. A bit error may or may not induce a system level message error—system-level errors will depend on the system protocol.

Bit errors that occur in devices in the data path are somewhat analogous to logic errors in memory devices, commonly known as single-event upsets. The main difference is that although the cross-section for memory bit errors has a physical geometry associated with it, the cross-section for a bit error that occurs in a clocked bit sequence is associated with not only a physical geometry, but also with a sensitive time window. The event must occur at a certain physical location and also within the decision window [Mars-94a, Reed-96].

5.1.2 Particle-Induced Bit-Error-Ratio Testing

It is desirable to collect bit error information in real time—that is, to detect, count and display the BER of an optical link as data is transmitted and detected by the link. Bit-error-ratio testing is one method of detecting bit errors in a clocked data sequence. At a minimum, a bit-error-ratio test determines the BER of an optical data link and/or the number of errors in a given time interval. (A specific test set may have other formats for displaying the data collected and more sophisticated tests may examine bus traffic at the protocol level.) For radiation characterization, we are interested in the number of errors that occur when we expose the system to a particle beam of known energy and flux. Such measurements are used to determine the error cross section while exposing each specific component of an optical data link to the test beam.

5.1.2.1 Proton-Induced SETs in Photodiodes that Cause Bit Errors

In this section we describe the use of a bit-error-ratio tester to investigate the mechanisms and effects of proton-induced single-event transients in a photodiode (PD) used in an optical data link. A diagram of the experimental setup used in this investigation [Mars-94a] is shown in **Figure 5.2**. The instrument control and data logging were done using customized software over GPIB interface. The PseudoRandom Number (PRN) sequence generator portion of the BERT generated the data stream. The bit-stream length was $(2^7–1)$, or 127 bits. A waveform generator (not shown) operating at 200, 400 and 1000 Mbps supplied the clock signal, which could be varied continuously for broadband data-link testing. The optical attenuator regulated the power of the optical signal incident on photodiode. An optical fiber could either route the light to the photodiode or be inserted into the lightwave meter so that the incident optical power could be measured. A 3D micro-manipulator stage was used to align the optical fiber with the photodiode. An oscilloscope was used to monitor photodiode output and maximize coupling efficiency between the fiber and the photodiode.

The photodiode used in these tests was an Epitaxx ETX 75 p-i-n fabricated with $In_{0.53}Ga_{0.47}As$. All circuitry other than the photodiode, including the transimpedance amplifier,

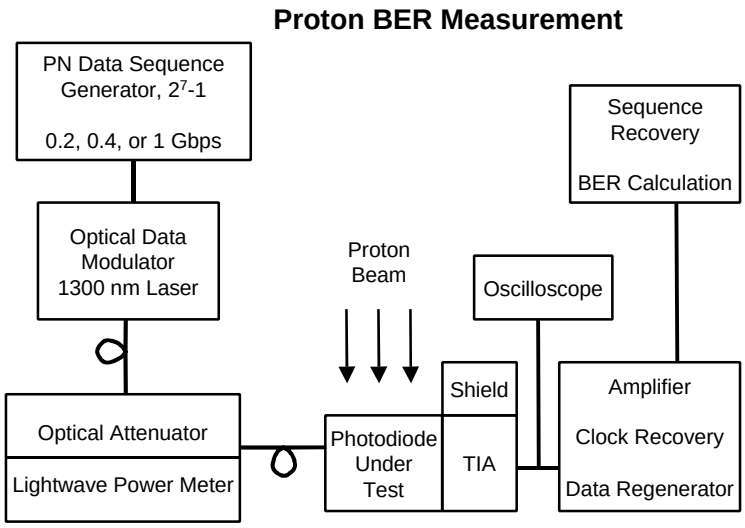

Figure 5.2. Block diagram of BER Test set-up. [Mars-94a]

was shielded from proton irradiation. The BERT performed clock and data recovery, calculated and reported the BER, and reported the number of errors that occurred during an exposure and the proportion of error free intervals. The proportion of error free intervals helps to identify single-bit errors induced by a single proton. Prior to any radiation exposure, the BER was measured to be better than 10^{-9}. This BER is sufficient to ensure that the link will be free from errors caused by noise during the time that it takes to make an irradiation.

Exposures to 63 MeV protons were carried out at Crocker Nuclear Laboratory, University of California [Mars-94, Dale-96, Mars-96]. A single exposure, with an accumulation of at least 100 errors, took a few minutes. After a proton exposure, the BER, number of errors, percent of error-free intervals, and proton fluence were recorded. (Recall that the error cross-section is found from the ratio of the number of errors to the proton fluence.)

First, let's consider the bit-error cross-section's dependence on optical power. (See **Figure 5.3**.) [Mars-94, Dale-96, Mars-96]. Here we plot the cross-section for various optical powers and a 400 Mbps operating frequency. The proton angle of incidence was 80 degrees. Notice that there are several orders of magnitude variation in cross section, depending on the optical power. The photodiode under exposure is incorporated into a broadband receiver that includes automatic gain control circuitry, and therefore an increase in the optical power sent to the detector increases the decision level of the receiver. As a result, the photodiode is less sensitive to proton-induced events that generate low current levels—so fewer protons cause errors. From this we see that one strategy for error reduction by system design would be to use brighter optical sources on the transmitter side. Another important consideration is the effect of network topology on the optical power incident on the photodiode. For example, star-coupler-based architectures often have inherently lower power loss than other topologies. The bit-error cross-section must be characterized across the entire range of optical powers that are of relevance to the system.

Next, let's consider the cross-section dependence on both proton angle of incidence and the optical power. **Figure 5.4** gives the results of measurements made on the proton-induced bit-error cross-section for various optical powers at four angles of incidence [Mars-94a, Mars-96].

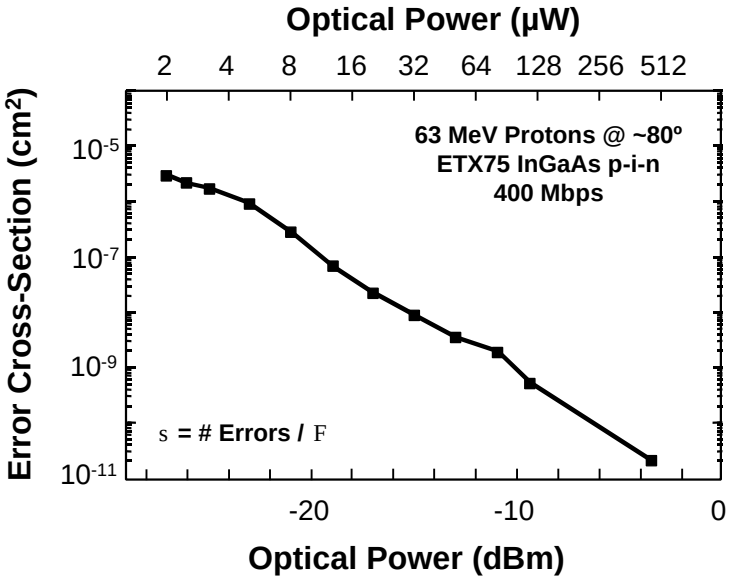

Figure 5.3. Variation of photodiode error cross-section over optical power. [Mars-94a, Dale- 96] Optical power considerations are critical when assessing impacts of radiation-induced bit errors on BER.

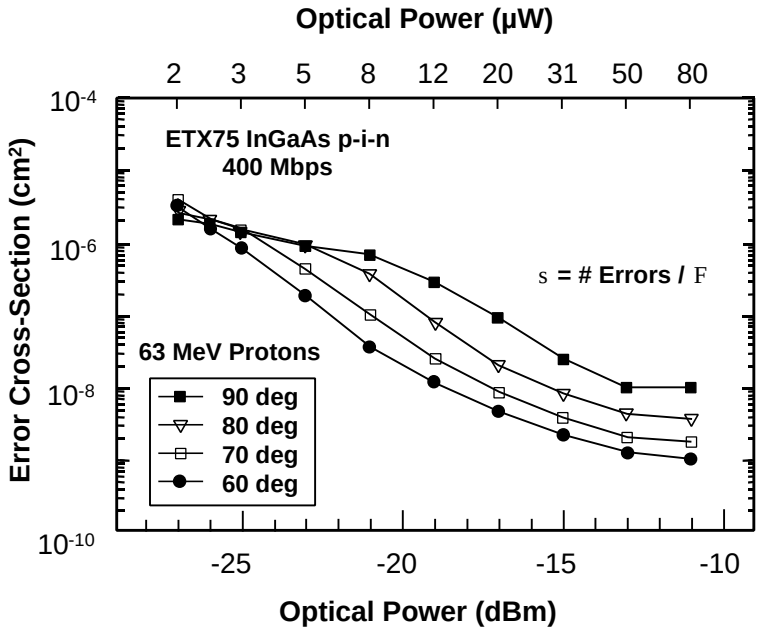

Figure 5.4. Proton-induced bit error cross-section for various optical powers and angles of incidence. [Mars-94a] These data demonstrate direct ionization mechanism for bit-errors in a photodiode.

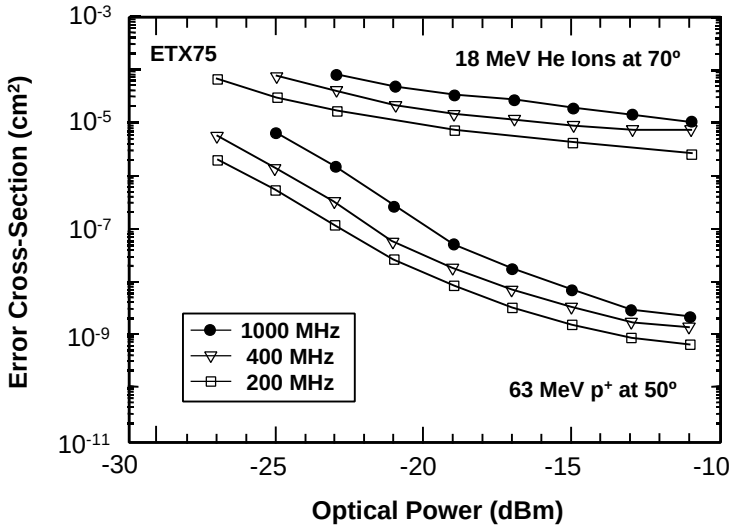

Figure 5.5 Frequency dependence of error cross section for various ions. [Mars-94a] System operating frequencies should be considered when characterizing bit-errors.

The angles are with reference to the normal to the photodiode surface. These data indicate that some of the proton-induced events are due to direct ionization, (as was also the case for the photodetectors in optocouplers, see section 4.4). Observing a few facts about the data illuminates the dynamics of the proton-induced direct-ionization effects. Notice that there is a sharp increase in cross-section with angle of incidence at high optical power. This is inconsistent with the hypothesis that indirect ionization is solely responsible for these bit errors. Probably the cross-section is some combination of direct- and indirect-ionization effects, and most likely dominated by direct-ionization effects. Also, notice that at low optical power there is very little change in the cross-section with angle of incidence. Correcting these cross-sections for angle of incidence shows that for low optical power, the cross-sections are near the geometric area of the photodiode. At this point the optical power is so low, and the receiver circuitry so sensitive that very low levels of ionization will induce a bit error. The dependence on optical power in this receiver with automatic gain control indicates an adjustment to the critical charge required for single-event transients to become bit errors. We will treat this topic in more detail in Section 5.2.2, where we discuss on-orbit BER calculations.

Finally, consider **Figure 5.5**, which shows the photodiode error cross-section dependence on operating frequency [Mars-94a, Mars-96]. Notice that for all optical powers for both protons and He ions the error cross section is linearly dependent on data rate. In [Reed-96] error-cross-section dependence on frequency was studied in detail, the next section summarizes this work.

5.1.2.2 General Discussion of Error-Cross-Section Dependence on Data Rate

At this point we will digress from our discussion of photonics for a moment to discuss frequency effects in general. Frequency effects on error cross-section have been observed and studied by several authors for several types of microelectronic and photonic devices [Turf-90, Schn-92, Buch-93, Turf-94, Mars-94a, Shog-94, Mars-95c, Buch-95, Reed-96]. Some of these papers focused on complete circuits while others studied device-level effects. Some found a linear relationship with frequency, while others found this relationship to be nonlinear. Testing

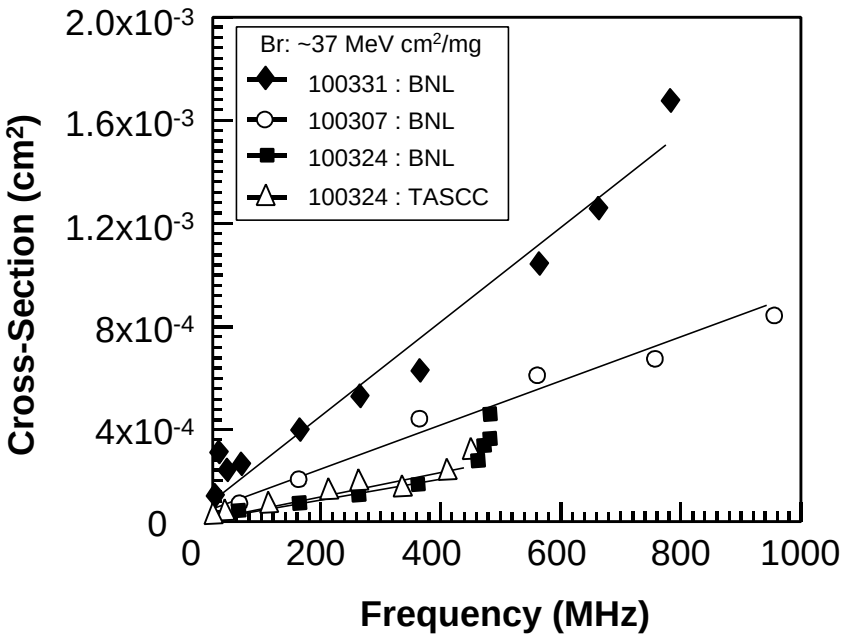

Figure 5.6. Cross-section data collected on several devices over various operating frequencies [Reed-96]. A linear relationship is observed for most cases except at the maximum operating frequency for the 100324. The departure from linear behavior can also be observed when testing at the maximum operating frequency of the test set-up (see Figure 5.7).

to date on fiber-links has shown a linear dependence on frequency. [Reed-96] presented a discussion of the origins of frequency effects in simple microelectronic devices. These results are particularly important when evaluating microelectronic support circuitry in fiber data links.

The data presented in [Reed-96] show that for a National Semiconductor voltage-level translator (100324), XOR (100307) and D flip-flop (100331) the relationship was linear until near the maximum operating frequency, **Figure 5.6**. The same study showed that for a proprietary microcircuit design the frequency effects were non-linear, **Figure 5.7**.

The linear relationship with data rate is easily understood by reviewing **Figure 5.1.A**. Each bit is sampled for a specified duration. There is a certain time window in which the radiation event must occur in order to be counted as an error. This window is called the vulnerable time window. The duration of the decision window and the probably the decay time of the transient event (defined by the circuit bandwidth) define the duration of vulnerable window. Increasing the frequency increases the number of vulnerable windows.

The data in **Figures 5.6** and **5.7** show that the cross-section increased dramatically as the data rate approached the maximum operating frequency of the test set or the device. For example, in **Figure 5.6** we see that at 440MHz the measured cross-section of the level translator increases rapidly away from the linear trend. This frequency was the maximum operational frequency for the device. Another example is shown in **Figure 5.7**: at frequencies greater than 1 Gsps the measured cross-section increases dramatically. These devices function at frequencies greater than 1 Gsps. The maximum operating frequency of the BERT used in this test is 1.2 Gsps. These data show that a dramatic increase in error cross-section occurs when operating near the maximum operating frequency of the test set or the device being tested.

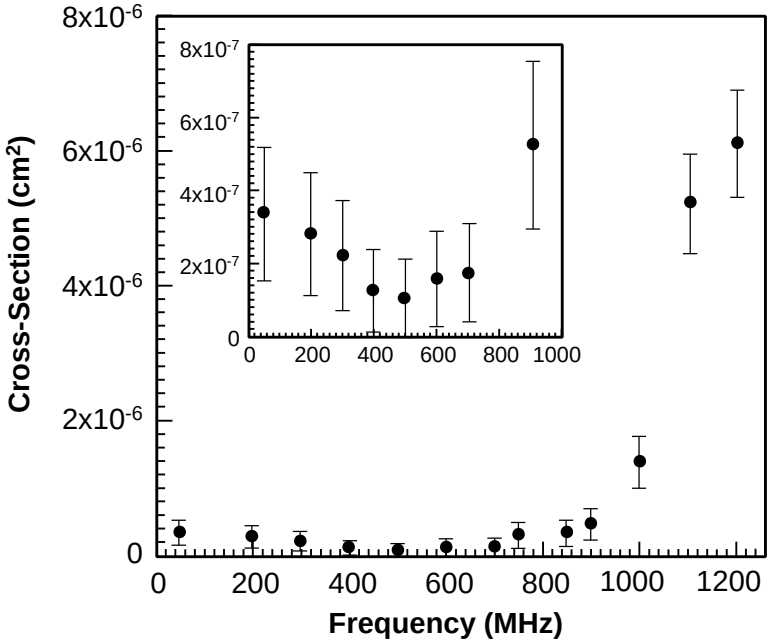

Figure 5.7. Cross-section data showing the nonlinearity of the relationship between cross-section and data rate; inset shows a blow-up of data at less than 1 GHz. [Reed-96] This result was repeatable.

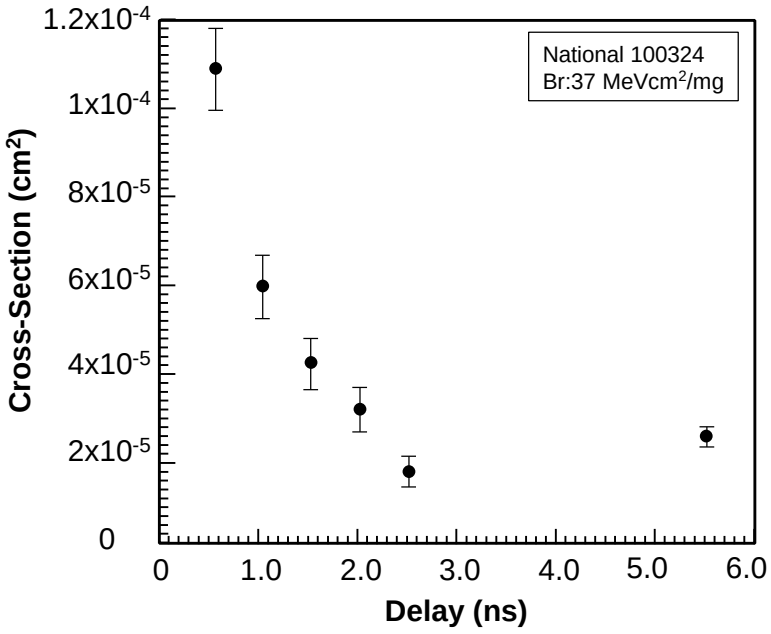

Figure 5.8. Cross-Section as a function of delay between the sample window and the data edge. This shows greater sensitivity when sampling near data transition. [Reed-96]

Figure 5.8 shows how the error cross-section increases as the decision window, and along with that the vulnerable window, is moved closer to the data transition. The delay is the time between a data transition and the leading edge of the decision window. This suggests that the increase in sensitivity is due to a loss of noise margin close to a data transition.

5.1.3 Optical Data Link Subsystem Level Radiation Effects Testing

In order to fully qualify an optical link for use in the space radiation environment, several issues must be addressed. Some of these can be addressed at the component level, while others must be quantified at the subsystem level. Section 2.2 gives an overview of the issues that must be addressed. The list below gives an overview of how some of these effects affect device performance in general.

- Total ionizing dose (TID): long term degradation of device performance, eventually leading to device failure. These effects can occur in passive optical components as well as optoelectronic and microelectronic devices.
- Examples of single-event effects (SEEs):
  - SEL, SEGR, SEB: single cosmic ray particle event that can cause the device to stop functioning. In some cases (especially SEL) this is recoverable. These effects can occur in microelectronic devices.
  - SEU, SET: Single-particle induced change in the logic-state of a digital device (SEU) or a temporary change in the output state of a analog device (SET). These effects can occur in optoelectronic and microelectronic devices.
- Displacement damage: long term degradation of device performance, eventually leading to device failure. These effects can occur in optoelectronic and microelectronic devices.

This section deals with the topic of *in situ* testing of fully functional optical data links that are representative of building blocks of an optical data network with fidelity to the hardware network layer and possibly also the protocol layer. First, as an example, proton testing on a specific optical system will described. Then, we will give results from several other system-level tests of optical data links. (In Section 5.3 we compare on-orbit results of some of these digital optical data links to predictions made using ground data.)

5.1.3.1 Ground Testing of a Digital Optical Data Bus

This section will describe system-level study of bit errors resulting from radiation effects. [Dale-96] The study was carried out on the STAR Fiber Optics Data Bus (FODB), which was designed by Boeing [Chap-93, Frit-94, Frit-95]. The STAR FODB is a 200 Mbps 32 node star-coupled fiber-based data bus. The star coupler is dual redundant; the data stream is Manchester encoded, and the system also allows for error checking. It uses 1300 nm multimode fiber and optoelectronics.

Figure 5.9 is a block diagram of a generic application of the STAR FODB. The Fiber Bus Interface Unit (FBIU) contains a transceiver (the transmitter and receiver) and support circuitry necessary to implement the protocol and form the host interface. Each host FBIU is connected to all others via the 32x32 optical star coupler. A block diagram of the FBIU is given in **Figure 5.10**.

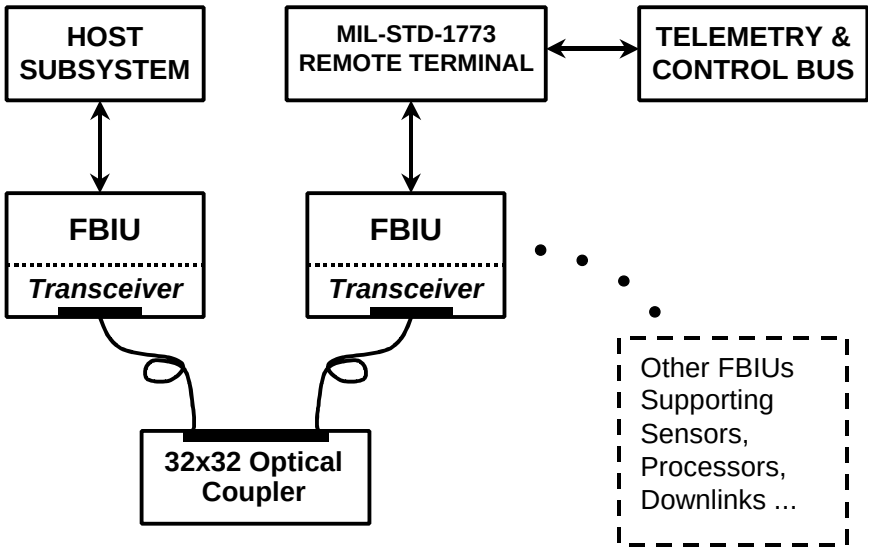

Figure 5.9. Schematic of a STAR FODB network. [Dale-96]

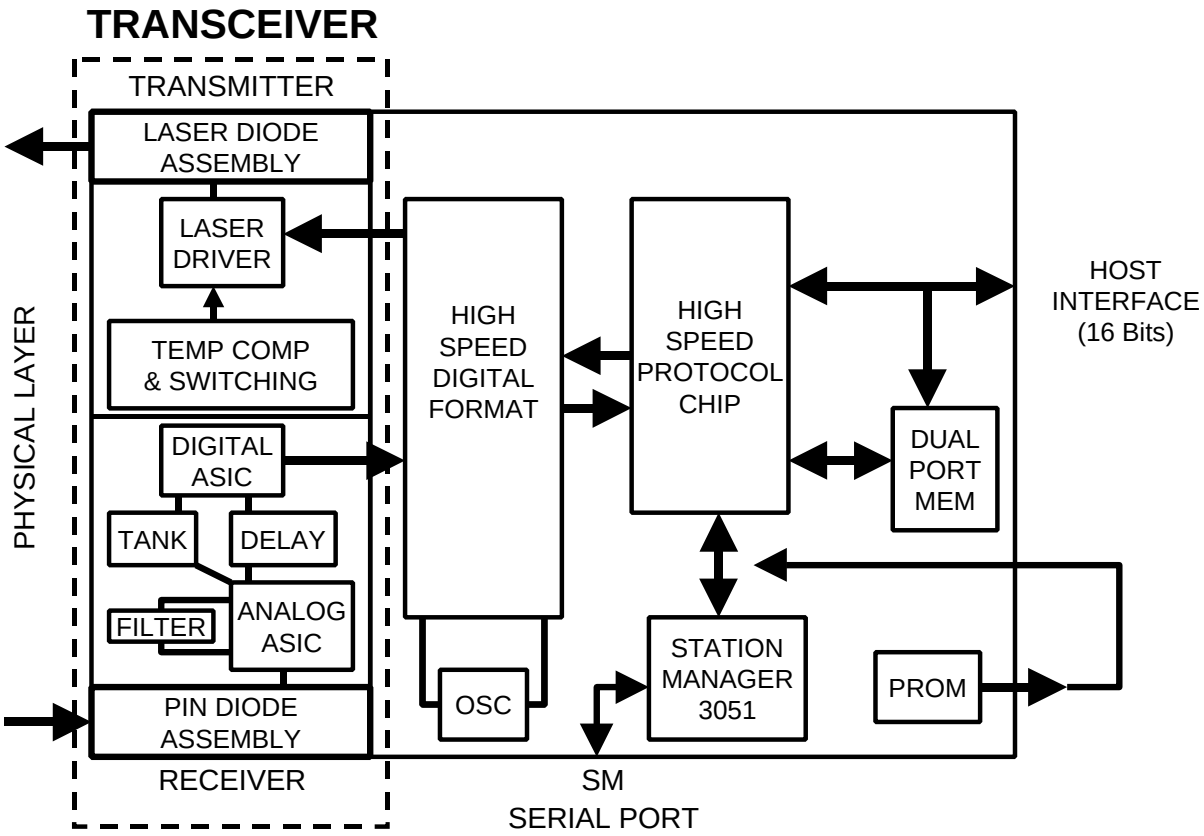

Figure 5.10. Schematic of a fiber optic bus interface (FBIU). [Dale-96]

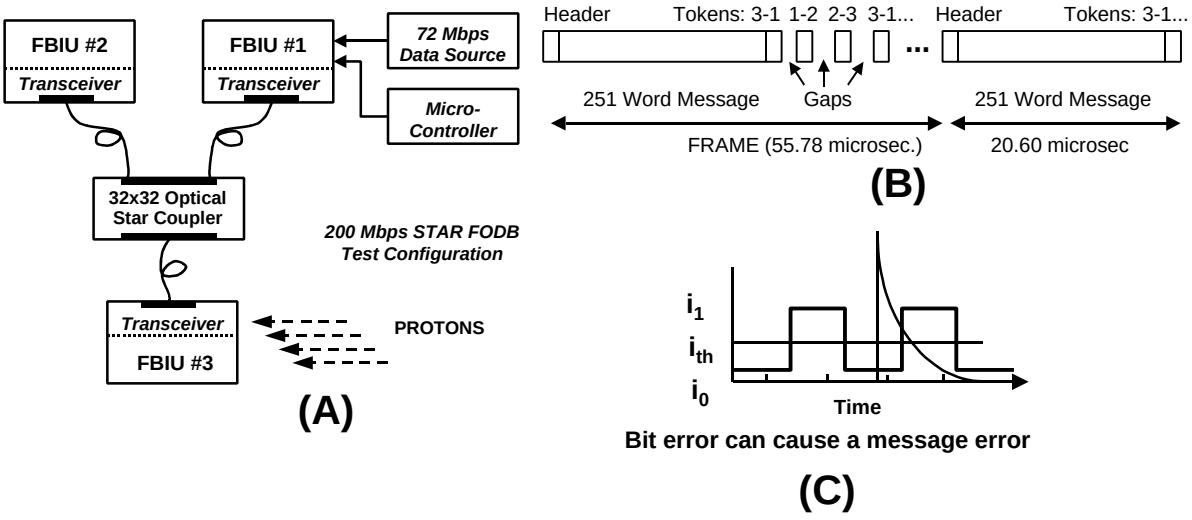

Figure 5.11. (A) Configuration of three FBIUs during proton system testing. (B) Message packet used during test. (C) SET induced bit error that can lead to a message error. [Adapted from Dale-96]

A detailed description of the FBIU can be found in [Frit-94]. Some of the key components are listed here. The photodiode is a 1300 nm laser diode, and the photodetector is the Epitaxx EXT75 p-i-n diode. The data formatter is a high speed GaAs ASIC that formats and deformats, encodes and decodes, and performs error checking. The protocol chip is a CMOS ASIC. The station manager is a CMOS micro-controller. The dual port memory is 3.3 V CMOS RAM. Clearly, there are several different issues that should be addressed when qualifying this hardware for use in the space radiation environment. Each device should be reviewed for its performance degradation and SEU sensitivities. Beyond that it is important to perform subsystem-level testing and analyses to understand how bit errors are generated, propagated and realized at the subsystem level to form message errors. Here we will describe some of the results from a proton-induced-bit-error-characterization study intended to assess proton-environment impacts at various test levels.

A depiction of a subsystem-level proton test on the STAR FODB is shown in **Figure 5.11.A**. The test-network configuration included three FBIUs, one of which was selected for irradiation. Complete testing of the system protocol (including recovery of the bus in response to the drop-out of an FBIU) required that at least three FBIUs be used. Errors were defined by the bus protocol [Chap-93, Frit-94]. Error logging during the irradiations was automatic. **Figure 5.11.B** depicts the message transfers used for these tests. Each frame had a 251 word long message, with each word having 16 bits. When messages were not being sent, a sequence of tokens (packets of information used to maintain network traffic according to the network protocol) was passed around the network. For these tests, a message error was defined as any loss of data—that is, any event that changed a bit in the message packet **Figure 5.11.C,** so all bit errors resulted in message errors. Errors in tokens were not counted as message errors.

A sequence of exposures was carried out for each component in the FBIU [Dale-96]. The measured error cross-sections for the entire transceiver are given in **Figure 5.12** as the triangles. Comparing this to results obtained on the photodiode module (upside down triangles) shows that the vast majority of the events are due to events in the photodiode. The squares in this figure

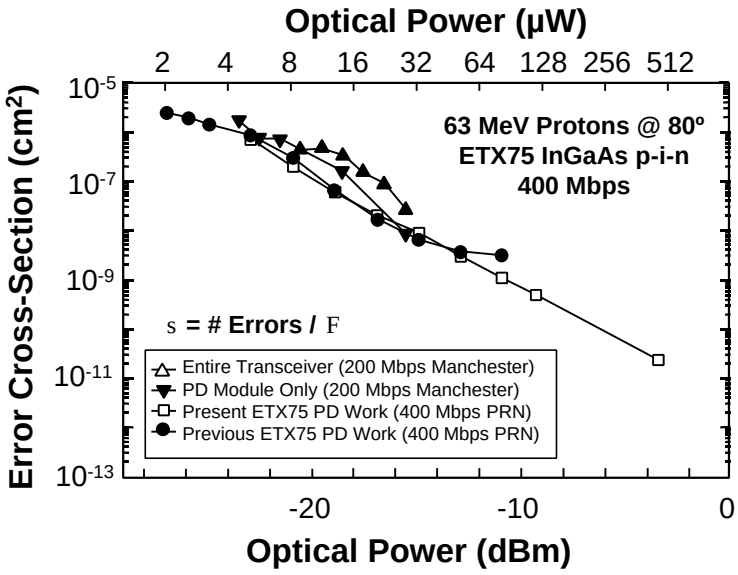

Figure 5.12. Comparison of message-error cross-section to error cross-section of photodiode. [Dale-96] Note that a majority of the errors are due to transients in the photodiode.

give the error cross-section measured on the photodiode from the generic BER tests, **Figure 5.3**. In this case the message errors measured at the subsystem level are well defined by the generic bit error (or BER) test results on the photodiode. This is not surprising since the receiver circuit used in the "generic" tests used some of the same components as the subsystem design, and more importantly, the components were used in similar ways in terms of detection concept, receiver sensitivity and bandwidth. These same components, if used in a significantly different receiver design, would exhibit different error-cross-section characteristics. Therefore, it is important to assure good component performance, but also to validate that performance with high-confidence models or particle radiation testing at the subsystem level.

Results from proton exposures of other components are detailed in [Dale-96]. Here we present a summary of the results. A small number of errors occurred when the protocol chip and the data formatter were exposed to more than 20krad(Si) of protons. No errors occurred during exposures of the station manager, which was a hardened micro-controller responsible for bus initialization, fault detection, and isolation. For this system configuration, TID-induced device degradation of the commercial dual port memory was a limiting factor for certain spaceflight missions. This was expected, and the testing was useful for determining the suitability of the present hardware for various missions as well as indicating a path for hardening the subsystem for more demanding missions.

5.1.3.1 Other Ground Test Results

Several subsystem-level tests of other fiber-optic data links have also been performed [LaBe-91a, LaBe-92a, LaBe-92b, LaBe-93a, LaBe-93c, LaBe-94a, LaBe-94b, Mars-95b, Frit-95, LaBe-96b, Mars-96, Cart-97, LaBe-98c]. The reader is encouraged to review these publications which give detailed discussions of the test setup and results. We give examples some of the these:

- Transients in photodiodes dominate system BER in most cases [Mars-96, Dale-96, Labe-98d, and references therein].

- In [LaBe-94a, LaBe-94b] the authors describe system level proton SEE test results on a data bus that uses the AT&T ODL200 transmitter and receiver and the Hot Rod protocol chip set from Gazelle Microcircuits. The test results showed that the microwave complementary bipolar integrated circuit support devices dominated the message-error sensitivity of the ODL200. Test results also showed that SEUs in the Hot Rod protocol chip set would dominated the BER. These results are somewhat unusual, given that for most systems tested, the photodiode is the major cause of bit-errors that lead to message errors. This example shows how SEU in support circuitry can dominate BER.
- Some bit-error cross-section can depend on particle flux and beam structure—for example, in systems that utilize message retries [Dale-92, LaBe-93a, LaBe-93c].
- Proton-Induced bit-error testing on a Fiber Channel (FC) transmitter and receiver is described in [Cart-97]. FC is an ANSI-standard for a high-performance serial data link. It includes a mix of point-to-point, network, and active intelligent interconnection topologies. Devices from AT&T and Force, Inc. were evaluated. The optical components in the AT&T devices where reasonably tolerant to bit-error effects, but SEUs in the link's logic portion interrupted operation and required a link re-initialization. Results on the Force devices showed them to also be tolerant to bit-error effects. However, during irradiation the transmitter experienced a repeatable unexplained high current condition.

The results of these fiber-optic-data-link radiation tests show the need to carefully characterize each component of the fiber-optic data link for appropriate SEE, TID and displacement damage effects (see Section 3). Some of these effects should be characterized at the subsystem level, while others can be characterized at the component level. Any device that can impact performance by causing system message errors should be well characterized under a system-like environment. The on-orbit message error rate will depend on the system protocol, message packet size, message encoding, error checking and correction, and other system and sub-system level characteristics. Similar considerations apply for BER for data link traffic below the protocol layer.

We should stress here that each in-situ test poses specific challenges. The test team should carefully weigh each segment of the test plan based on the requirements and functionality of the system or subsystem under test. Some important considerations are listed below:

- Determine limitations when performing subsystem-level heavy ion and proton testing. For example, packaging may limit heavy-ion bit-error testing and TID may limit proton testing.
- The system being tested should simulate actual spacecraft intra-satellite optical data link system operation. So that the test will determine when bit errors propagate through the system and cause message errors.
- Consider how mitigation approaches may impact testing and results.
- Individual expose each component of the optical data link during system level SEE testing.
- Consider whether component-level TID testing is needed to quantify the risks of parametric and functional failure of support ASICs, RAM or other support devices.

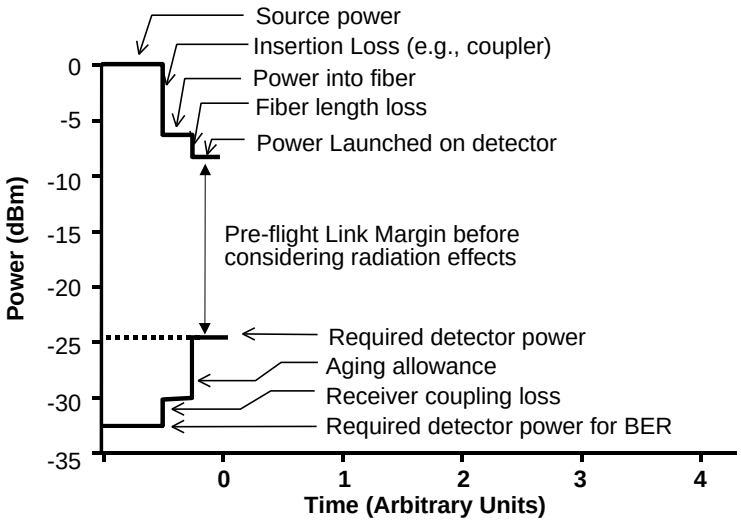

Figure 5.13. Plot of pre-launch system power budget (after Figure 3.14). The abscissa is now mission duration as opposed to fiber length.

- Consider whether component-level SEE testing for SEL, heavy-ion-induced bit errors or other effects is needed.
- Characterize the network over the full range of optical powers relevant to the network.. (Optical power incident on photodiodes critically affects BER.)
- Consider the effects of the orientation of the photodiode in the receiver package. (This can dramatically affect SEE test results and should be explored to gain meaningful information for error rate predictions.
- Consider the effects of radiation-induced darkening in passive optical components during the test. (Such degradation can decrease the optical power incident on the photodiode and must be distinguished from loss of responsivity in the photodiode itself.)

5.2 Assessing Radiation Effects on Optical Digital Data Link Performance Metrics

Assessing performance of an optical data link for the space radiation environment requires consideration of the effects of TID, displacement damage, and SEE on the optical digital data link performance metrics described in Section 3.3. General considerations for system-level assessment of radiation effects on spaceflight hardware has been described in [LaBe-96a, Gate-96, LaBe-98b, Kinn-98, Heid-99]. In this section we discuss the issues that are specific to fiber-optic data links. First we consider how TID and displacement damage impact the power budget. Next, we discuss the techniques for predicting on-orbit BER, and the impact of power budget on BER. Lastly, a brief discussion of approaches for bit-error mitigation is then given.

5.2.1 TID and Displacement Damage Impacts on Power Budget

A power budget analysis for an optical-fiber link was discussed in Section 3.3. Such an analysis of the pre-launch power-budget margin for the optical link can also be conducted for radiation effects (see **Figure 5.13**). The abscissa is relabeled in arbitrary units of time (instead of

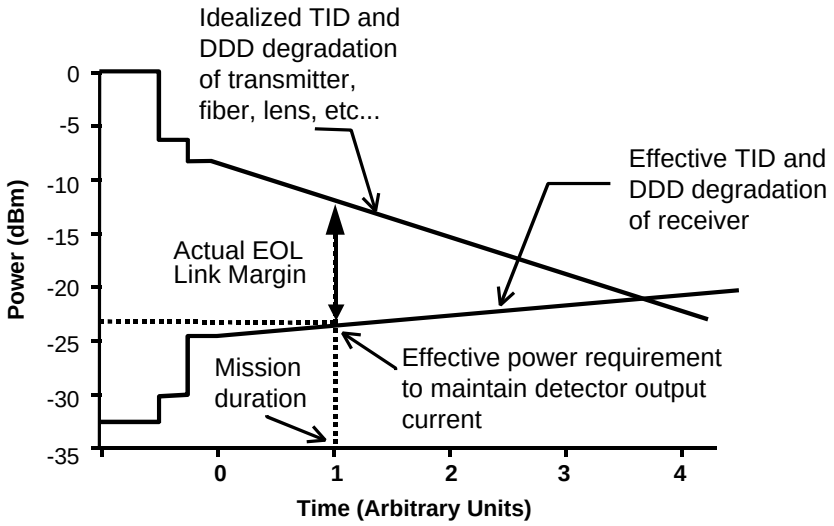

Figure 5.14 Idealized radiation induced degradation of power -budget margin. When the power incident on the detector falls below the bottom line the system BER will be above the specification limits.

length as in **Figure 3.17**). As a fiber-based system is exposed to the space radiation environment, the power budget margin will decrease as a result of several effects. **Figure 5.14** shows graphically how these effects impact link margin (note that this figure is a cartoon and is for demonstration purposes only). The slope of the top line represents idealized TID and displacement damage effects as the mission time increases. This line takes into account effects such as degradation of source optical power and the signal as it passes through the fiber and optics components such as lenses. The slope of bottom line represents idealized TID and displacement damage impacts on the optical power needed to maintain the required system BER. The upward slope reflects, for example, displacement damage degradation of the photodiode responsivity. For the hypothetical mission life marked on the time axis, the power incident on the detector at the end of the mission life will be –12 dBm. The power requirement for maintaining system BER is –23dBm. So, the net EOL link margin is 11 dB. A power-budget-margin analysis must be preformed that considers radiation-induced degradation effects to ensure sufficient EOL margin to maintain a functioning optical link.

5.2.2 Impacts of Radiation-Induced Bit Errors on On-Orbit BER

Traditional proton-induced on-orbit error rate calculations [Pete-97] assume indirect ionization to be the dominant mechanism for upset, and so they proceed as follows. The error cross-section is measured at various proton energies. These data are then fit using Bendel curves. The error rate is computed by direct integration of the on-orbit flux-energy curves with the Bendel curve-fit to the error cross-section data. Traditional heavy ion-induced error-rate calculations [Pete-97] assume that direct ionization is the dominant mechanism for upset. For these calculations, the error cross-section is measured at various effective LETs. The error-rate calculation assumes that the sensitive volume is a right rectangular parallelepiped. One then fits the graph of cross-section vs. LET to a Weibull distribution and calculates the error rate by convoluting this function with the LET spectra appropriate for the mission environment.

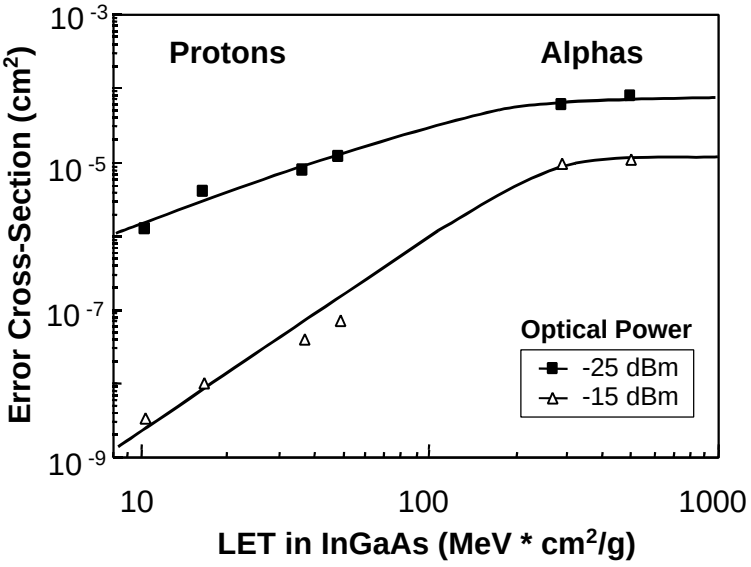

Figure 5.15. Plot of the 400 Mbps data in Figures 5.4 and 5.5 using conventional techniques to correct LET and cross-section for beam angle. [Adapted from Mars-94a]

All traditional approaches for computing on-orbit error rates separate the contributions due to direct and indirect ionization effects. Although such techniques are adequate for predicting error rates for most microelectronic devices used in support circuitry for fiber optic data links, separate consideration of direct and indirect mechanisms is not the best approach for predicting proton-induced error rates for optical data links where bit errors occur due to direct ionization from protons in photodiodes.

5.2.2.1 Proton-Induced Transients in Photodetectors and On-Orbit BER

Direct ionization by protons striking photodiodes can be the dominant source of single-event induced bit errors in digital optical data links (see Section 5.1.2.1). As discussed above, traditional proton SEE rate prediction approaches that only consider indirect ionization effects are inadequate for links that are susceptible to errors caused by proton direct-ionization.

References [Mars-94a, Mars-96, Mars-99] show that for fiber-link applications that use photodiodes that are very susceptible to SETs due to proton direct ionization, bit error data can be analyzed in terms of particle LET. The authors use standard methods from heavy-ion upset calculations to account for geometric effects of changes in incident particle angle, including: a) using "effective LET" to account for the increased charge deposited in the sensitive volume particles at grazing incidence, and b) the decreased cross-sectional area projected by the sensitive volume as the particle angle of incidence increases. The resulting plot presents convincing evidence that it is possible to understand the data using the conventional methods of fitting a Weibull distribution to a plot of error cross section vs. effective LET (see **Figure 5.15)**. The plot shows the cross section for a bit error while operating the link at 400 Mbps for various values of effective LET in InGaAs (note units are MeV cm^2 / g). The data for LETs < 100 MeV * cm^2 / g are from proton exposures, while data for LET > 100 MeV * cm^2 / g are from He exposures.

Predicting the proton-induced on-orbit bit-error rates using data like that in **Figure 5.15** was demonstrated in [Mars-94a, Mars-96]. The approach was to determine the best Weibull fit to the

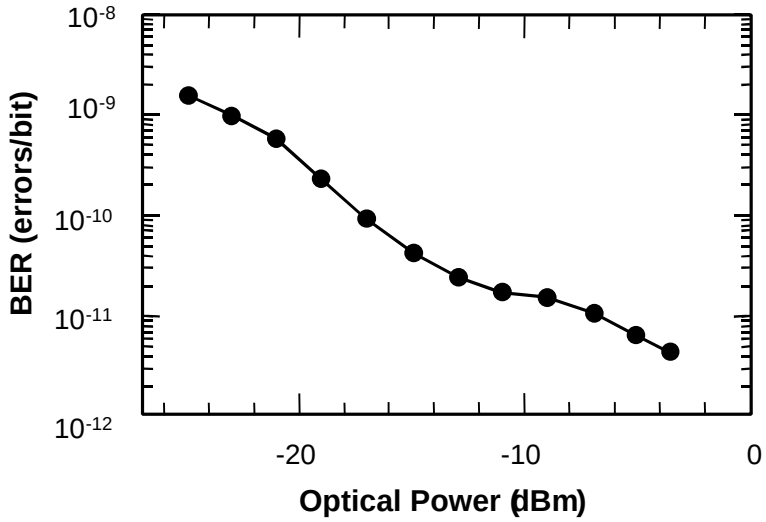

Figure 5.16. Predicted on-orbit BER during solar particle event at various optical powers [Adapted from Mars-94a]

data and use the standard tools of rate calculation for heavy-ion induced SEE to calculate the proton-induced error rate in the photodiode. **Figure 5.16** shows the predictions of such calculations for various optical powers for a 400 Mbps application during a solar particle event. (Recall that the error cross-section data vary with data rate, so any error rate calculation on any clocked device must consider the application operating frequency [Mars-94a, Reed-96].) This type of calculation assumes that bit errors are dominated by direct ionization effects at all angles.

5.2.2.1.1 Methods for Predicting On-Orbit SETs for Mixed Direct and Indirect Effects

In the paragraphs above we address the specific case where proton-induced direct ionization is the dominant mechanism for SETs in photodetectors (this has been the case for most high bandwidth fiber-optic data links.) SETs in other optical data link configurations can be a mixture of direct and indirect effects. One specific case is high-speed optocouplers, which can be thought of as simplified optical data links. Accurate predictions of SETs in a photodetectors like those used in optocouplers, must include a combination of direct and indirect effects [LaBe-97, Reed-98, John-99b]. Characterization of SET cross section of any data link over angle of incidence will reveal which mechanism (direct ionization or indirect ionization) is dominant.

In [LaBe-97], the authors suggest using a combination of the existing traditional methods for predicting SETs in for optocouplers. Ground data is used to determine the angle where direct ionization effects begin to dominate the cross-section. One then applies traditional approaches for direct ionization effects for angles greater than this cutoff and uses indirect-ionization methods indirect effects for angles less than this cutoff.

In [John-99b] an empirical approach was suggested for photodetectors used in optocouplers. This approach requires data to be collected at several angles of incidence and at several proton energies. One then integrates these data over the proper on-orbit proton spectra. The first step is to integrate the cross-section over all angles at each energy. Angular data like that in **Figure 4.5** must be collected at all energies and then integrated over all angles to arrive at an effective cross-section curve like that in **Figure 5.17**. The next step is to integrate this effective cross-section with the space proton environment.

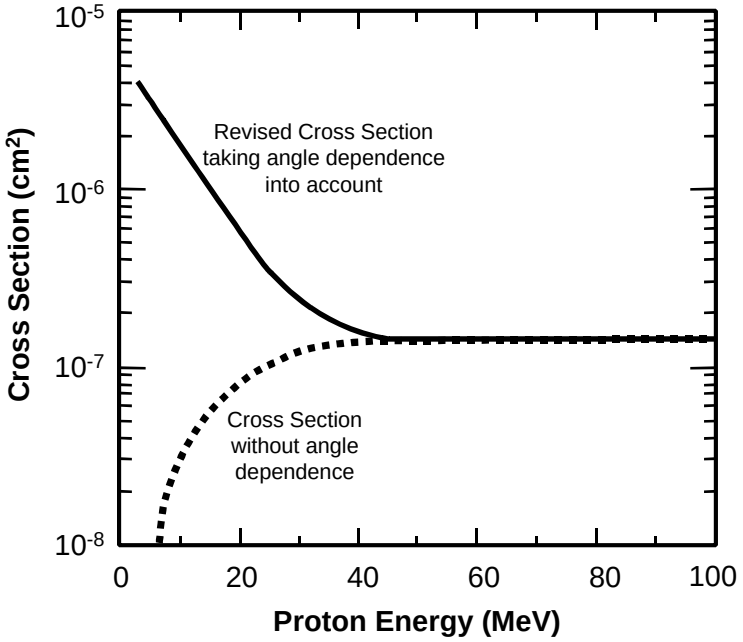

Figure 5.17. Effective cross-section—including the angular distribution like that in Figure 4.5—for various proton energies on the HP6N134. [John-99]

Note : A detailed formulation of a model for computing proton-induced transients in photodetectors or photodiodes that incorporates direct and indirect ionization effects, i.e. directly incorporates angular effects, has not been published to date. The reader should keep in mind that not all device-level effects cause system level errors.

5.2.2.2 Optical Link On-Orbit BER and Message Error Considerations

The previous sections demonstrate that the BER of an optical data link decreases as the optical power incident on the photodiode increases in links that employ automatic gain adjustment. **Figure 5.18** shows a hypothetical example of this effect. In this plot, we have assumed a bit-error rate like that in **Figure 5.16** and 2) that the optical power incident on an ideal photodiode degrades as in the top curve in **Figure 5.14.** (We note that the data in Figure 5.14 is idealized and does not represent a quantitative analysis of the relative contribution of each link component to performance degradation.) The radiation environment was assumed to be typical of an anomalously large solar proton event. To accentuate the role of incident optical power, we have also assumed constant receiver response (no degradation) from launch to mission EOL. Assuming an initial optical power of 0 dBm yields the curve traced by the triangles, the squares represent the results for the same system assuming an additional initial source optical power of just 5 dBm. Operating the source output 5 dB higher decreases the radiation-induced BER.

Another consideration is the complex problem of computing the on-orbit rate for message errors from ground based data. These calculations are dependent on the network protocol and how message errors are defined. This calculation may be as simple as collecting *in situ* message error data on each sensitive component, computing the message error rates for each and then summing them up to get and aggregate rate. In most cases it is not as simple as that, Section 5.3 suggests references to find information on this type of calculation for a optical link network that resends failed messages.

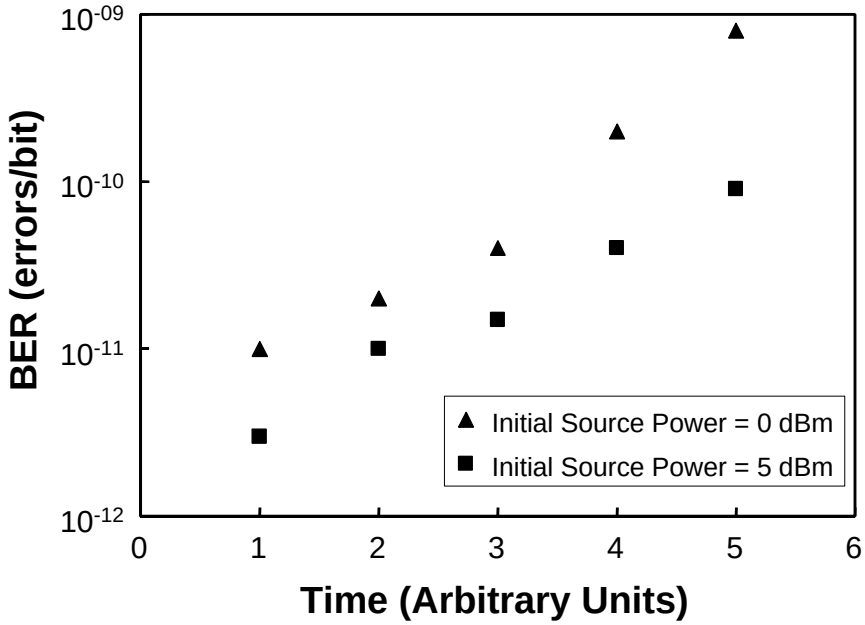

Figure 5.18. SEE-induced bit errors can be reduced by increasing link margin. This figure illustrates such a reduction for the case where the source power has been increased. These data also demonstrate how BER might change over mission life. These data are based on the idealized curve in Figure 5.14.

5.2.3 Bit Error Mitigation Approaches

There are many ways to mitigate bit errors—at the component level as well as the subsystem and system levels. Such mitigation techniques almost always involve tradeoffs between performance and error mitigation. We direct the reader to the several references to fiber data link systems given above for a detailed description of mitigation schemes. As with any system, computing the net on-orbit error rate can be complicated by the use of error mitigation techniques. Some examples are described here:

- Reduce detector depletion layer thickness. This decreases the target size and limits charge collection. Indirect band gap (Si) diodes have thicker depletion regions than do direct band gap (III-V) diodes [Mars-96].
- Reduce the photodiode area. Again this reduces the target size, but it also reduces the received optical power. As such, the amount of area reduction possible may be limited.
- Over-sample and compare single data bits. Over-sampling is not possible at high data rates where the duration of the transient event is on the same order as a bit period [Thel-94].
- Use encoding and parity checking to detect errors and enable retry commands for error correction. The impact is effectively a 50% loss of bandwidth. This technique also requires buffer memory and a handshaking architecture that can be difficult to implement in high data rate systems [LaBe-93c].

- Increase the optical power incident on the photodiode. This decreases the photodiode's sensitivity to particle-induced ionization, but must be weighed against other system considerations such as power budget [Dale-96].
- Use multi-level filtering and receiver design approaches such as those used in Boeing's implementation of the AS1773 [Bone-96]. (See the next section for a more complete description of this mitigation approach.)
- Use good system engineering practices for handling SEEs at the system level. This will minimize the effects of device errors on the BER, and perhaps even more important, applying these techniques will minimize the risk that TID, DDD, or SEE will cause degradation in overall spacecraft performance. Several papers and short courses address this topic for general applications [LaBe-96a, Gate-96, LaBe-98b, Kinn-98, Heid-99].

5.3 Ground Testing Results and On-Orbit Use of Selected Digital Optical Data Links

Several optical components and optical links have been used or tested in spaceflight hardware. The Long Duration Exposure Facility (LDEF), launched in 1978, [Tayl-91b, John-92] was the first experiment to examine fiber-optics in space. LDEF orbited for 5 ¾ years and then was retrieved. The dose levels varied from 200 to 25,000 rads. No significant attenuation was observed for any of four data links, each operating at 830nm.

In 1993 Boeing developed the Photonics Space Experiment (PSE) [Cros-93, Frit-93]. The PSE was a five-segment set of experiments designed to measure the performance of selected fiber optic data links and certain components over a 5 year mission. It contained experiments that measured the long term TID degradation of optical fibers and passive components. The fibers included step and graded index multimode fibers designed to operate at 850 and 1300nm. It also studied the on-orbit stability of a laser diode and selected LEDs. Finally the first on-orbit BER test of a full function MIL-STD 1773 was performed. Preliminary on-orbit results were presented in [Frit-96]. The results favored using these components and data links in space systems.

The NASA Small Explorer Program's implementation of a fiber-optic data bus, named Small Explorer Data System (SEDS), was used to transfer telemetry and commands between subsystems. The standards community identifies the SEDS fiber-optic system structure as MIL-STD-1773. This 1 MHz star bus is a slave/master configuration that has two sides, side A and the redundant side B. The messages are Manchester encoded and can be up to 32 words long. In 1995 the standard was revised to include data transmission at either 1 Mbps or 20 Mbps. The new standard was renamed AS-1773 [A-1773]. The functional requirements of AS-1773 remained the same as MIL-STD-1773. A detailed discussion of the bus protocol can be found in [A-1773]. One notable error detection and correction feature for this standard is that after every received message the receiving node sends a short return message to the master identifying the status of the received message. The status message tells the master to retransmit the message if the transfer was unsuccessful. Retransmission of a message pack can be suppressed.

Two generations of the MIL-STD-1773 SEDS data bus have been developed. Major changes to the link from one generation to the other were mechanical and electrical, but the same optical components were used in both generations. The first generation SEDS (SEDSI) data bus was used on NASA's Solar Anomalous Magnetospheric Particle Explorer (SAMPEX). SAMPEX was launched in July 1992. The SEDSI radiation test effort is described in [LaBe-93a, LaBe-

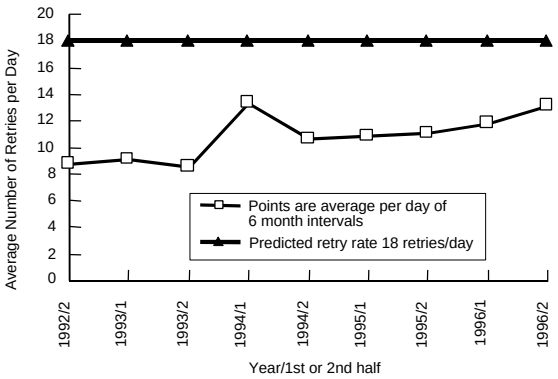

Figure 5.19. Comparison of predicted retry rate to the measured value for SEDSI on SAMPEX. [LaBe-97c]

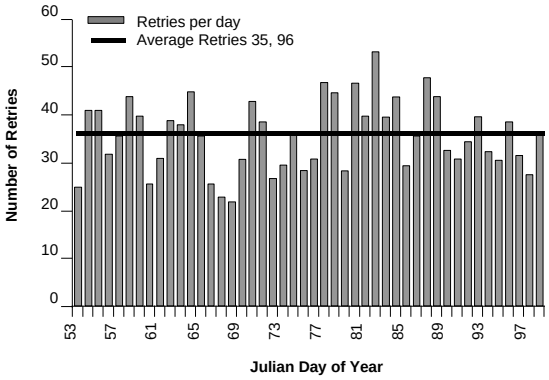

Figure 5.20 Comparison of predicted retry rate to the measured value for SEDSII on HST. [LaBe-97c]

93c]. The second generation of SEDS (SEDII) was used on the Hubble Space Telescope (HST) Solid State Recorder (SSR). The SSR was installed on HST in February 1997. A comparison of the radiation performance of the first and second generation SEDS data bus was given in [LaBe-98c]. The data of [LaBel93c,LaBel98c] show that the photodiode is the sensitive component to radiation-induced message errors. This work compared on-obit message error data to predictions made from ground data for proton-induced errors. The ground results were identical for the two generations. (This is not unexpected because the same optical components were used in both generations.)

The operation of SEDSI on SAMPEX has been successful. No bus outages or failed messages have occurred. However, there have been several corrupted data messages that required a retransmission of the message for correction. Typical numbers of message retransmissions are shown in **Figure 5.19**. This figure also shows the predicted number of retransmissions. Also as expected, most of the retransmissions have occurred in the SAA.

The number of bus SSR SEDSII retransmissions per day for the first two months of operation is plotted in **Figure 5.20**. SEDSII on HST is fully operational. No bus outages have occurred. Errors requiring retransmission have occurred with a frequency of about 1 every 2 days. These errors are believed to result from software or hardware error rather than single-event effects. An error cross-section calculation and on-orbit prediction approach for multiple retransmissions based on a binomial distribution for the retry probability and the cross section for single message errors was developed in [LaBe-93c, and revisited in LaBe-98c].

A space experiment based on AS-1773 using a Boeing transceiver [Bone-96], has been developed, radiation tested in the lab, and flown on board the Microelectronics and Photonics TestBed (MPTB) [LaBe-96b, Jack-96]. The goal of the experiment was to fully simulate the AS-1773 spacecraft bus. We note that operating frequency was fixed at 20 Msps. The experiment was reconfigurable between two modes of operation: transmission could be reversed so that data flowed between two subsystems in either direction—but not simultaneously. The Boeing transceiver utilized 1300 nm InGaAs photodetector and GaAs LED, the design employed several mitigation techniques:

- A small volume photodetector was used to minimize charge collection.

- The analog preamplifier circuitry had excess drive to minimize the pulse widths of SETs
- It utilized a proprietary asynchronous digital data reconstruction to filter narrow-width SETs produced in the photodiode and the preamplifier.
- The transceiver electronics were fabricated in a radiation hardened, 1.2 μm, thin epi-layer CMOS process.
- The system used a proprietary clock-recovery architecture.
- The optical fiber used is radiation-tolerant.

Ground testing showed that the SETs in the photodiode would be the most sensitive source of radiation-induced message-errors [LaBe-96b]. The data link has seen very few errors [Jack-99]. This is mainly due to the decreased size of the photodiode. (We should note that the link has been exposed to a relatively low proton fluence while operating in MPTB host spacecraft's highly elliptical orbit.) These on-orbit results confirm the ground results, which demonstrated the effectiveness of the hardening solution. Although on-orbit bit errors are occurring during one of the modes of operation, these are hardware related and are not radiation induced.

The on-orbit robustness of these digital optical data links—confirmed by ground testing and modeling—shows that intra-satellite digital communications can be achieved with little or no radiation-induced performance degradation.

6.0 Radiation Effects in Emerging Optical and Optoelectronic Technology

This section will focus on recent radiation-effects testing of technology that could eventually be used in digital optical data transfer system in spaceflight applications. The intent is not to be exhaustive, but rather to give the reader a sense of radiation-effects issues for the state-of-the-art technology.

A glance at these technologies and the associated radiation effects issues will show that the future for high-speed (>1Gsps) optical data links in spaceflight application is very promising. However, the path toward this goal will not be without its challenges, from the perspective of design as well as that of radiation-effects issues. SEU and SET effects are certain to be among the more complex issues that engineers and radiation-effects researchers will face in implementing these technologies into spaceflight hardware.

- [LaBe-98a] listed vertical cavity surface emitting lasers and Metal-Semiconductor-Metal (MSM) photodetectors as two technologies that have strong potential for use in spaceflight high-speed optical data link. VCSELs are high-speed, small-scale (< 10 μm diameter) top emitting lasers. These devices can be fabricated to form an array of light emitters with each individual device having very small beam divergence. An account of testing for proton-induced radiation effects in VCSELs can be found in [Paxt-97, Barn-99]. These data show that VCSELs demonstrate excellent performance for most spaceflight applications. More detail on VCSELs can be found in segment II of this Short Course.
- MSMs are high-speed (10s-100s GHz) photodetectors. Fabrication techniques used in making MSM vary greatly. They use Schottky barriers with semiconductor sandwiched between [Mars-97] the interdigitized electrodes, see **Figure 6.1**. Like VCSELs, they are small-scale and can be fabricated to form arrays. Proton-induced bit-error tests on MSMs [Mars-97] showed the same trends for SETs over angle and optical power as those shown in photodiodes (see Section 4.4). However, the acceptance angle for direct ionization effects is much narrower than that for p-i-n diodes, and the MSM cross section has a stronger dependence on optical power. This leads to the possibility that MSM could be fabricated to be much less sensitive to radiation induced increases in BER than are p-i-n diodes. The MSM used in this study proved to be robust to TID and DDD effects.
- Several commercial vendors have developed fiber-optic transceivers. A world wide web search on May 25, 2000 for "fiber-optic transceiver" uncovered over 1200 pages. The list below is a subset of the list of vendors.
  - Telebyte, Inc—http://www.telebyteusa.com/index.htm
  - TC Communications—http://www.tccomm.com/LAN.htm
  - 3Com—http://www.3com.com
  - Agilent Technologies (formerly HP)—http://www.agilent.com/
  - Lasermate Corporation—http://www.lasermate.com/

Some of these transceivers may use technologies that are very robust to the space radiation environment. Careful radiation effects characterization would need to be carried out to evaluate each transceiver's susceptibility to TID, DDD, and SEE. Results from proton-induced SEE testing on two of these links show the trends similar to those described in Section 5 of this Short Course [OBry-00].

- Wavelength-Division Multiplexers (WDMs) combine the signals transmitted from several sources—each source operating at a different wavelength—and pass the signal through a single fiber and then separates out the various signals by wavelength (see **Figure 6.2)**. There are

several methods of combining and separating an optical signal according to its wavelength. [See for example Agra-97.] The methods vary from those using passive components like lenses to those using a combination of active and passive components—such as those in Mach-Zehnder interferometers. (Recall that Mach-Zehnder interferometry applies an electric field to an optical material to shift its refractive index.)

Radiation-effects testing on a fused biconical-taper WDM was described in [Guti-94]. They found that radiation had very little effect on optical power loss of the signal passing through the WDM. However, there was a small, but not insignificant increase in the individual channel signal loss to other channels.

Polymer optical waveguides are another promising technology. Polymer traces can be placed on flexible sheets of materials such as Kapton. These can then be laminated onto multi-layer boards using standard lamination processes. Typical waveguide dimensions are 1 mil square. Polymer optical waveguides can be used to transfer light from one side of a printed circuit board to another (see **Figure 6.3)**. One obvious application of this technology is in WDMs. Radiation-effects testing has been done for some polymer waveguides [VanE-96].

- Erbium-Doped Fiber Amplifiers (EDFAs) are passive optical power amplifiers. Optical power gain can be achieved as light travels through an Er doped silica-based fiber [Desu-93]. There are several potential applications for this technology in spaceflight hardware—use in WDMs being one. EDFAs are known to be much more sensitive to radiation than classical silica fibers. [Will-98, Hens-98 and references therein] offer excellent reviews of radiation effects in EDFAs. One issue of great importance for use of these fibers in space-based systems is whether one can predict their performance in the space radiation environment from ground data. [Will-98] carefully addresses this issue.
- High speed (> 1 GHz) support electronics are required for Gbps data rates and beyond. GaAs MESFET and bipolar emitter-coupled logic (ECL) are mature technologies that can operate in the GHz regime. Other III-V and Si semiconductor technologies are currently expected to reach speeds much greater than 1 GHz. TID testing on GaAs, ECL, SiGe, and CMOS SOI has proven these technologies to be sufficiently robust for the space environment TID effects. SEU testing at high data-rates (>1GHz) on ECL, GaAs, and SiGe technologies has shown them to be sensitive to radiation-induced bit errors, which would add to the BER. Growing GaAs with a buried layer at low temperatures has been shown to be effective at mitigating SEUs [Mars-95a]. We direct the reader to some of the more recent discussions of the radiation tolerance of these technologies : ECL [Reed-96, O'Bry-00, and references therein], CMOS SOI [Brot-97], SiGe [Mars-00], and GaAs [Mars-95c, Weat-97, and references therein]; these are just starting points, we suggest a the reader review more recent IEEE TNS for up to date information on the radiation tollerance of these emerging semiconductor microcircuits.

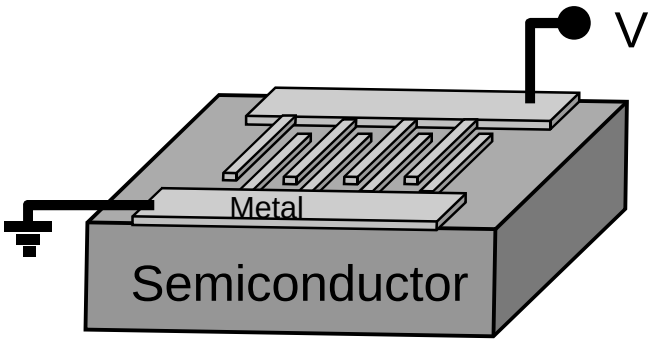

Figure 6.1 Cartoon of a MSM photodetector showing the interdigitized electrodes.

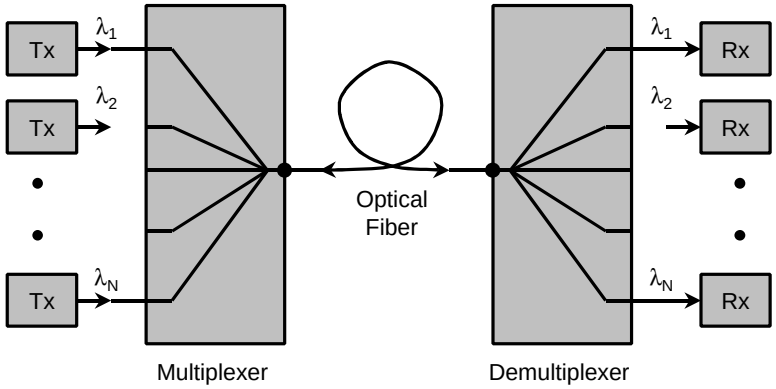

Figure 6.2. Block diagram of a WDM. Individual subsystem's transmit (Tx) data at different wavelengths. Each receiver (Rx) is tuned to accept data at a defined wavelength. Some WDM use wavelength tunable components.

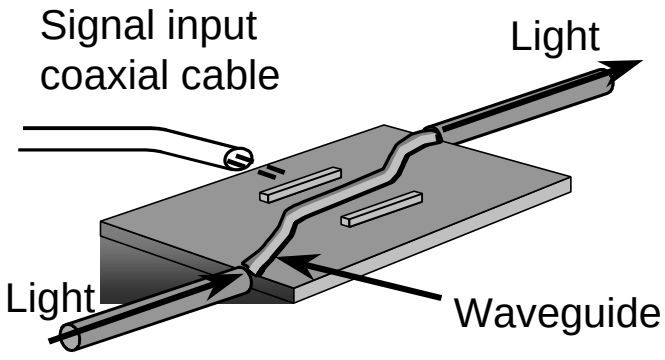

Figure 6.3. A polymer waveguide trace laid on a PCB configured in a Mach-Zehnder interferometer.

➢ Wavelength-Division Multiplexers (WDMs) combine the signals transmitted from several sources, each operating at a different wavelength, pass the signal through a single fiber and then separates out the various signals by wavelength (see **Figure 6.2)**. There are several methods of combining and separating an optical signal according to its wavelength. [See for example Agra-97.] The methods vary from those using passive components like lenses to those using a combination of active and passive components—such as those in Mach-Zehnder interferometers. (Recall that Mach-Zehnder interferometry applies an electric field to an optical material to shift its refractive index.)

Radiation-effects testing on a fused biconical-taper WDM was described in [Guti-94]. They found that radiation had very little effect on optical power loss of the signal passing through the WDM. However, there was a small, but not insignificant increase in the individual channel signal loss to other channels.

Polymer traces can be placed on flexible sheets of materials such as Kapton. These can then be laminated onto multi-layer boards using standard lamination processes. Typical waveguide dimensions are 1 mil square. Polymer optical waveguides can be used to transfer light from one side of a printed circuit board to another (see **Figure 6.3)**. One obvious application of this technology is in WDMs. Radiation effects testing on some polymer waveguides can be found [VanE-96].

➢ Erbium-Doped Fiber Amplifiers (EDFAs) are passive optical power amplifiers. Optical power gain can be achieved as light travels through an Er doped silica based fiber [Desu-93]. There are several potential applications for this technology in spaceflight hardware—use in WDMs being one. EDFAs are known to be much more sensitive to radiation than classical silica fibers. [Will-98, Hens-98 and references therein] offer excellent reviews of radiation effects in EDFAs. One issue of great importance for use of these fibers in space-based systems is whether one can predict their performance in the space radiation environment from ground data. [Will-98] carefully addresses this issue.

➢ High speed (> 1 GHz) support electronics are required for Gbps data rates and beyond. GaAs MESFET and bipolar emitter-coupled logic (ECL) are mature technologies that can operate in the GHz regime. Other III-V and Si semiconductor technologies are currently expected to reach speeds much greater than 1 GHz. TID testing on GaAs, ECL, SiGe, and CMOS SOI has proven these technologies to be sufficiently robust to space environment TID effects. SEU testing at high data-rates (>1GHz) on ECL, GaAs, and SiGe technologies has shown them to be sensitive to radiation induced bit errors, which would add to the BER. Growing GaAs with a buried layer at low temperatures has shown to be effective at mitigating SEUs [Mars-95a]. We direct the reader to some of the more recent discussions of the radiation tolerance of these technologies : ECL [Reed-96, O'Bry-00, and references therein], CMOS SOI [Brot-97], SiGe [Mars-00], and GaAs [Mars-95c, Weat-97, and references therein]; these are just starting points, we suggest a the reader review more recent IEEE TNS for up to date information on the radiation tollerance of these emerging semiconductor microcircuits.

7.0 Summary and Conclusions

We began this segment of the Short Course with a brief overview of the space radiation environment, summarizing the basic space radiation effects important for microelectronics and photonics and giving an example of a typical mission's radiation environment requirements.

We then gave an overview of intra-satellite digital optical data link systems, including a general discussion of the digital optical data link, some link components, and a brief description of optical link power budget and bit error ratio.

The subsequent discussion of radiation effects in optical and optoelectronic components focused on degradation of passive optical components and SETs in photodiodes. We briefly mentioned DDD degradation of source output power and laser turn-on threshold. We discussed in some detail the characterization of TID induced signal attenuation resulting from darkening in passive transmission medium. (Proper choice of fiber can largely resolve this issue.) Radiation-induced transients in photodetectors were seen to pose a significant concern for data link performance in space missions. DDD degradation of detector output current and TID and DDD increase in background noise were seen to be significantly less of a radiation effects problem.

We noted that radiation effects in support circuitry—though not covered in this segment of the short course—could also threaten data link performance—or even data link survival. Significant threats included: TID and DDD parametric and functional failure, SEUs in logic, SEL in CMOS, and SETs in linear devices. Proper design can resolve most, if not all these issues.

From device effects, we went on to consider the system response of optical data links to the space radiation environment. First a discussion of system-level SEE ground testing was given that stressed the importance of understanding the contributions of bit errors in all devices in the data path to the system BER. A clear understanding of the system response to radiation induced errors is critical. The system protocol and employed mitigation approaches determine when and how radiation induced errors impact the system functionality. Simple component level testing cannot illuminate these issues. A carefully designed test plan will simulate the spacecraft subsystems use the optical data link, note that this is also true for data link that utilize an electronic physical layer. SETs due to proton-induced direct ionization p-i-n photodiodes and direct and indirect ionization phototransistors were seen to pose specific challenges. Proper characterization was seen to demand that cross-section measurements be made of over the entire system phase space of beam angle, optical power and operating frequency. The potential frequency dependence of bit errors in other support circuitry was emphasized. Finally, we reemphasize that without *in situ* testing to determine the bit-error ratio and the multiple-error ratio, one cannot determine how device level effects impact system level performance (with protocol layer), that is, whether or not a particular device effect translates into a system effect.

The discussion of ground-based, system-level testing was followed by a discussion of system level assessment of data link performance in the space radiation environment, emphasizing the importance of managing TID and DDD effects in sources and passive transmission media. We emphasized that these degradation effects could be avoided with proper device selection and/or mitigated by proper management of the system's optical power budget. We also saw that predicting on-orbit, radiation-induced BER in support electronics is possible using standard on-orbit error rate calculation tools, but that a modified approach is needed to account for the contribution by SETs in photodiodes.

Lastly, we looked at some state-of-the-art technologies and found that the prospects for high-data-rate (>1 GHz) fiber-optic data links looks to be excellent in the near term.

The bottom line is: Designers must consider radiation effects when making decisions about optical data transfer system configuration and protocol, hardware design (especially the receiver) and device selection. A proper hardness assurance program at the component level, careful electrical, optical, and optoelectrical designs, and well thought-out system protocol will result in a qualified fiber optic data link for use in the space radiation environment.

8.0 Acknowledgments

We would like to thank each person in the Radiation Effects and Analysis Group and the Radiation Physics Office at NASA Goddard Space Flight Center for their support. Specifically we would like to thank Paul Marshall, Cheryl Marshall, Janet Barth and Ken LaBel for their insightful technical discussions, guidance and careful review of this work. This course would not have been possible had they not been willing to let us tap into their vast knowledge of this subject matter. Thank you. We would also like to thank Martha O'Bryan for her support in formating the graphics and text in the written and oral presentation of this Short Course. We would also like to thank Janet Jew and Christian Povey for their excellent review of this segment of the Short Course.

Like most of our adventures, we would not have completed this one had it not be for the forgiving support of our families.

9.0 References

[A-1773] "Fiber optic mechanization of a time division multiplex data bus," AS-1773, The Society of Automotive Engineers (SAE), 1995.

[Agra-97] G.P. Agrawal, Fiber-Optic Communication Systems, 2nd edition, New York, Wiley, c1997.

[Barn-84] C.E. Barnes and J.J. Wiczer, "Radiation effects in optoelectronic devices," Sandia Report, SAND84-0771, 1984.

[Barn-86] C.E. Barnes, "Radiation hardened optoelectronic components: sources," Proc. SPIE, vol. 616, pp. 248-252, 1986.

[Barn-90] C. Barnes, L. Dorsky, A. Johnston, L. Bergman, and E. Stassinopoulos, "Overview of fiber optics in the natural space environment," in Fiber Optics Reliability: Benign and Adverse Environments IV, Proc. SPIE, 1990, vol. 1366, pp. 9-16.

[Barn-99] C. Barnes, G. Swift, S. Guertin, J. Schwank, M. Armendariz, G. Hash, K. Choquette, "Proton irradiation effects in oxide-confined certicle cavity surface emitting laser (VCSEL) diodes," to be published in the Procs. of 1999 RADECS.

[Bart-97] J. Barth, "Modeling space radiation environments," Notes from 1997 IEEE Nuclear and Space Radiation Effects Conference Short Course.

[Bart-98] Private comunications, 1998.

[Bone-96] R.K. Bonebright, J.H. Kim, R.A. Hughes, J.W. Clement, T.M. Bocek, E.Y. Chan, J.H. Nitardy, and C. Hong, "Development of dual-rate MIL-STD-1773A data bus transceiver," ion 1773 DR SPIE

[Bosc-99] D. Boscher, S. Bourdarie, A. Vacaresse, "Contribution of physical modeling to engineering models of the radiation belts," to be published in the Procs. of 1999 RADECS.

[Bris-93] J. Bristow and J. Lehman, "Component tradeoffs and technology breakpoints for a 50 Mbps to 3.2 Gbps fiber optic data bus for space applications," Proc. SPIE, vol. 1953, pp. 159-169, 1993.

[Brot-97] C. Brothers, R. Pugh, P. Duggan, J. Chavez, D. Schepis, D. Yee, S. Wu, "Total-dose and SEU characterization of 0.25 micron CMOS/SOI integrated circuit memory technologies," IEEE Trans. on Nucl. Sci., vol. NS-44, pp. 2134 –2139, 1997.

[Buch-93] S. Buchner, K. Kang, D. Krening, G. Lannan, and R. Schneiderwind, "Dependence of the SEU window of vulnerability of a logic circuit on magnitude of deposited charge," IEEE Trans. on Nucl. Sci., vol. NS-40, no. 6, pp. 1853-1857, 1993.

[Buch-95] S. Buchner, A. B. Campbell, D. McMorrow, J. Melinger, M. Masti, and Y. J. Chen, "Modification of single event upset cross section of an SRAM at high frequencies," RADECS 95, pp. 326-332, 1995

[Cart-97] M.A. Carts, P.W. Marshall, C.J. Marshall, K.A. LaBel, M. Flanegan, J. Bretthauer, "Single event test methodology and test results of commercial gigabit per second fiber channel hardware," IEEE Trans. Nucl. Sci., Vol. 44, No. 6, pp. 1878-1884, 1997.

[Chap-93] M. de La Chapelle, A. W. Van Ausdale, and M. E. Fritz, "The STAR-FODB (fiber optic data bus) program," in Proc. GOMAC '93 Conf., pp. 395-397.

[Cros-93] D. Cross, M. Fritz, D. Haakenson, C. Hoeflein, R. Hodges, S. Kelnhofer, J. Lam, and M. Summerhays, "The Boeing photonics space experiment," Photonics for Space Environments I, vol. SPIE-1953, pp. 116-26, 1993.

[Dale-92] C.J. Dale , and P.W. Marshall, "Radiation response of 1300 nm optoelectronic components in a natural space environment," Proc. SPIE, vol. 1791, pp. 224-232, 1992.

[Dale-93a] C.J. Dale, P.W. Marshall, B. Cummings, L. Shamey, and A. Holland, "Displacement damage effects in mixed particle environments for shielded spacecraft CCDs," IEEE Trans. Nucl. Sci., Vol. 40, No. 6, pp. 1628-1637, 1993.

[Dale-93b] C.J. Dale, and P.W. Marshall, "Candidate NRL space experiments for the Microelectronics and Photonics Test Bed," SPIE Proc. on Photonics for Space Environments, vol. 1953, pp. 17-22, 1993.

[Dale-95] C.J. Dale, P.W. Marshall, K.A. Clark, M. de La Chapelle, M.E. Fritz, and K.A. LaBel, "Fiber optic data bus space experiment on board the microelectronics and photonics test bed (MPTB)," Photonics for Space Environments III, vol. SPIE-2482, p. 285, 1995.

[Dale-96] C.J. Dale, P.W. Marshall, M.E. Fritz, M. de La Chapelle, M.A. Carts, and K.A. LaBel, "System radiation response of a high performance FODB," IEEE Trans. on Nucl. Sci., vol. NS-43, no.3, p 1030, 1996.

[DeLa-94] M. Delaus, "Radiaiton concerns in state-of-the-art processing technology," Notes from 1994 IEEE Nuclear and Space Radiation Effects Conference Short Course.

[DeRu-93] J.DeRuiter, "Survivable ring architecture for spaceborne applications," Proc.SPIE,vol. 1953, pp. 128-135, 1993.

[Desu-93] E. Desuvire, Erbium-Doped Fiber Amplifiers, Principles and Application, New York: John Wiley and Sons, Inc., 1993.

[Dodd-99] P. Dodd, "Basic mechanisms for single event effects," Notes from 1999 IEEE Nuclear and Space Radiation Effects Conference Short Course.

[Dres-98] P. V. Dressendorfer, "Basic mechanisms for the new millenium," Notes from 1998 IEEE Nuclear and Space Radiation Effects Conference Short Course.

[Dres-89] Dressendorfer, P. V., Ma, T. P., Ionizing Effects in MOS Devices and Circuits, New York: John Wiley and Sons, 1989.

[Dyer-98] C. S. Dyer, "Space radiation environment dosimetry," Notes from 1997 IEEE Nuclear and Space Radiation Effects Conference Short Course.

[Emil-96] D.W. Emily, "Total dose response of linear bipolar microcircuits," Notes from 1996 IEEE Nuclear and Space Radiation Effects Conference Short Course.

[Endo] Nikkei Science, Inc. of Japan, image by K. Endo

[Evan-93] B.D. Evans, H.E. Hager, B.W Hughlock, "5.5-MeV proton irradiation of a strained quantum-well laser diode and a multiple quantum-well broadband LED," IEEE Trans. on Nucl. Sci., vol NS-40, no. 6, pp. 1645 –1654, 1993

[Flee-95] D.M. Fleetwood, "A first principles approach to total-dose hardness assurance," Notes from 1995 IEEE Nuclear and Space Radiation Effects Conference Short Course.

[Frie-84a]. E.J. Friebele, C.G. Askins, M.E. Gingerich, and K.J. Long, "Optical fiber waveguides in radiation environments, II," Nucl. Inst. Meth. in Phys. Res. B1, 355-369 (1984).

[Frie-84b] E.J. Friebele, K.J. Long, C.G. Askins, and M.E. Gingerich, "Radiation response of optical fibers and Selfloc Microlenses at 1.3μm," Fiber Optics in Adverse Environments II, Proc. SPIE, vol. 506, pp. 202-208, 1984.

[Frie-85] E.J. Friebele, K.J. Long, C.G. Askins, M.E. Gingerich, M.J. Marrone, and D.L. Griscom, "Overview of radiation effects in fiber optics," Crit. Rev. Tech.:Opt. Materials in Radiation Environ., P. Levy and E.J. Friebele,Ed. Bellingham, WA: SPIE, 1985, vol. SPIE-541, pp. 70-88.

[Frie-91] E.J. Friebele, "Photonics in the space environments," Notes from 1991 IEEE Nuclear Space Radiation Effects Conference Short Course.

[Frit-93] M.E. Fritz, et al., "The Boeing photonics space experiment," SPIE Proceedings, vol. 1953, pp. 116-126, April 1993.

[Frit-94] M.E. Fritz, B.E. Daniels, M. de La Chapelle, D.A. Cross, A.W. Van Ausdale, "The STAR FODB program," SPIE Proc. on Photonics for Space Environments II, vol. 2153, 1994.

[Frit-95] M.E. Fritz, M. de La Chapelle, and A.W. Van Ausdale, "Boeing's STAR FODB test results," Photonics for Space Environments, vol. SPIE-2482, pp. 226-235, 1995.

[Frit-96] M.E. Fritz, G. Berg, D.A. Cross, and M.C. Wilkinson, "Photonics space experiment on-orbit results," SPIE Proceedings, vol. 2811, pp. 106-115, Aug. 1996.

[Gall-96] Galloway's short course

[Gate-96] M. Gates, K.A. LaBel, J. Barth, A. Johnston, and P.W. Marshall, "Single event effects criticality analysis," NASA Report, See NASA GSFC Radiation Effects & Analysis Home Page, http://flick.gsfc.nasa.gov/radhome.htm, 1996.

[Gris-94] D.L. Griscom, M.E. Gingerich, and E.J. Friebele, "Model for dose, dose-rate, and temperature dependence of radiation induced loss in optical fibers," IEEE Trans. Nucl. Sci., vol. NS-41, no. 3, pp. 523-527, 1994.

[Gros-93] S. Gross, "ATM-based protocol for Gbps ring networks," in Proc. Gomac '93 Conf., p. 399.

[Guti-94] R.C. Gutierrez, G.M. Swift, S. Dubovitsky, R.K. Bartman, C.E. Barnes, and L. Dorsky, "Radiation effects on fused biconical taper wavelength division multiplexers," IEEE Trans. Nucl. Sci., vol. NS-41, no. 6, p1950, 1994.

[Hash-94] S. G. L Hash et al. T Hash, G.L.; Schwanck, J.R.; Shaneyfelt, M.R.; Sandoval, C.E.; Conners, M.P.; Sheridan, T.J.; Sexton, F.W.; Slayton, E.M.; Heise, J.A.; Foster, C.C., "Proton irradiation effects on advanced digital and microwave III-V components,", IEEE Trans. Nucl. Sci. vol. NS-41, pp. 2259-2266, 1994

[Heid-99] W.F. Heidergott, "System level mitigation strategies," Notes from 1999 IEEE Nuclear and Space Radiation Effects Conference Short Course.

[Hens-92] H. Henschel, O. Köhn, and H.U. Schmidt, "Radiation sensitivity of fibre optic couplers," SPIE, Optical Materials Reliability and Testing, vol. 1791, pp. 151-163, 1992.

[Hens-97] H. Henschel, O. Kohn, W. Lennartz, S. Metzger, H.U. Schmidt, J. Rosenkranz, B. Glessner, B.R.L. Siebert, **"**Comparison between fast neutron and gamma irradiation of optical fibres," Proc. RADECS 1997, pp. 430 –438, 1997

[Hens-98] H. Henschel, O. Köhn, H.U. Schmidt, J. Kirchhof, and S. Unger, "Radiation-induced loss of Rare Earth doped silica fibres," IEEE Trans. Nucl. Sci.,vol. NS-45, no.3, p 1552, 1998.

[Hinr-98] P.F. Hinrichsen, A.J. Houdayer, A.L. Barry, J. Vincent, "Proton induced damage in SiC light emitting diodes," IEEE Trans. Nucl. Sci. vol. NS-45, pp. 2808-2812, 1998.

[Hous-98] S.L. Houston and K.A. Pfitzer, "A new model for the low altitude trapped proton environment," IEEE Trans. on Nucl. Sci., vol. NS-45, no.6, pp. 2972-2978, 1998.

[Hsie-81] C.M. Hsieh, P.C. Murley, R.R. O'Brien, "A field-funneling effect on collection alpha-particle generated carriers," IEEE Electron Device Letters 2, p. 103, 1981

[Hugh-90] B.W. Huglock, G.S. LaRue, and A.H. Johnston, "Single-Event upset in GaAs E/D MESFET," IEEE Trans. Nucl. Sci.,vol. NS-37, no.6, p 1894, 1990.

[Jack-99] G.L Jackson, K.A. LaBel, C.J. Marshall, J.L. Barth, J. Kolasinski, C.M. Seidleck, P.W. Marshall, "Preliminary flight results of the Microelectronics and Photonics Test Bed NASA dual rate 1773 (DR1773) fiber optics data bus experiment," Procs. 1999 GOMAC, pp. 340-344, 1999.

[Jack-96] G.L. Jackson, K.A. LaBel, M. Flanegan, C. Dale, P.W. Marshall, R.K. Bonebright, J.H. Kim, E. Y. Chan, T. M. Bocek, C. White, "The Microelectronics and Photonics Test Bed dual rate 1773 fiber optics data bus experiment," SPIE Proc. for Photonics for Space Environments, Vol. 2811, pp.116-127, 1996.

[Jord-93] A.F. Jordan, "On the brink: Fiber optic LAN's for avionics and space," Defense Electronics, vol. 25, no. 11, pp.43-47, 1993

[John-92] A.R. Johnston and E.W. Taylor, "A survey of the LDEF fiber optic experiments," JPL Report D-10069, Nov. 10, 1992.

[John-94] A.H. Johnston, G.M. Swift, B.G. Rax, "Total dose effects in conventional bipolar transistors and linear integrated circuits," IEEE Trans. Nucl. Sci. vol. NS-41, pp. 2427-2436, 1994.

[John-99a] A.H. Johnston, B.G. Rax, L.E. Selva, C.E. Barnes, "Proton degradation of light-emitting diodes," IEEE Trans. Nucl. Sci. vol. NS-46, pp. 1781-1789, 1999

[John-99b] A.H. Johnston, T. Miyahira, G.M. Swift, S.M. Guertin, L.D. Edmonds, "Angular and energy dependence of proton upset in optocouplers," IEEE Trans. Nucl. Sci. vol. NS-46, pp. 1335-1341, 1994

[Kinn-98] J.D. Kinnison, "Achieving reliable, affordable systems" Notes from 1998 IEEE Nuclear and Space Radiation Effects Conference Short Course.

[Koga-94] R. Koga, R.J. Ferro, D.J. Mabry, S.D. Pinkerton, D.E. Romeo, J.R. Scarpulla, T.K. Tsubota, M. Shoga, "Ion-induced sustained high current condition in a bipolar device," IEEE Trans. Nucl. Sci. vol. NS-41, pp. 2172-2178, 1994

[LaBe-91a] K. LaBel, E.G. Stassinopoulos, and G.J. Brucker, "Transient SEU's in a Fiber Optic System for Space Application," IEEE Trans. Nucl. Sci., vol. 38,no. 6,1991.

[LaBe-92a] K.A. LaBel, "A spacecraft fiber optic data system – radiation effects," RADECS 91: IEEE Proceedings from, La-Grande Motte, France, Sept. 1991, pp. 412-415, vol. 15.

[LaBe-92b] K.A. LaBel, J.A. Cooley, E.G. Stassinopoulos, P. Marshall, C. Crabtree "Single event test methodology for integrated optoelectronics," SPIE Proceedings of Integrated Optical Circuits II, Boston, MA, vol. 1794, Sept. 1992, pp. 225-233.

[LaBe-93a] K.A. LaBel, E.G. Stassinopoulos, P.W. Marshall, E.L. Petersen, C. Dale, C. Crabtree, and C. Stauffer, "Proton irradiation SEU test results for the SEDS MIL-STD-1773 fiber optic data bus: integrated optoelectronics," SPIE Proc. for Photonics for Space Environments, Vol. 1953, pp. 27-44, 1993.

[LaBe-93b] K.A. LaBel, M. Flanegan, P. Marshall, C. Dale, and E.G. Stassinopoulos, "Space flight experience and lessons learned with NASA's first fiber optic data bus," Second European Conference: RADECS 1993 Proc., pp. 221-225, 1993.

[LaBe-93c] K.A. LaBel, P. Marshall, C.Dale, C.M. Crabtree, E.G. Stassinopolous, J.T. Miller and M.M. Gates, "SEDS MIL-STD-1773 fiber optic data bus: Proton irradiation test results and spaceflight SEU data," IEEE Trans. Nucl. Sci., vol. 40, no. 6, pp. 1638-44, 1993.

[LaBe-94a] K.A. LaBel, D.K. Hawkins, J.A. Cooley, C.M. Seidleck, P. Marshall, C. Dale, M. M. Gates, H.S. Kim, and E.G. Stassinopoulos, "Single event effect ground test results for a fiber optic data interconnect and associated electronics," IEEE Trans. Nucl. Sci., vol. 41, no. 6, pp. 1999-2004, 1994.

[LaBe-94b] K.A. LaBel, P.W. Marshall, C.J. Dale, E.G. Stassinopoulos, A. Johnston, C.M. Crabtree, and H.S. Kim, "Single event effects on associated electronics for fiber optic systems," Proc. SPIE, vol 2215, pp. 74-93, April 1994.

[LaBe-95] K.A. LaBel, A.K. Moran, D.K. Hawkins, A.B. Sanders, E.G. Stassinopoulos, R.K. Barry, C.M. Seidlick, H.S. Kim, J. Forney, P. Marshall, and C. Dale, "Single-event effect proton and heavy-ion test results in support of candidate NASA programs," 1995 IEEE Radiation Effects Data Workshop Record, pp. 16-32, July 1995.

[LaBe-96a] K.A. LaBel, and M.M. Gates, "Single-event-effect mitigation from a system perspective," IEEE Trans. Nucl. Sci., NS-42, no. 2, pp. 654-660, April 1996.

[LaBe-96b] K.A. LaBel, M. Flanegan, G. Jackson, D. Hawkins, C.J. Marshall, P.W. Marshall. D. Johnson, C. Seidleck, R.K. Bonebright, J.H. Kim, E. Y. Chan, T. M. Bocek, and B. Bartholet, "Preliminary ground test radiation results on NASA's MPTB dual-rate 1773 experiment," SPIE Proc. for Photonics for Space Environments, Vol. 2811, pp.128-135, 1996.

[LaBe-97] K.A. LaBel, P.W. Marshall, C.J. Marshall, M. D'Ordine, M. Carts, G. Lum, H.S. Kim, C.M. Seidleck, T. Powell, R. Abbott, J. Barth, E.G. Stassinopoulos, "Proton-induced transients in optocouplers: in-flight anomalies, ground irradiation test, mitigation and implications," IEEE Trans. Nucl. Sci. vol. NS-44, pp. 1885-1892, 1997.

[LaBe-98a] K.A. LaBel, "Applying state of the art commercial and emerging technologies to space systems," Notes from 1998 IEEE Nuclear and Space Radiation Effects Conference Short Course.

[LaBe-98b] K.A. LaBel, A.H. Johnston, J.L. Barth, R.A. Reed, C.E. Barnes, "Emerging Radiation Hardness Assurance (RHA) Issues: A Nasa Approach For Space Flight Programs," IEEE Trans. Nucl. Sci. vol. NS-45, pp. 2727-2736, 1998

[LaBe-98c] K.A. LaBel, R.A. Reed, H. Leidecker, J. Barth, P.W. Marshall, C.J. Marshall, C. Seidleck, "Comparison of MIL-STD-1773 fiber optic data bus terminals: single event proton test irradiation, in-flight space performance, and prediction techniques," IEEE Trans. on Nucl. Sci., NS-44, no. 3, 1998.

[LaBe-98d] K.A. LaBel, C.J. Marshall, P.W. Marshall, M.O. Ott, C.M. Seidleck, D.J. Andrucyk, "On the suitability of Fiber Optic Data Links in the space radiation environment: a historical and scaling technology perspective," 1998 IEEE Aerospace Engineering Conference Proc., V 4, pp. 421-434, 1998.

[Lach-98] G. Lachs, Fiber Optic Communications : Systems, Analysis, and Enhancements, New York, McGraw-Hill, c1998.

[Lee-99] S.C. Lee, Y.F. Zhao, R.D. Schrimpf, M.A. Neifeld, K.F. Galloway, "Comparison of lifetime and threshold current damage factors for multi-quantum-well (MQW) GaAs/GaAlAs laser diodes irradiated at different proton energies," IEEE Trans. Nucl. Sci. vol. NS-46, pp. 1797-1803, 1999

[Lema-91] P.J. Lemaire, "Reliability of optical fibers exposed to hydrogen: Prediction of long term loss increases," Opt. Eng. 30, 780-789 (1991).

[Lera-99] J.L. Leray, "Total dose effects: modeling for the present and future," Notes from 1999 IEEE Nuclear and Space Radiation Effects Conference Short Course.

[Mars-92] P.W. Marshall, C.J. Dale, and E.A. Burke, "Space radiation effects on optoelectronic materials and components for a 1300 nm fiber optic data bus," IEEE Trans. Nucl. Sci., vol. 39, no. 6, pp. 1982-1989, 1992.

[Mars-93a] P. Marshall, C. Dale, and K. LaBel, "Charged particle effects on optoelectronic devices and bit error rate measurements on 400 Mbps fiber based data links," in Proc. RADECS Conf., Saint Malo, France, Sept. 13-16, 1993, pp. 266-271.

[Mars-93b] P.W. Marshall, K.A. LaBel, C.J. Dale, J.P. Bristow, E.L. Petersen, and E.G Stassinopoulos, "Physical interactions between charged particles and optoelectronic devices and the effects on fiber based data links," Proc. SPIE, vol. 1953, pp. 104-115, 1993.

[Mars-93] P. Marshall, J. Cutchin, and T. Weatherford, "Space radiation effects in a GaAs C-HIGFET logic family suitable for satellite data transmission above 1 Gbps," in Proc. GOMAC '93 Conf., pp. 227-229.

[Mars-94a] P.W. Marshall, C.J. Dale, M.A. Carts, and K.A. LaBel, "Particle induced bit errors in high performance data links for satellite data management," IEEE Trans. Nucl. Sci.,vol. NS-41, no.6, pp. 1958-65, 1994.

[Mars-94b] P.W. Marshall, C.J. Dale, E.J. Friebele, and K.A. LaBel, "Survivable fiber-based data links for satellite radiation environments," SPIE Critical Review CR-14, Fiber Optics Reliability and Testing, pp. 189-231, 1994.

[Mars-95a] P.W. Marshall, C.J Dale, T.R. Weatherford, M.A.Carts, D. McMorrow, A. Peczalski, S. Baier, J. Nohava, J. Skogen "Heavy ion immunity of a GaAs complementary HIGFET circuit fabricated on a low temperature grown buffer layer," IEEE Trans. Nucl. Sci.,vol. NS-42, no.6, p. 1850, 1995.

[Mars-95b] P.W. Marshall, C.J. Dale, M.E. Fritz, M. de La Chapelle, M.A. Carts, and K.A. LaBel, "Total ionizing dose and single particle effects in a 200 Mbps star-coupled fiber optic data bus," Proc. of SPIE Conference on Photonics for Space Environments III, Proc. #2482, 1995.

[Mars-95c] P.W. Marshall, C.J Dale, T.R. Weatherford, M. La Macchia, and K.A. LaBel, "Particle induced mitigation of SEU sensitivity in high data rate GaAs HIGFET technologies," IEEE Trans. Nucl. Sci.,vol. NS-42, no.6, pp. 1844-1854, 1995.

[Mars-96] P.W. Marshall, C.J. Dale, and K.A. LaBel, "Space radiation effects in high performance fiber optic data links for satellite management," IEEE Trans. Nucl. Sci.,vol. NS-43, no.3, pp. 645-653, April 1996.

[Mars-98] C.J. Marshall, P.W. Marshall, M.A. Carts, R.A. Reed, K.A. LaBel, "Proton-induced transient effects in a Metal-Semiconductor-Metal (MSM) photodetector for optical-based data transfer," IEEE Trans. on Nucl. Sci., vol. NS-45, pp. 2842-2848, 1994

[Mars-99] P.W. Marshall and C.J. Marsahll, “Proton effect and test issues for satellite designers,” Notes from 1999 IEEE Nuclear and Space Radiation Effects Conference Short Course.

[Mess-86] G. C. Messenger, M. S. Ash, The Effects of Radiation on Electronic Systems, New York : Van Nostrand Reinhold Co., c1986.

[Mess-97] G. C. Messenger, M. S. Ash, Single Event Phenomena, New York: Chapman and Hall, 1997.

[McCl-94] S. McClure, R.L. Pease W. Will, G. Perry, “Dependence of total dose response of bipolar linear microcircuits on applied dose rate,” IEEE Trans. Nucl. Sci. vol. NS-41, pp. 2544-2549, 1994

[McDo-00] McDonald, P. T. et al. to be published in Proceedings of the GOMAC/HEART Conference, March, 2000.

[McMo-96] D. McMorrow, T.R. Weatherford, S. Buchner, A.R. Knudson, J.S. Melinger, L.H. Tran, and A.B. Campbell, “Single event effects in GaAs devices and circuits,” IEEE Trans. Nucl. Sci.,vol. NS-43, no.2, pp. 628-624, 1996.

[Miya-79] T. Miya, Y. Terunuma, T. Miyoshita, Electron. Lett. 15, 106, 1979

[OBry-99] M.V. O'Bryan, K.A. LaBel, R.A. Reed, J.W. Howard, J.L. Barth, C.M Seidleck, P.W. Marshall, C.J. Marshall, H.S. Kim, D.K. Hawkins, M.A. Carts, K.E. Forslund,”Recent radiation damage and single event effect results for microelectronics,” 1999 IEEE Radiation Effects Data Workshop Record, pp. 1-14, July 1999.

[OBry-00] M.V. O’Bryan, C.M. Seidleck, M.A. Carts, K.A. LaBel, R.A. Reed, J.L. Barth, C.J. Marshall, D.K. Hawkins, A. Sanders, J. Forney, J.W. Howard, H.S. Kim, R. Ladbury, P. Marshall, D. Roth, E. Nhan, J. Kinnison, K. Sahu, S. Kniffin, to be published in the 2000 IEEE Radiation Effects Data Workshop Record, 2000

[Ott –97] M. Ott, J. Plante, J. Shaw, M.A. Garrison Darrin, “Fiber optic cable assemblies for space slight: issues and remedies,” Paper number 975592 AIAA/SAE World Aviation Congress, Anaheim, CA. 1997.

[Paxt-97] A.H. Paxton, R.F. Carson, H. Schone, E.W. Taylor, K.D. Choquette, H.Q. Hou, K.L. Lear, M.E. Warren, “Damage from proton irradiation of vertical-cavity surface-emitting lasers,” IEEE Trans. Nucl. Sci., vol NS-44, no. 6, pp. 1893 –1897, 1997.

[Pala-98] J.C. Palais, Fiber Optic Communications, 4th edition, Prentice Hall, Upper Saddle River, N.J., c1998.

[Pete-97] E.L. Petersen, “Single event analysis and prediction,” Notes from 1997 IEEE Nuclear and Space Radiation Effects Conference Short Course.

[Powe-93] J.P. Powers,.An Introduction to Fiber Optic Systems, Aksen Associates ; Homewood, IL : Irwin, c1993.

[Rax-99] B.G. Rax, A.H. Johnston, T. Miyahira, “Displacement damage in bipolar linear integrated circuits,” IEEE Trans. on Nucl. Sci., volume NS-46, pp. 1660 –1665, 1999.

[Ream-95] D. V. Reames, “Solar Energetic Particles: A Paradigm Shift,” Revs. Geophys. (Suppl.), 33,585, 1995.

[Reed-96] R.A. Reed, M.A. Carts, P.W. Marshall, C.J. Dale, S. Buchner, M. La Macchia, B. Mathes, D., McMorrow, “Single Event Upset cross sections at various data rates,” IEEE Trans. Nucl. Sci. vol. NS-43, pp. 2862 –2867, 1996.

[Reed-98] R.A Reed, P.W. Marshall, A.H. Johnston, J.L. Barth, C.J. Marshall, K.A. LaBel, M. D'Ordine, H.S. Kim, M.A. Carts, “Emerging Optocoupler Issues With Energetic Particle-Induced Transients And Permanent Radiation Degradation,” IEEE Trans. Nucl. Sci. vol. NS-45, pp. 2833 –2841, 1998.

[Schn-92] R. Schneiderwind, D. Krening, S. Buchner, and K. Kang, “Laser confirmation of SEU experiments in GaAs MESFET combinational logic,” IEEE Trans. on Nucl. Sci., vol. NS-39, no. 6, pp. 1665-1670, 1992.

[Shog-94] M. Shoga, K. Jobe, M. Glasgow, M. Bustamante, E. Smith, and R. Koga, “Single event upset at Gigahertz frequencies,” IEEE Trans. on Nucl. Sci., vol. NS-41, no. 6, pp. 2252-2266, 1994.

[Stap-95] W.J. Stapor, “Single-event effects qualification,” Notes from 1995 IEEE Nuclear and Space Radiation Effects Conference Short Course.

[Tayl-90] E.W. Taylor, “Behavior of coupled waveguide devices in adverse environments,” SPIE, Fibre Optics, vol. 1314, pp. 155-167, 1990.

[Tayl-91a] E.W. Taylor, “Ionization-induced refractive index and polarization effects in $LiNbO_3$:Ti directional coupler waveguides,” J. Lightwave Tech., vol. 9, no. 3, pp. 335-340, 1991.

[Tayl-91b] E.W. Taylor, J.N. Berry, A.D. Sanchez, R.J. Padden, and S.P. Chapman, “Preliminary analysis of PL experiment #701, space environment effects on operating fiber optic systems,” in LDEF-69 Months in Space- First Post Retrieval Symposium, Report No. NASA CP-3134, pp. 1257-1282, 1991.

[Tayl-92a] E.W. Taylor, “Radiation effects in guided wave devices,” SPIE, Integrated Optical Circuits II, vol. 1794, pp. 54-61, 1992.

[Tayl-92b] E.W. Taylor, J. Berry, A.D. Sanchez, R.J. Padden, S. DeWalt, and S. Chapman, “First operational space fiber optic data links orbited aboard the Long Duration Exposure Facility-lessons learned,""1992 DOD Fiber Optics Conference Proceedings.

[Teag-72] M.J. Teague,”A model for the starfish flux in the inner radiation zone,” X-602-72-487, NASA/Goddard Space Flight Center, Greenbelt, MD, December 1972.

[Thel-94] D. Thelen, S. Rankin, P.W. Marshall, K.A. LaBel, M.A. Krainak, “Dual-rate MIL-STD-1773 fiber optic transceiver for satellite applications,” Proc. of SPIE Conference on Photonics for Space Environments II, Proc. #2215, pp.101-112, 1994.

[Turf-90] T.L. Turflinger and M.V. Davey, “Understanding single event phenomena in complex analog and digital integrated circuits,” IEEE Trans. on Nucl. Sci., vol. NS-37, no. 6, pp. 1832-1838, 1990.

[Turf-94] T.L. Turflinger, M.V. Davey, and B.M. Mappes, “Single event effects in analog-to-digital converters: device performance and system impact,” IEEE Trans. on Nucl. Sci., vol. NS-41, no. 6, pp. 2187-2194, 1994.

[Tylk-96] A.J. Tylka, J.H. Adams, Jr., P.R. Boberg, B. Brownstein, W.F. Dietrich, E.O. Flueckiger, E.L. Petersen, M.A. Shea, D.F. Smart, E.C. Smith, :CREME96 a revision of the cosmic ray effects on microelectronics code,” IEEE Trans. Nucl. Sci.,vol. NS-43, no.6, pp. 2758-2766, 1996.

[VanE-96] T.E. Van Eck, D.G. Girton, J.A. Marly, S.P. Ermer, W.W. Anderson, L.E. Robinette, G.K. Lum, and J.W. Garrett, “Space environment testing of polymer photonic modulators,” SPIE, vol. 2911, pp. 25-28, 1996.

[Weat-97] T.R. Weatherford, P.W. Marshall, C.J. Marshall, D.J. Fouts, B. Mathes, and M. La Macchia, "Effects of low temperature buffer layer thickness and growth temperature on the SEE sensitivity of GaAs HIGFET circuits," IEEE Trans. Nucl. Sci.,vol. NS-44, no.6, 1997.

[Weis-90] J.D. Weiss, "The radiation response of a Selfoc microlens," J. Lightwave Technol.,vol. 8, no. 7, pp.1107-1109, 1990.

[Wicz-86] J.J. Wiczer, "Radiation hardened optoelectronic components: Detectors," Proc. SPIE, vol. 616, pp. 254-266, 1986.

[Will-98] G.M. Williams and E.J. Friebele, "Space radiation effects on Erbium-doped fiber devices: sources, amplifiers, and passive measurements," IEEE Trans. Nucl. Sci., vol. NS-45, no.3, p 1531, 1998.

[Widm-87] A.X. Widmer, U.S. Patent 4,667,517, 12 May, 1987

[Wino-92] P.S. Winokur, "Total-dose radiation effects (from the perspective of the experimentalist)," Notes from 19XX IEEE Nuclear and Space Radiation Effects Conference Short Course.

[Xaps-98] M.A. Xapsos, G.P. Summers and E.A. Burke, "Probability model for peak fluxes of solar proton events," IEEE Trans. Nucl. Sci.,vol. NS-45, no.6, pp. 2948-2953, 1998.

[Xaps-00] M.A. Xapsos, R.J. Walters, G.P. Summers, J.L. Barth, E.G. Stassinopoulos, R. Messenger, and E.A. Burke, "Characterizing solar proton energy spectra for radiation effects," presented at the IEEE NSREC 2000.

[Zhao98] Y.F. Zhao, R.D. Schrimpf, A.R. Patwary, M.A. Neifeld, A.W. Al-Johani, R.A. Weller, and K.F. Galloway, "Annealing Effects on Multi-Quantum Well Laser Diodes after Proton Irradiation," IEEE Trans. Nucl. Sci., Vol. 44, pp. 2826-2832, 1997.

[Zieg-84] J.F. Ziegler, J.P. Biersack, and U. Littmark, The Stopping and Range of Ions in Solids. New York: Pergamgon, 1884.

10.0 List of Acronyms

AE8	model for trapped electron environment
AP8	model for trapped proton environment
APD	Avalanche PhotoDiodes
BER	Bit Error Ratio
BERT	Bit Error Ratio Tester
CME	Coronal Mass Ejections
CRRESELE	model for trapped electron environment
CRRESPRO	model for trapped proton environment
DDD	Displacement Damage Dose
EDFA	Erbium-Doped Fiber Amplifier
ELDRS	Enhanced Low Dose Rate Sensitivity
EOL	End Of Life
FBIU	Fiber Bus Interface Unit
FODB	Fiber Optics Data Bus
Gbps	Giga-bits per second
GLAS	Guided Laser Altimeter System
GRC	Galactic Cosmic Rays
HST	Hubble Space Telescope
LED	Light-Emitting Diode
LET	Linear Energy Transfer
LDEF	Long Duration Exposure Facility
Mbps	Mega-bits per second
MPTB	Microelectronics and Photonics TestBed
MSM	Metal-Semicondictor-Metal
NRZ	NonReturn-to-Zero
NSREC	Nuclear and Space Radiation Effects Conference
p-i-n	p-intrinsic-n
PRN	PseudoRandom Number
RADECS	Proceedings from the Radiation Effects in Components and Systems Conference
RZ	Return-to-Zero
SAA	South Atlantic Anomaly
SAMPEX	Solar Anomalous Magnetospheric Particle Explorer
SEB	Single-Event Burnout
SEDS	Small Explorer Data System
SEDSI	first generation SEDS
SEDSII	the second generation of SEDS
SEE	Single-Event Effects
SEGR	Single-Event Gate Rupture
SEL	Single-Event Latchup
SET	Single-Event Transient
SEU	Single-Event Upset
SSR	Solid State Recorder
TID	Total Ionizing Dose
TNS	Transactions on Nuclear Science

VCSEL	Vertical Cavity Surface Emitting Laser
WDMs	Wavelength-Division Multiplexers